NOAA TM ERL ARL-39

A UNITED STATES DEPARTMENT OF COMMERCE PUBLICATION

NOAA Technical Memorandum ERL ARL-39

U.S. DEPARTMENT OF COMMERCE
NATIONAL OCEANIC AND ATMOSPHERIC ADMINISTRATION
Environmental Research Laboratories

Atmospheric Transport and Diffusion in the Planetary Boundary Layer

July 1971-June 1972

Air Resources
Laboratories
SILVER SPRING,
MARYLAND
June 1973

ENVIRONMENTAL RESEARCH LABORATORIES

AIR RESOURCES LABORATORIES

IMPORTANT NOTICE

Technical Memoranda are used to insure prompt dissemination of special studies which, though of interest to the scientific community, may not be ready for formal publication. Since these papers may later be published in a modified form to include more recent information or research results, abstracting, citing, or reproducing this paper in the open literature is not encouraged. Contact the author for additional information on the subject matter discussed in this Memorandum.

NATIONAL OCEANIC AND ATMOSPHERIC ADMINISTRATION

U.S. DEPARTMENT OF COMMERCE
National Oceanic and Atmospheric Administration
Environmental Research Laboratories

NOAA Technical Memorandum ERL ARL-39

ATMOSPHERIC TRANSPORT AND DIFFUSION IN THE PLANETARY BOUNDARY LAYER JULY 1971 - JUNE 1972

I. Van der Hoven, Editor

Contributors

J. K. Angell
A. B. Bernstein
D. J. Bjorem
H. L. Boen
C. R. Dickson
G. A. Herbert
J. F. Sagendorf
G. E. Start
L. L. Wendell

Annual Research Program Review
July 1971 - June 1972
for
U. S. Atomic Energy Commission

Air Resources Laboratories
Silver Spring, Maryland
June 1973

DISCLAIMER

The Environmental Research Laboratories, National Oceanic and Atmospheric Administration, U.S. Dept. of Commerce, does not approve, recommend or endorse any proprietary product or proprietary material mentioned in this publication. No reference shall be made to the Environmental Research Laboratories, or to this publication furnished by the Environmental Research Laboratories, in any advertising or sales promotion which would indicate or imply that the Environmental Research Laboratories approves, recommends or endorses any proprietary product or proprietary material mentioned herein, or which has as its purpose an intent to cause directly or indirectly the advertised product to be used or purchased because of this Environmental Research Laboratories publication.

The findings of this report are not to be construed as an official Department of Commerce position, unless so designated by other authorized documents.

TABLE OF CONTENTS

LIST OF FIGURES

LIST OF TABLES

PREFACE

In accordance with the letter of agreement of July 13, 1971, with the U.S. Atomic Energy Commission, Division of Reactor Development and Technology, the Air Resources Laboratories have continued their study of atmospheric transport and diffusion in the planetary boundary layer, micrometeorology, diffusion climatology, and the application of this work to the disposal of radioactive waste gases into the atmosphere. The research is technically administered and supervised through the Air Resources Environmental Laboratory of the Air Resources Laboratories. The work is performed at the Air Resources Laboratories Headquarters in Silver Spring, Maryland, and at the Air Resources Idaho Falls Laboratory, National Reactor Testing Station, Idaho. Any inquiry on the research being performed should be directed to the editor, Isaac Van der Hoven, Chief, Air Resources Environmental Laboratory, Air Resources Laboratories, National Oceanic and Atmospheric Administration, 8060 - 13th Street, Silver Spring, Maryland 20910.

ATMOSPHERIC TRANSPORT AND DIFFUSION IN THE PLANETARY BOUNDARY LAYER

AIR RESOURCES LABORATORIES ANNUAL RESEARCH PROGRAM REVIEW FOR THE ENVIRONMENTAL SAFETY BRANCH DIVISION OF REACTOR DEVELOPMENT AND TECHNOLOGY U. S. ATOMIC ENERGY COMMISSION

1. URBAN PLANETARY BOUNDARY LAYER STUDIES (OKLAHOMA CITY)

1.1 Introduction

In a continuing effort to learn something about the effect that a city has on the low-level windfield, we carried out an extensive observational program near Oklahoma City from mid-September to mid-October 1971. A number of factors led to the choice of Oklahoma City for this program. The most important ones were a meteorologically instrumented 500 m tower (the WKY TV tower, with meteorological equipment installed and operated by NOAA's National Severe Storms Laboratory); the relative flatness of the surrounding terrain so that the city itself could reasonably be assumed to be the only disrupting element in the flow; and the expected prevalence of steady, moderate to strong southerly winds, which greatly simplified the design of the observational network and permitted accumulation of an "ensemble" of observations under similar meteorological conditions.

The measurement program consisted of four separate parts: (1) fast-response sensors were mounted on the WKY tower at two levels to accurately measure the stress tensor and other turbulence statistics needed for proper interpretation of the other data; (2) tetroons were released at sites upwind from the city, the release points being varied as circumstances dictated, but were always chosen so that the tetroons would pass close to the WKY tower, with the tracking radar situated about 8 km from the tower; (3) pilot balloon soundings (and some radiosondes) were taken by a mobile network of five stations arranged in three different configurations, those of greatest interest being a line along the mean wind direction, passing through the heart of the city, and including a station adjacent to the WKY tower; (4) slow-response wind measurements were made on a continuous basis at five levels of the WKY tower and at about 30 m above the ground with a network of nine stations occupying a region some 80 x 130 km centered around Oklahoma City.

These four measurement activities contributed to six distinct goals: (1) to repeat the comparison of pibal and tower wind measurements carried out in 1970 (see NOAA Tech. Memos. ERL ARL-28, 1971 and ERL ARL-32, 1972) but with better quality control and greater precision; (2) to determine

the spatial variations in the windfield in the lowest 2 km, as induced by the presence of the city; (3) to compare features of the windfield determined from a line of pibal stations with the same features determined from a series of tetroon flights passing close to that line of stations; (4) to compare the "Eulerian" covariance of horizontal and vertical velocity measured with fast-response sensors mounted on a tower with the "Lagrangian" covariance of horizontal and vertical velocity determined from a series of tetroon trajectories; (5) to determine the feasibility of using standard pibal and radiosonde techniques to determine the vertical variation of wind, geostrophic wind, and acceleration in the lowest 2 km; and to test the technique of determining the shearing stress by vertical integration of the geostrophic departure; (6) to test a technique developed at the National Reactor Testing Station (NRTS) for determining trajectories from a network of near-surface wind measurements. Since analysis of the data is currently underway, it is now most appropriate to describe the program in detail by breaking it down according to measurement program.

1.2 The WKY Tower Measurements

Slow-response measurements of wind speed and direction were made at five levels on the tower — approximately 26, 44, 90, 266, and 444 m above the surface. Slow-response temperature measurements were made at these same levels and also at the surface and 177 and 355 m. These data were recorded continuously throughout the program and were subjected to vastly improved quality control procedures than in 1970. In addition, fast-response measurements of three wind components, using orthogonal arrays of propeller anemometers were made at 177 and 355 m; these were recorded in analog form while tetroon and/or pibal operations were in progress. They are discussed in greater detail in section 1.5.

1.3 Three-Dimensional Tetroon Trajectories

Constant volume balloon (tetroon) flights near Oklahoma City during September-October 1971 provide information on the influence of an isolated urban area on the horizontal and vertical airflow in unstable and relatively stable conditions. The tetroons were tracked by an M-33 radar. Launch mobility was provided by a large truck fitted out as an inflation van. Tetroon positions were obtained at 1-sec intervals and stored on magnetic tape. These 1-sec readings were later averaged to yield 30-sec average tetroon positions and derived velocities. As usual, transponders were attached to the tetroons to permit accurate positioning at very low elevation angles. The tetroons were inflated to float at a mean height 300 m above ground, since one purpose of the experiment was to compare Reynolds stresses derived from the tetroons with the stresses derived in the conventional fashion from fixed-point instruments (Gill props) on the 450-m WKY tower.

The solid lines in figure 1 crudely estimate the partitioning of Oklahoma City according to building type. The small area labeled 1 represents the downtown area with buildings as high as 40 stories (120 m), area 2 the semibuilt-up industrial and commercial areas with buildings about 10 stories (30 m), area 3 the residential area, and area 4 the rural area. The dashed lines indicate terrain height about sea level at 40-m intervals. The slight variation in terrain height is mainly associated with the three river systems in the area: the Cimarron River to the north, the North Canadian River that passes through the southern edge of Oklahoma City, and the Canadian River that passes about 30 km south of Oklahoma City, or near Norman, Oklahoma. The locations of the instrumented TV tower and the tetroon-tracking radar are also indicated in figure 1.

Figure 2 shows sequential tetroon trajectories for the first 2 days of October. To make the city's influence on the trajectories more obvious, we have doubled the east-west scale with respect to the north-south scale. The dots indicate tetroon positions at 3-min intervals, the flight numbers are given at the ends of the trajectories, and the time (CDT) when the tetroons passed over the center of the city are shown in parentheses. At this location, the wind consistently backed during the day; therefore, tetroons released in the morning tended to pass to the east of downtown and those released in the evening, west of downtown.

Quite apparent on morning flights 19, 20, and 24 is the tendency for the tetroons to turn toward the left looking downwind (toward lower pressure) as they pass over the city; in most cases this is followed by a return nearly to the original track. Complete compensation is prevented by the diurnal backing of the wind. In the afternoon, this turning is not so obvious, and instead wave-like oscillations occur over the city. The single evening trajectory (flight 23) in figure 2 is nearly straight.

To obtain a generalized picture of the turning, examine the mean tetroon trajectories in figure 3; these are based on five flights passing over the city from 0900 to 1200, 1200 to 1500, and 1500 to 1800 CDT. The wind speeds are so nearly the same (13 to 14 m sec^{-1}) along all the tracks that the averaging procedure causes little smoothing, but to ensure a minimum of distortion, the coordinate axis for the averaging was centered on the city's center and not on the launch site. Between 0900 and 1200 CDT, the trajectory turning (backing) over the city at about 300 m amounted to 9°, probably illustrating the additional frictional effect induced by the city. Because of this turning the trajectory beyond the city shifted about 2 km laterally from that shown by the light dashed lines. Inasmuch as trajectories either side of the city presumably do not undergo such a shift, downwind of the city there is lateral trajectory convergence to the left and lateral trajectory divergence to the right of the city looking downwind. This lateral mass convergence and divergence could be compensated for either by ascending and descending motion, respectively, or by an increase in wind speed while it moves downwind to the right of the city. Without simultaneous tetroon flights, it is difficult to tell which is the

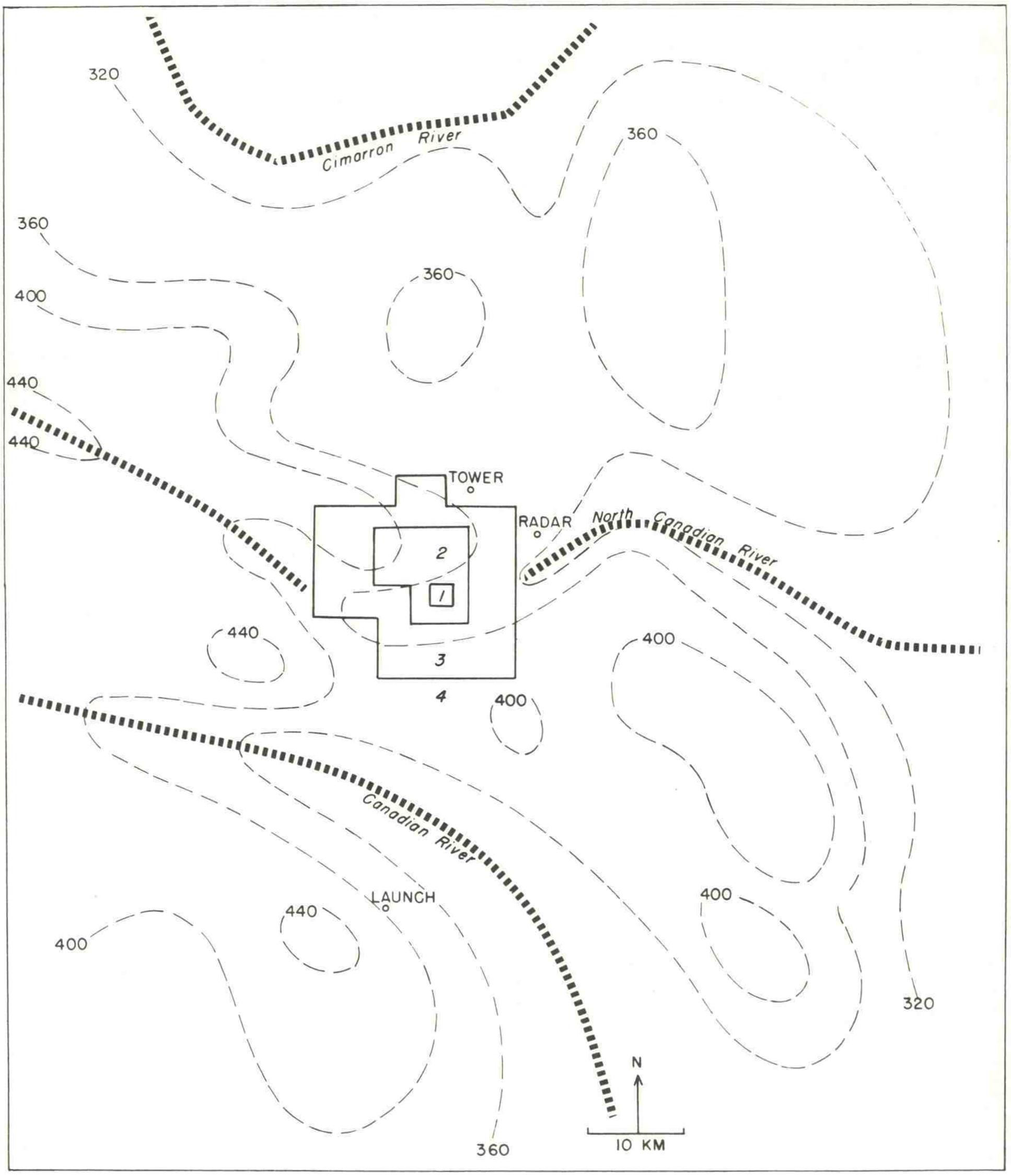

Figure 1. Map showing the radar, tower, the partitioning of the city according to building type (see text), and the terrain height in meters MSL (dashed lines).

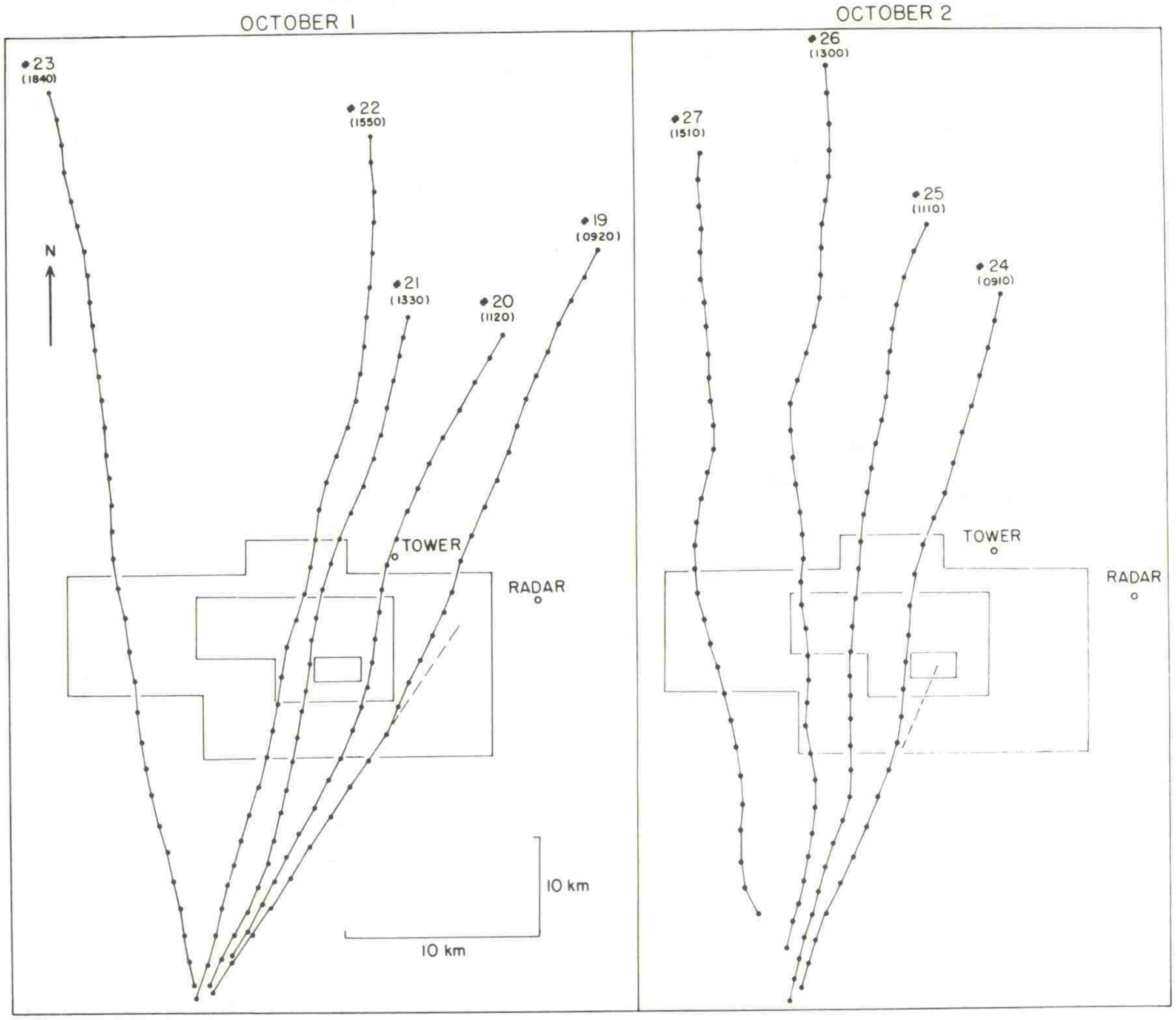

Figure 2. Sequential tetroon trajectories. The dots are tetroon positions at 3-min intervals; flight numbers and passage (LT) over city center are indicated at trajectory end. The E-W scale is double the N-S scale.

case. Between 1200 and 1500 CDT, the mean trajectory backing over the city amounted to only 3°, but the backing began farther upwind and extended farther downwind from the city than at the earlier times. Thus, in this case also the lateral trajectory displacement amounted to about 2 km. Note that in early afternoon, even in the mean, wave-shaped trajectory oscillations are set up by the city and appear to extend at least 50 km downwind. Between 1500 and 1800 CDT, the mean trajectory passing west of downtown turns eastward at a 5° angle downwind of the city, but there is no apparent upstream effect; however, this may be because the launch site was too close to the city. The impression that late in the day the city acts as an obstacle to the flow is confirmed in figure 4 by the mean trajectories for 1800 to 2100 CDT. The two outer trajectories are each the average of two trajectories, and under the relatively stable

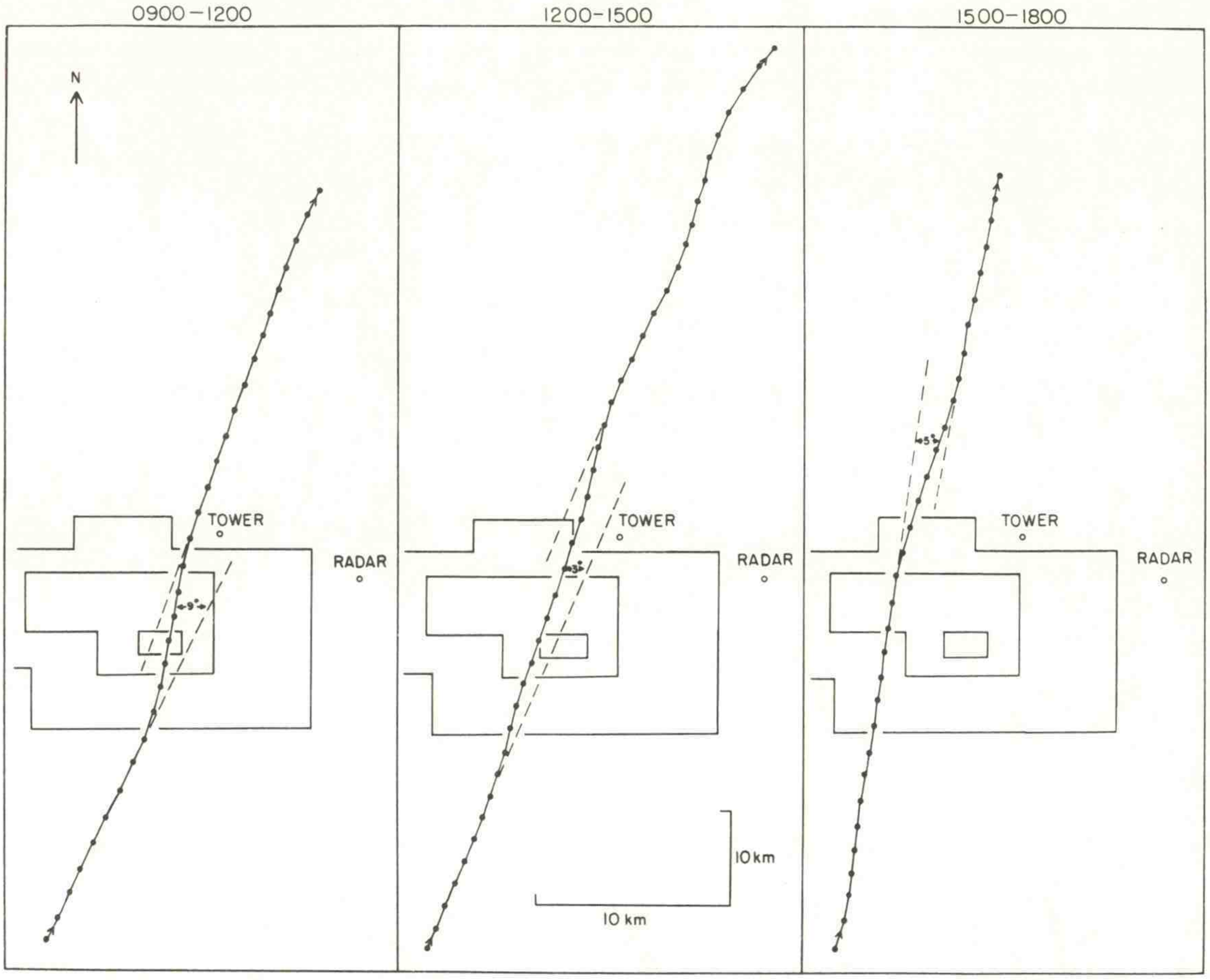

Figure 3. Mean tetroon trajectories across the city determined by averaging five flights each period. The dashed lines illustrate the mean lateral trajectory displacements caused by the city; the mean angular turning is also shown. The E-W scale is double the N-S scale.

conditions prevailing at this time, note that the air tends to bend around the city somewhat like the flow of water around a rock. The mean angular turnings are small, only about 4°, but an opposing lateral trajectory displacement of about 2 km occurred each side of the city, resulting in an overall lateral trajectory convergence in the lee of the city of about 4 km. Once again, simultaneous flights would be required to see if this lateral convergence was compensated for by an upward air motion or increase in wind speed.

The two individual trajectories in figure 4 crossed the center of the city at 1820 and 1950 CDT, respectively. The point of interest is that the city center induced a fairly pronounced wave-shaped oscillation at 1820, but there is no evidence of such an oscillation at 1950. Apparently, as

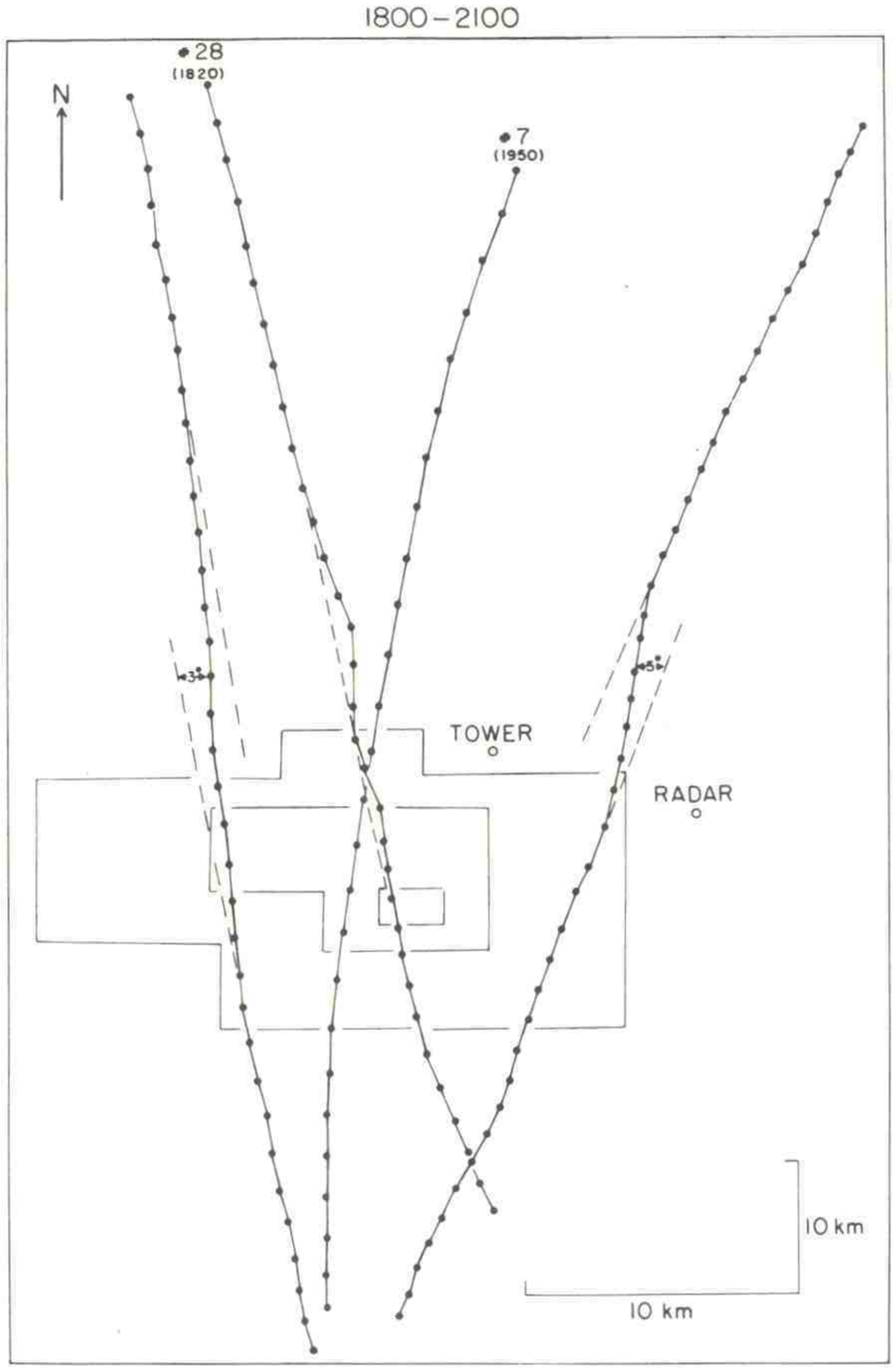

Figure 4. Tetroon trajectories across the city. The trajectories farthest west and east are each based on the average of two individual trajectories. Dots show tetroon positions at 3-min intervals.

the atmospheric stability increases, the effect the city has on the airflow at heights of 300 m becomes very small. This is consistent with the experience at Columbus, Ohio (Angell et al., 1971), where the influence of the city is mostly evident below 200 m.

Figure 5 shows the mean tetroon height traces for the five flights in each of four time periods, whose mean horizontal trajectories appear in figures 3 and 4. The heights have been averaged with respect to distance from the city's center. The city-induced upward air motion is a maximum in the late afternoon, but is also apparent during the morning, with respective mean upward motions of 0.7 and 0.3 m sec^{-1}. The point of maximum tetroon height moves farther downwind as the day progresses, but in general it is centered almost over the city. Because the restoring force acts to return the tetroon to its equilibrium (isopycnic) float surface, this result may be misleading. A computer program estimates the air parcel vertical motion from the tetroon vertical motion. This program will be run for all the Oklahoma City flights, but this has not yet been accomplished. Preliminary results indicate, as expected, that the actual air parcel vertical motion above the city is considerably larger than that indicated by the tetroons, and that in general the crest of the air parcel trajectory is several kilometers downwind of the city.

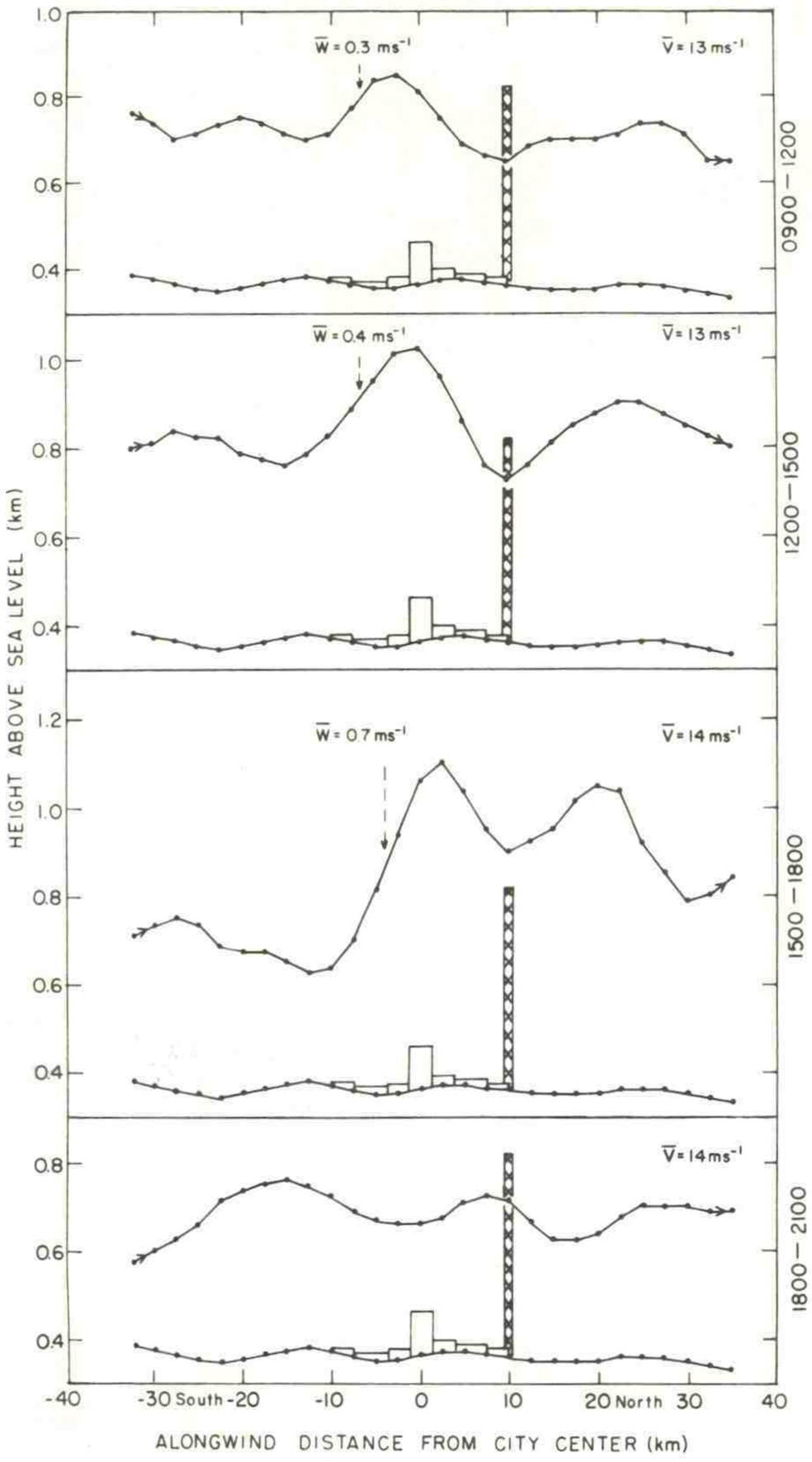

Figure 5. Mean tetroon height upwind and downwind of city center based on five flights each period (indicated by dots at 3-min intervals). Schematic representations of the tower and Oklahoma City buildings are shown. Mean tetroon speed is shown at the right, mean vertical velocity at center.

An interesting feature of figure 5 is that the TV tower appears to be very near the trough in the standing-wave pattern over the city, so that there should be relatively little mean vertical motion at the tower. In other words, by pure coincidence, for conditions prevailing during the experiment the tower was approximately one-half the standing-wavelength from the center of the city.

In the evening, the tetroons descended slightly over the city, the opposite of their daytime behavior. This may be because so little vertical air motion occurred in the evening that the tetroons basically followed their isopycnic float surface, which descended over the relatively warm city (heat island effect). During the day, the isopycnic surfaces may also dip over the city, but this effect on the tetroon height traces is completely masked by the strong vertical air motions occurring in daytime.

One purpose of the experiment was to compare the Reynolds stress measured from sequential horizontal and vertical velocities along the tetroon trajectories with the stress measured in the conventional manner on the TV tower. The tower data are not yet available so that comparisons are not now possible. However, it is of interest to see how the tetroon-derived stress over the city compares with that over the countryside. For this preliminary investigation, we assume that the first hour of tetroon flight in the southerly flow was basically over the city (after the first hour, the tetroons were near the tower) and that the second hour of flight was over the country.

Figure 6 shows the mean urban and rural tetroon-derived stress as a function of time. The urban stress is always greater than the rural stress, as would probably be anticipated. Furthermore, although the rural stress is a maximum in midafternoon, as might be expected because of the strong convection occurring then, the urban stress is a maximum (nearly 2.5 dynes cm^{-2}) in the morning. This shift in peak value to the morning is probably because the mean tetroon trajectory was directly over the downtown area (fig. 3). Thus, this implies that the city, particularly its center, induces an anomalously large downward transport of momentum.

An interesting point still to be investigated is the extent to which the standing-wave pattern associated with the city causes the relatively large downward transport of momentum over the city. This will be estimated from the cospectra of longitudinal and vertical velocity. This is of special interest because the momentum flux associated with the standing wave cannot show up in the momentum flux obtained at a fixed point, namely on the TV tower. Thus, the possibility exists that conventional tower estimates of momentum flux are seriously wrong in locations near cities or hills where standing-wave patterns are well established. Of course, aircraft measurements would yield representative flux estimates under such conditions.

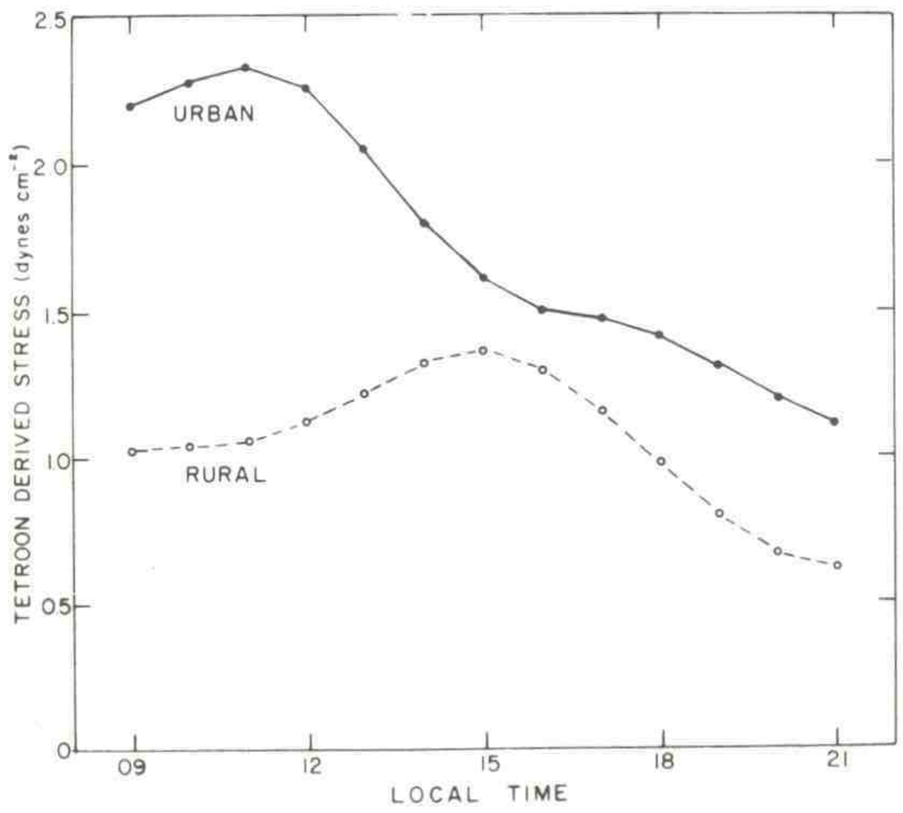

Figure 6. Tetroon-derived longitudinal Reynolds stress as a function of time for flights over the city (solid line) and over rural areas (dashed line).

1.4 Pibal - Radiosonde Measurements

This program consisted of three different phases. In Phase I, a line of five stations was set up, oriented with the prevailing wind from roughly 25 km upwind of the downtown area to 25 km downwind, passing through the downtown area and past the WKY tower. In Phase II, the five stations were situated in the four corners and at the center of a rectangle roughly 80 by 120 km, with the center station at Tinker Air Force Base just outside Oklahoma City. In this phase, radiosondes as well as pibals were taken. In Phase III, five theodolites were set up adjacent to the WKY tower; each balloon was tracked by all five theodolites, permitting evaluation of each sounding along 10 baselines of varying length and orientation, assessment of observer accuracy, and comparison of pibal-determined winds with those measured on the tower. In all three phases, we used only double-theodolite tracking. Baselines were, wherever possible, at least 750 m long, and the basic data period was 2 hr during which 20 balloons were tracked at each station. Each balloon was tracked for 10 min and reached a height of roughly 1.5 to 2.0 km. To permit tracking at this pace, two teams of observers were stationed at each site; the first team tracked the first balloon, and halfway through this sounding, the second team began tracking the second balloon, etc.

Phase I was from September 27 to October 1, the synoptic pattern was steady, and the wind blew directly along the line of stations. Data were collected during 11 different 2-hr periods on these 5 days, and because of the unchanging overall picture, these 11 periods may be combined into a single ensemble. Preliminary examination of the soundings indicates a far greater diurnal variation than had been expected, undoubtedly due in part to diurnal changes in geostrophic wind associated with the large-scale terrain slope (as described, for example, by Bonner and Paegle, 1970), but also very likely due in part to the thermal and roughness field associated with the urban area.

Phase III was on October 14 and 15. The weather was good, and data were collected during five 2-hr periods. Examination of these data has not started.

1.5 Fast-Response Wind and Temperature Fluctuation Measurements

1.5.1 Objective

The principal objective of this program was to estimate the momentum and heat flux, using the eddy correlation method, at sufficient height on the WKY tower to represent flow conditions above the surface layer in the planetary boundary layer. The estimates of the momentum flux in particular are to be compared with similar measurements derived from balloon and profile data gathered near the tower and from tetroon measurements. Considerable emphasis will be placed on the low-frequency fluctuation to find long-period oscillations in the measurements of the vertical

component of the wind, which may be induced by the dynamics of flow over the city.

1.5.2 Instrumentation

The selection of a sensor to measure the orthogonal components of the wind was determined by the following factors. First, measurements of the momentum flux were desired above 300 m; therefore, a fairly rugged system, requiring only periodic maintenance and calibration was needed. Second, nonuniformity of the local terrain and vegetation near the tower would make any measurements below 40 m suspect. In this height range, the long wavelength end of the inertial subrange is about 1/10 the height. Thus to measure the high frequency contribution to the momentum flux, we needed a sensor with a distance constant of less than 2 m. What is commonly referred to as a Gill propeller-type anemometer, described by Holmes et al. (1964), meets these general requirements. Wind tunnel tests reported by Camp et al. (1970) show the distance constant is dependent upon the angle of attack with a maximum value of 1.2 m at longitudinal directions that decreases to about 0.4 m at transverse flow directions.

Three individual propeller units (Young, Model Number 27100) were assembled to form an orthogonal array by constructing a central mounting block (fig. 7). The aluminum block was 10 cm in diameter and 5 cm thick. The arm support holes were precision drilled to guarantee the angle between the respective propeller shafts of 90° $\pm$ 0.1°, the accuracy suggested by Kaimal and Haugen (1969) for accurately determining the momentum flux. At the risk of adding slightly to the distance constant, a shaft extender was used on the vertical pointing propeller to unify the response in transverse flow conditions. The propeller shaft connects to a small generator (53 mV m^{-1} sec^{-1}), and signal wires transmit the voltages to the base of the tower. Two such arrays were constructed.

Obtaining a level array to the accuracy ($\pm$ 0.1°) suggested by Kaimal and Haugen (1969) at 300 m above ground presented a much bigger problem. Following the procedures suggested by Dunbar (private communication) a sensitive electronic level monitor was constructed. The sensors (Hamlin, Model Number 106), variable resistance type bubble levels (fig. 7), were mounted on the aluminum mounting block parallel to the axis of the horizontal propeller shafts. The position accuracy of the electronic level sensors was checked and found to represent the horizontal plane defined by the propeller shafts within the limits specified above. An a-c bridge circuit was constructed to measure the resistance of the level indicators. The bridge circuit was "portable," and the level indicators were useful in positioning the array after calibrations. Sufficient signal wires were available to allow monitoring of the level sensors from the base of the tower at the beginning and end of each run.

A sensitive thermometer, consisting of a five-junction thermopile (No. 40 copper/constantan), was constructed to measure temperature fluctuations to allow us to estimate the heat flux. Both the sensing junction

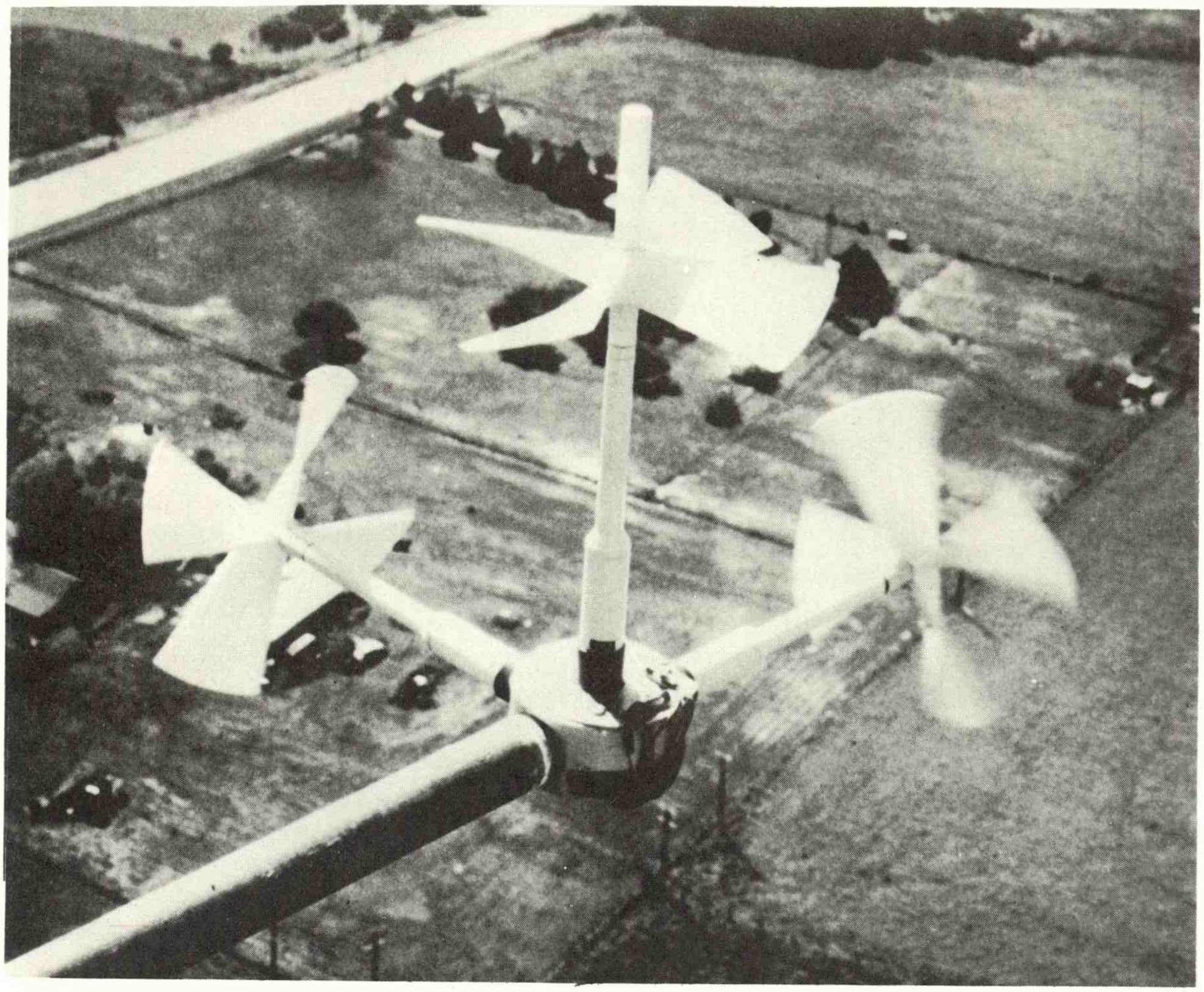

Figure 7. The orothogonal propeller anemometer used in the study. The shaft extender is clearly visible atop the vertical pointing anemometer and the bubble levels are to the right at the base of that component.

and the reference junction were mounted in an aspirated radiation shield (Climat, Model Number 061-1) similar to that used to shield the temperature gradient measuring system. The reference junction was enclosed in an epoxy mass to lengthen its time constant to agree with that of the gradient sensor. Tests showed that when mounted in the aspirator, the sensor junction had a time constant of about 1 sec (1/e time), and the reference junction was about 70 sec. Airflow in the shield was computed to be 3 m sec^{-1}.

1.5.3 Exposure

As discussed in a preceding section, one of the important objectives of this study was to measure the effect of a city on a relatively uniform

flow. Thus, on the WKY tower, located NNE of downtown Oklahoma City, the primary measurements (wind and temperature) were taken from the SW side. The support for the orthogonal wind system was constructed to extend from the tower arms used to mount the profile system, as shown in figure 8. In this position, the center of the array extended 4.2 m from the face of the tower and had its major axis pointing in a 240° ± 2° direction. Thus, winds blowing down the center of the orthogonal wind system blow from 195°. Throughout the measurement program, wind and temperature fluctuation sensors were 354 m above ground. The aerovane was removed to avoid any possibility of interference. The second system was 158 m above ground throughout most of the test; temperature fluctuations were not measured at the lower level.

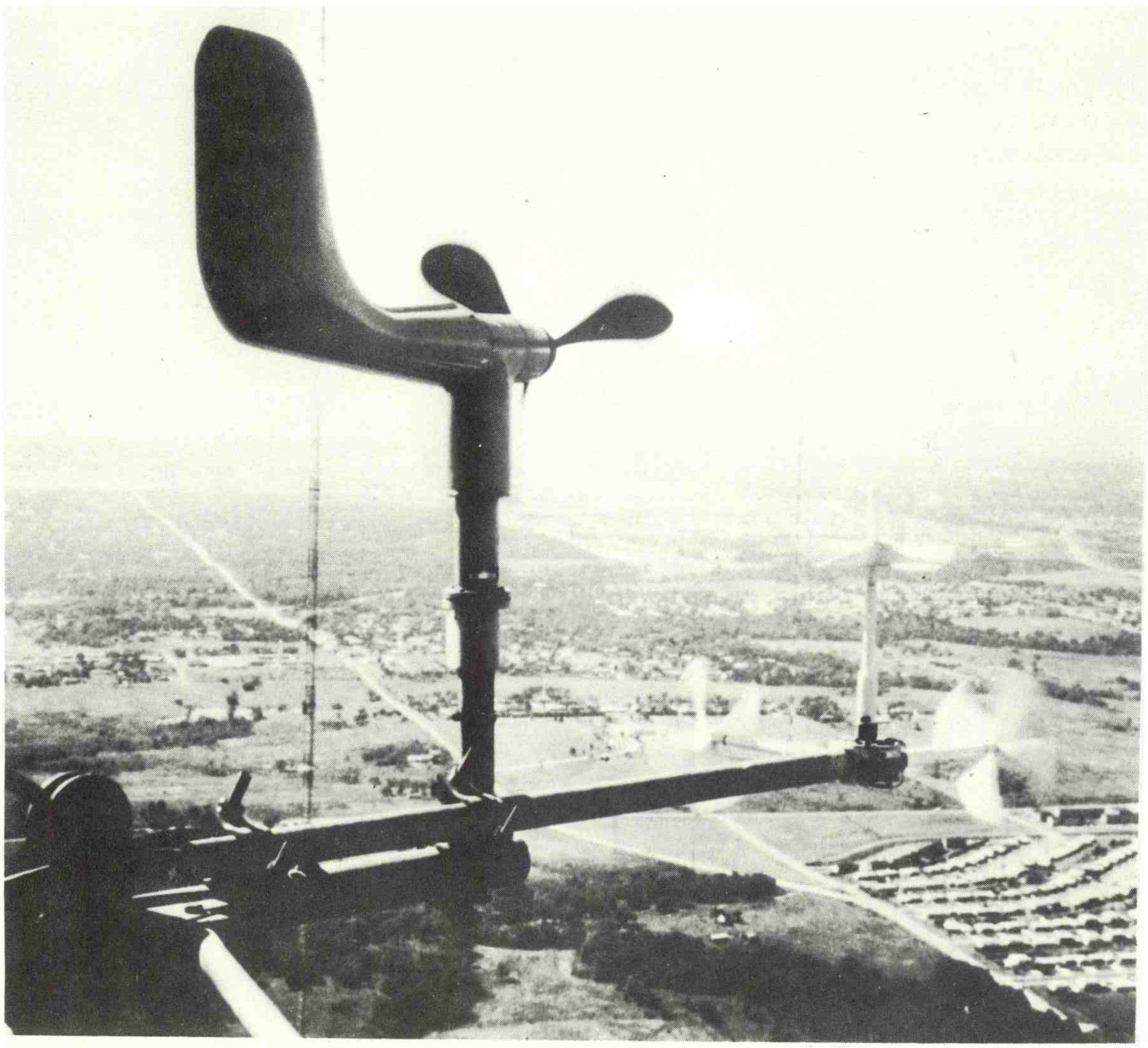

Figure 8. The orthogonal propeller anemometer in the extended position. At this time the propeller anemometer and the aerovane were being compared, normally the aerovane was removed to avoid interference.

The two primary factors that influence the accuracy of the wind component measurements, deviation from a cosine response and flow interference caused by the tower, are wind direction dependent. Maximum accuracy was obtained when the wind direction was 195° ± 40°, or within 5° of being transverse to one of the horizontal sensors. According to Gill et al. (1967), the effect the tower has on the measurements is less than 2 percent in this direction sector, if we assume the anemometer extends 3 m from the tower. This approximately true since a tower is about 3.1 m on a side and the anemometer extends 4.2 m. Tower effects do not exceed 5 percent until wind direction fluctuations exceed 195° ± 80°. Winds from 310° through north to 80° cannot be analyzed due to tower interference. The calibration error caused by a deviation from a cosine response at transverse attack angles, when the propeller is changing direction of rotation, can be minimized when a data run can be subdivided into periods when the flow is longitudinal and when it is transverse. Such subdivisions were generally possible in the stronger wind conditions; major problems were encountered though when winds were light and variable. Although an analytic expression for the calibration has been proposed by Drinkrow (1972), it was not used; rather, a table of values based on figure 3 from Holmes, et al. (1964) was used to correct for deviations from a cosine response.

1.5.4 Signal Conditioning, Recording, and Calibrating

All signals were transmitted to ground level by shielded cables; nonetheless, a considerable amount of high frequency noise was acquired. A simple first-order filter, with cut-off frequency of 13 Hz, limited the noise on all six anemometer signals. The gain of the amplifier and the input bias were changed from one run to the next in order to maintain an optimum signal level at the input to the recorder. All signals, including a zero level and bias voltage, were recorded in FM mode on a 14-track analog magnetic tape recorder. The six wind channels were also monitored on a multichannel stripchart recorder.

A voltage calibration, zero and ± 200 mV, was performed on each amplifier at the beginning and end of each run in order to document gain and bias settings. At four times during the tests, a calibration signal was applied from the anemometer using a constant speed (1800 rpm) motor to spin the anemometer shafts; propellers were removed during this process. The range in the values from each anemometer was less than 1/2 percent of the calibration value. Thus a single set of calibration voltages was used for all of the records.

The sensors operated from September 24 through October 12, 1971, and recorded 77 hours of data, the mean wind direction was between 160 and 220° for 47 hr of this period. Of the remaining 30 hr of data, approximately one-half are not useful because directions were more northerly and tower influences will not be negligible. All tapes were digitized at the NRTS computer facility. The digitizing rate was 10 observations/sec, and the resolution is ± 1 part in 8192. The data will be subdivided into

20-min blocks for editing and computing of basic statistics — the mean, variance, skewness, and kurtosis. The spectra and cospectra will be computed for longer periods, in most cases 60 to 100 min long.

1.6 Mesoscale Windfield and Transport Analysis

The network of wind stations used in this experiment was set up specifically for this study. Except for the NRTS mesonetwork, it was ARL's first attempt to establish a mesoscale network of wind observations for a field experiment. The wind observations obtained for the Los Angeles experiment (see NOAA Tech. Memo. ERL ARL-32, 1971) were obtained from stations previously established for other purposes; this caused some of the data to be of questionable value because of sensor height and location.

Since the area surrounding Oklahoma City is moderately populated, it was possible to mount the wind sensors approximately 30 m high on existing towers. Figure 9 shows the positions of the eight wind stations in the 90 x 130 km area centered on the WKY tower. Wind data were also extracted at 44, 266, and 444 m for use in the analyses. The configuration of the network provided optimum coverage of south-to-north tetroon flights.

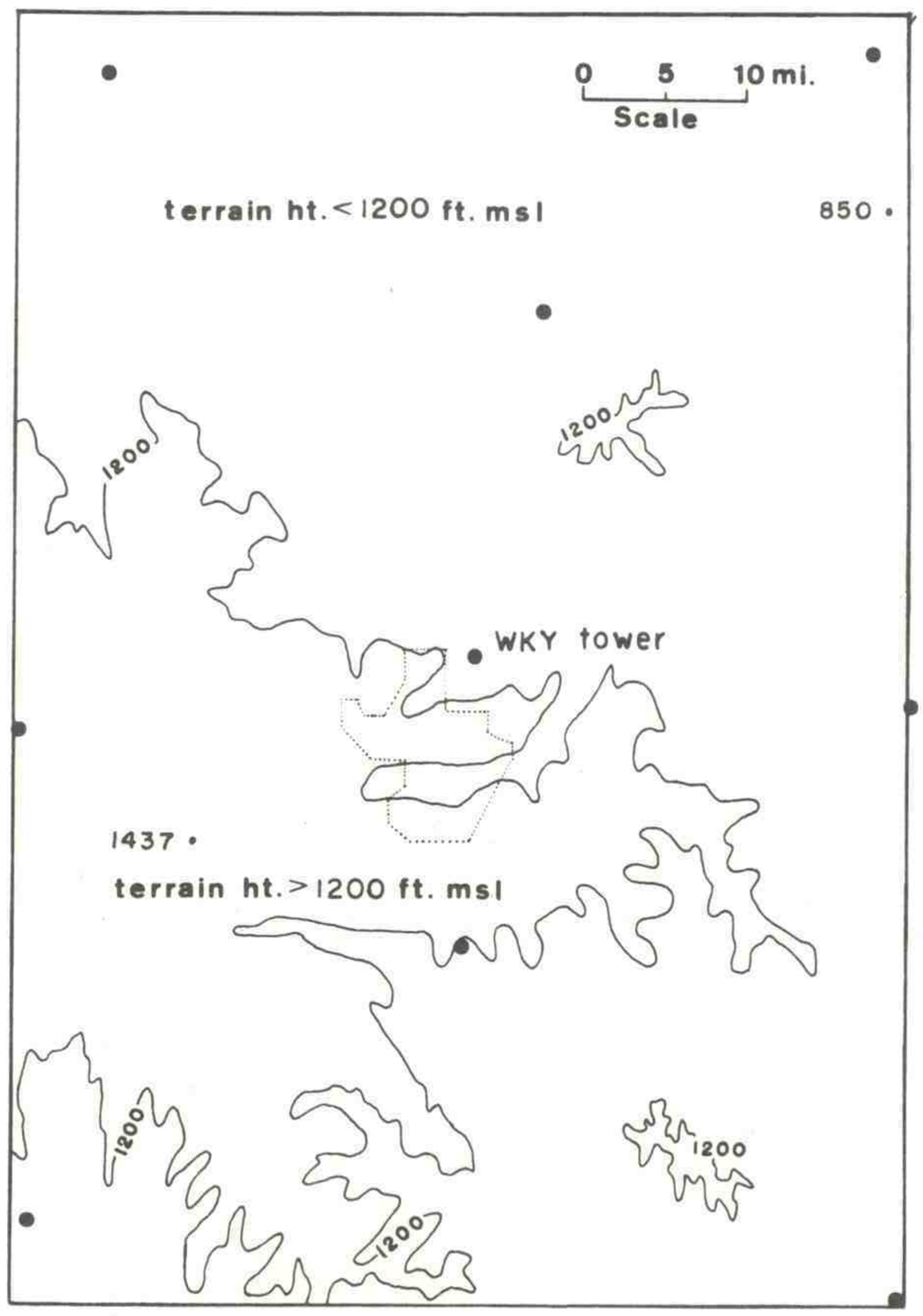

Figure 9. Wind station network configuration for Oklahoma study. Flat topography is indicated by the 1200-ft contour.

The local topography provided an interesting contrast to the terrain characteristics of the upper Snake River Plain. The height difference between the highest point on the grid (about 440 m) to the lowest point (about 260 m) is about 180 m in a distance of about 90 km. This represents an average slope of about 2×10^{-3}, or about 1/5 of the slope over the NRTS mesonetwork, and would indicate a more gently varying terrain. On a scale of less than a kilometer, however, the Oklahoma terrain may vary by over 30 m in a distance of 400 m, which is considerably rougher than the NRTS terrain. The most noticeable terrain feature within the boundaries of the grid is the protrusion of the slightly higher ground from the west. Oklahoma City is on a peninsula of this slightly higher ground with the terrain sloping downward and away from the city to the north, east, and south.

The wind data set from the mesonetwork was from September 21 through October 12, 1971. The wind speed and direction on the strip charts were averaged over 20-min periods and recorded on punch cards for editing and transfer to disc storage.

Windfield plots every 3 hr, similar to those for the NRTS network, were produced and examined. There were no wind patterns that could be recognized systematically with mesoscale features observed in the data set. Under the conditions of a very weak synoptic-scale pressure gradient, there seemed to be a slight influence of the higher ground to the west, as indicated by the nighttime westerly winds. This phenomenon would probably occur more during July and August when daytime heating is greater.

The most severe horizontal variations in the windfields of this data set seem to be associated with the fronts passing through the area. An example of this is shown in figure 10. For 6 days previous to this series, the windfields showed southerly flow with very little horizontal variation. Shortly after 0400 CDT October 2, a weak front passed the northwest corner of the grid and proceeded southeastward causing the spatial variation shown in the series of plots. This frontal system was accompanied by a considerable amount of thundershower activity, which would account for much of the horizontal variation. By 0700 October 3, the front was 80 km southeast of Oklahoma City and the windfield pattern is once again quite uniform, but with winds from the north.

The overall conclusion one might draw from the windfield plots of this data set is that the primary influences on the flow through the grid were the synoptic-scale pressure patterns and frontal systems. Figure 11 shows an interesting circulation pattern, of a larger scale than the grid, passing through the area on October 11. A frontal system oriented east-west through southern Kansas moved slowly toward the area during the period but did not pass through, while the flow through the area rotated through 360°.

The transport of hypothetical particles from the WKY tower for the 22-day period of the experiment is depicted with the same type of trajectory plots that were produced for the NRTS (Wendell, 1970). The high

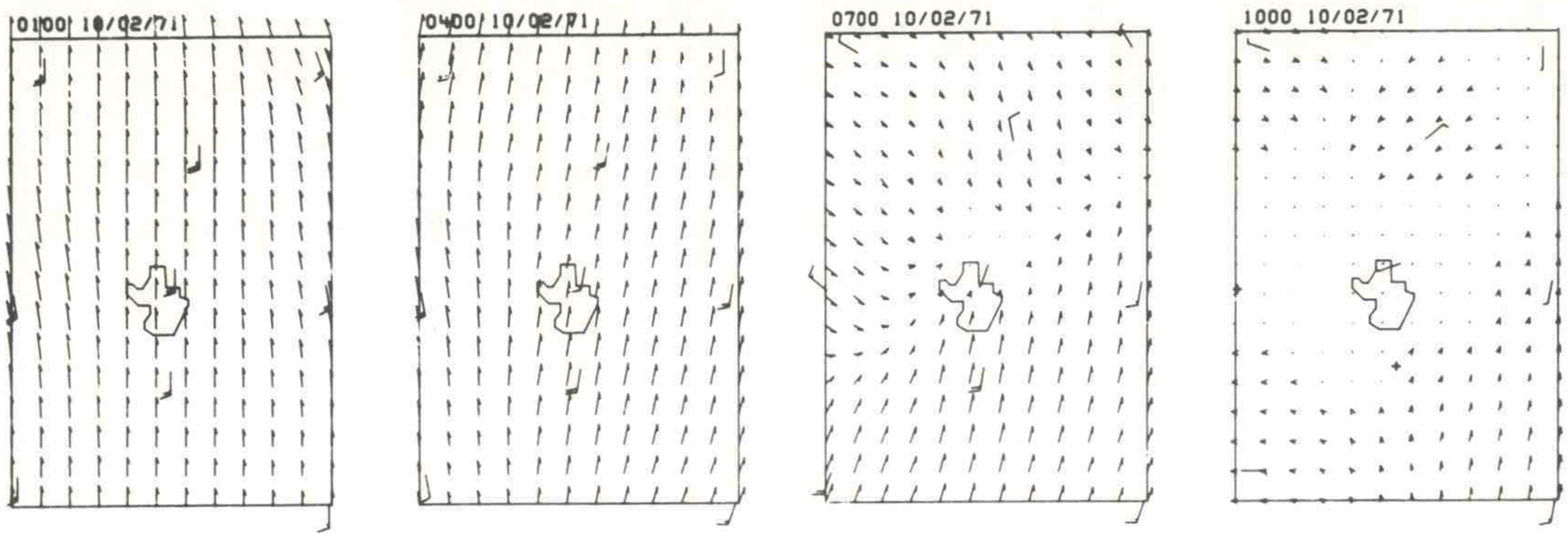

Figure 10. Windfields as a front left the Oklahoma mesonetwork. Grid spacing for the random-to-grid interpolution is 8 km. Wind vector scaling is 11 m sec^{-1} per grid unit.

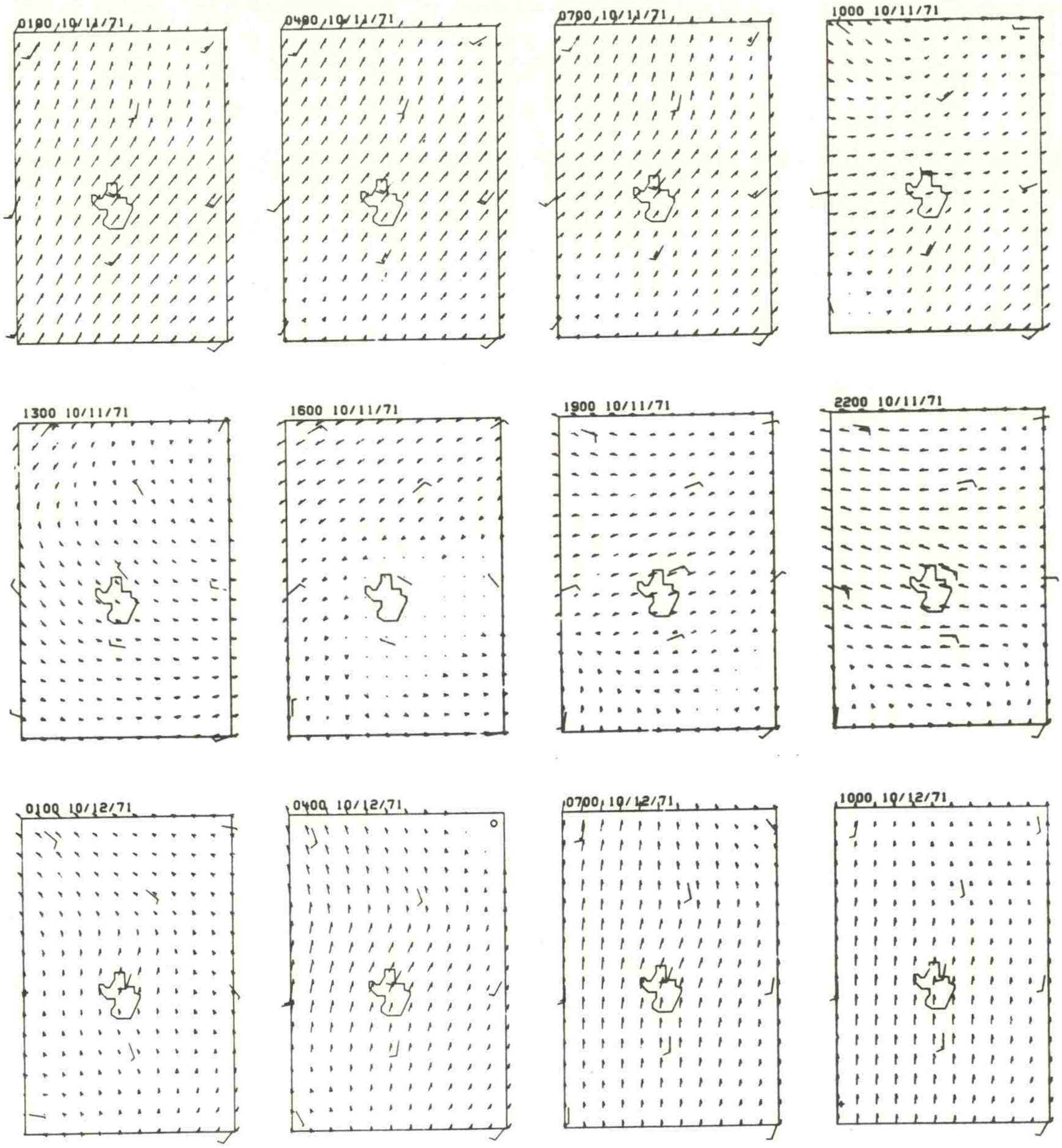

Figure 11. Windfields showing almost a complete rotation. See figure 10 for other details.

percentage of southerly flow is indicated by the fact that 18 out of 42 plots had all 12 trajectories exit the northern boundary. A 4-day period that this occurred is shown in figure 12. A close examination of these plots reveals a persistent phenomenon. For the daytime releases, beginning at 0800 CDT, the trajectories of the particles released at 1-hr intervals shift toward the west, but for the night releases the trajectories shift toward the east. This behavior was observed for all the 18 cases of sustained southerly flow. It would seem to be related to the diurnal oscillation in the southerly flow observed in long-term averages by Bonner

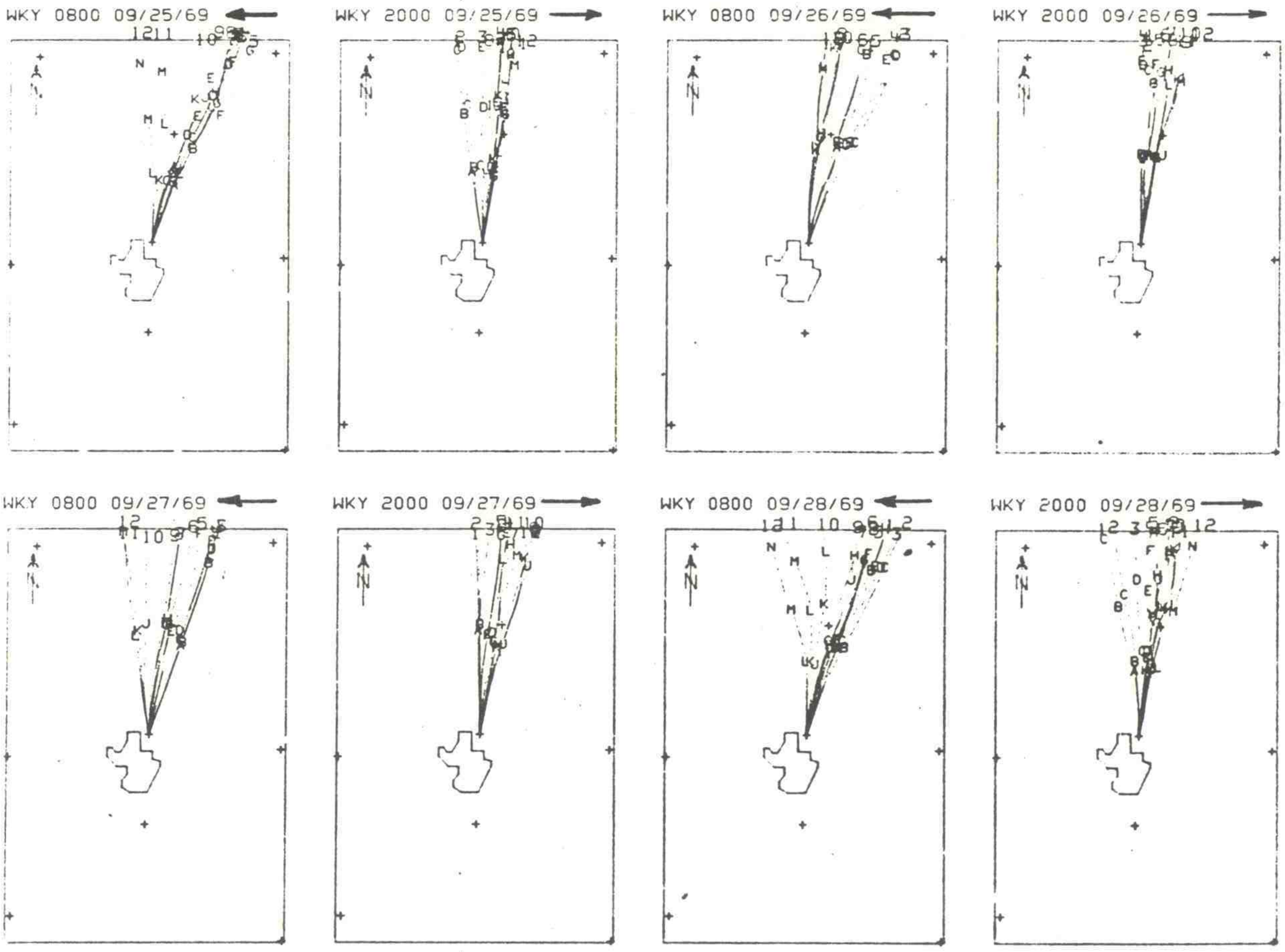

Figure 12. Trajectory plots at 1-hr intervals showing the paths of hypothetical particles advected with 20-min averaged windfield data. Each plot contains 12 particle trajectories with the release time for the first particle shown at the top of the plot. The arrow at the top of each plot indicates the general direction of the wind change shown by the trajectories.

and Paegle (1970). They attributed the oscillation to the alternate heating and cooling of the sloped terrain. A reexamination of the windfield plots indicates that the phase of the oscillation agrees well with their observations.

An oscillation of this type would have important implications in both accidental and routine releases of an effluent. For the emergency situation, the ability to anticipate a 15 to 30° turning of the wind would be important. Under a sustained and controlled effluent release, the relationship of the oscillation to the diurnal variation in stability would be helpful in determining the area that would receive the highest long-term dose.

Of the remaining 24 trajectory plots, three indicated sustained easterly flow, seven sustained northerly flow, four sustained westerly flow, and 10 a dispersion over a significant portion of the grid. In these 10 sets only five contained evidence of the spreading being caused by curved streamlines. This observation is confirmed by the differences shown in comparing the windfield trajectories with those produced by the source wind only.

Trajectory plots for the same data set were produced using the WKY wind as if it applied over the whole grid. The results of a comparison of the areas covered by the two sets of plots are shown in table 1. Examples of these comparisons are shown in figure 13. The first two show poor agreement in terms of area covered. The third comparison (0800 CDT, October 11, 1971) agrees well in spite of the large spread in the trajectories. This release period corresponds to the occurrence of the rotating windfield discussed above (fig. 11). An interesting feature in this situation is that a seemingly significant amount of spatial variation occurred caused by curved streamlines from 1000 CDT on the 11th to 0700 CDT on the 12th, but it is lateral to the direction of transport and causes little discrepancy in the single-station trajectories. The last

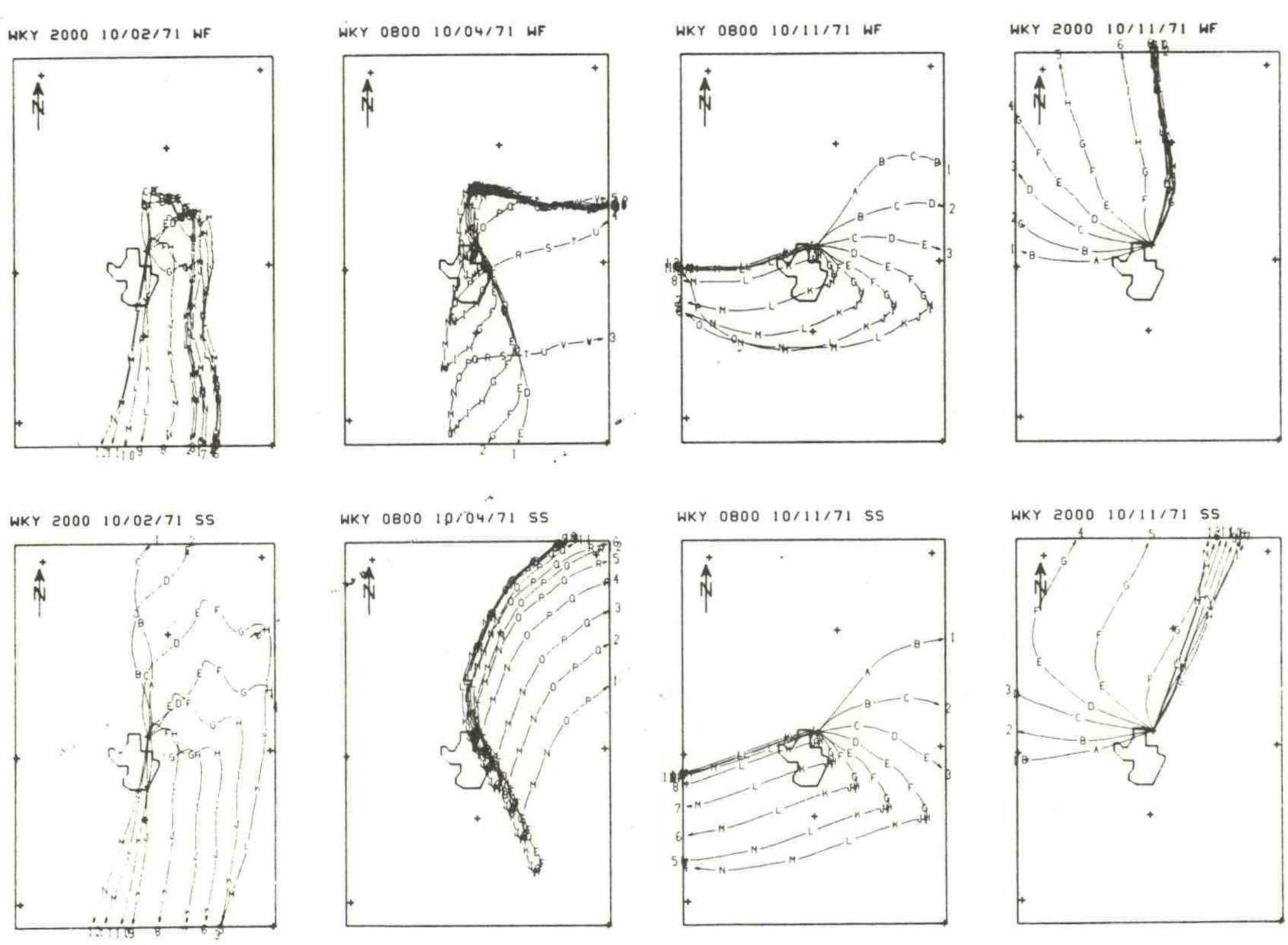

Figure 13. Windfield (WF) - single station (SS) comparisons. See fig. 12 for other details.

Table 1. Comparison of Area Covered by Windfield and Single Station Trajectories

Area Agreement	Number of Cases	Percent of Total
Good (90% to 95% mutually covered)	27	64
Fair (70% mutually covered)	9	22
Poor (<70% mutually covered)	6	14

comparison in figure 13 is a continuation of the October 11 release. If we consider area coverage alone, there is fair agreement in the plots, but individually, the last nine of the 12 trajectories show significant differences.

To compare trajectories of individual particles computed with windfield and single-station data, we calculated separation distances and stored them according to distance traveled by the particle in the windfield. Some statistical results of these comparisons are shown in table 2. The number of particles on the grid is strongly dependent on the grid geometry. The distances from the source to the boundaries are about 43 km east and west, 65 km to the north and south, and about 77 km to the grid corners. There is a distinctive drop in the number of particles available for comparison as each of these distances is exceeded, indicating a high percentage of relatively straight trajectories. The separation statistics of table 2 indicate that, for the period of this data sample, inside a 32-km radius a particle being advected by the source wind would be within 8 km of its position in the windfield for at least 70 to 80 percent of the time. At a distance of 48 km, with about 89 percent of the particles still on the grid, the average separation is 14 km and growing rapidly. This would cause serious problems only for unexpected short releases of material. The favorable area comparisons would show single-station transport to be a reasonable approximation for long-term controlled releases.

Even though it was not their primary purpose, the tetroons flown through the grid provided a valuable source of information on the flow above the tower network. There were 54 flights that were compared with simultaneous windfield trajectories. The average heights of these flights varied as follows: 24 flights at or below 300 m (above the ground), 25 flights above 300 m, and five flights above 610 m. The average height for all the flights was 380 m above the ground. A trajectory plot was produced for each tetroon flight including also the trajectory of a hypothetical particle carried by the windfield. Information was printed at 15-min intervals on the positions, separation, speed, and direction of the tetroon and particle. Figure 14 shows examples of these plots. The primary

Table 2. Statistics on Separation of Particles Advected by the Windfield and Particle Movement by the Source Wind Only.

*D_{WF} (km)	N_P	S_{mean} (km)	σ_s (km)	S_{min} (km)	S_{max} (km)	Percent of Particles in Four Separation Categories			
						8	8-24	24-40	40 km
0800 to 1900 CDT									
16	126	1.6	2.6	21.6	0.0	96.8	3.2	0.0	0.0
32	126	7.4	10.6	66.4	0.5	78.6	14.3	4.0	3.2
48	112	14.8	18.7	98.0	1.8	41.1	50.0	1.8	7.1
64	75	22.7	23.5	121.0	3.7	13.3	58.7	20.0	8.0
80	17	44.5	30.2	117.0	9.7	0.0	35.3	17.6	47.1
96	13	60.8	28.4	114.0	17.4	0.0	7.7	23.1	69.2
2000 to 0700 CDT									
16	120	1.4	1.3	5.7	0.2	100.0	0.0	0.0	0.0
32	120	8.0	9.9	61.2	0.2	68.3	26.7	2.5	2.5
48	111	14.0	15.3	91.9	0.3	47.7	35.1	2.6	4.5
64	53	28.6	20.8	78.6	1.6	22.6	24.5	26.4	26.4
80	8	49.1	19.0	90.0	21.3	0.0	13.5	35.0	62.5
96	6	37.4	16.2	57.4	17.9	0.0	33.3	16.7	50.0

*D_{WF} - distance traveled by windfield advected particles.

N_P - number of windfield particles still on grid.

S - particle separation.

transport factors are wind speed and direction shear with height. Since the tetroons were generally well above the level of the network sensors, the average speed of the tetroons was always greater than the average speed of the particle. A logarithmic extrapolation of the average speed of the particle in the windfield to the average tetroon height was within $\pm$ 15 percent of the average tetroon velocity in 47 percent of the cases. The errors in the extrapolation seemed to be fairly evenly distributed on the high and low side, providing no reason to bias the extrapolation for better accuracy. Thus, this series of primarily daytime tetroon flights indicates that a logarithmic extrapolation of the 30-m wind speed in the network to the height of interest should generally provide a reasonable estimate of the transport speed in the lowest 610 m.

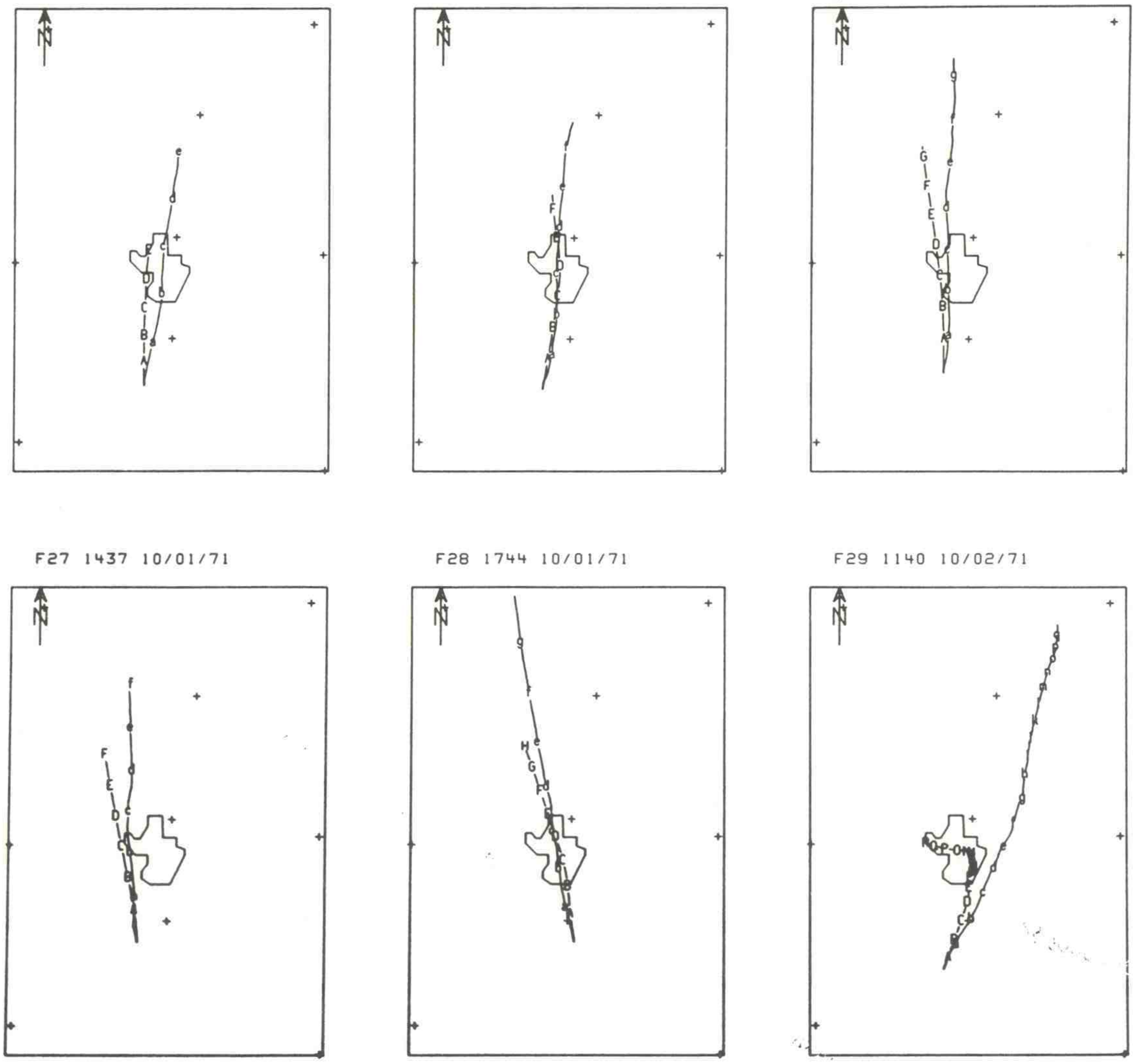

Figure 14. Tetroon (lower case) and windfield trajectory comparisons at 15-min intervals. Release times shown at the top of the plots.

For transport, a more important consideration than speed shear is direction shear. Varying amounts of direction shear were observed in the trajectory comparisons. For the 50 applicable cases, the breakdown on the average direction difference between the tetroon trajectory and the windfield generated trajectory is shown in table 3. These results verify, in a general sense, the basic physical principle that surface friction will cause cross-isobaric flow in the lower levels when the wind turns to the right with increasing height. In a southerly wind, almost 70 percent of the flights show an average of an 8° shift to the right. There seemed to be no significant correlation of the amount of shear with average

Table 3. Average Direction of Tetroon Trajectory with Respect to Windfield Trajectory.

Wind Direction	Left	Centered	Right	Total
Southerly	1* (5)**	11	23 (8)	35
Northerly	2 (10)	3	5(12)	10
Westerly	2 (12)	2	0	4
Easterly		1		1
Total	5 (10)	17	28 (9)	50

* number of cases

** average number of desgrees deviation to the left or right of the windfield trajectory

tetroon height, but for the southerly flow the variation around the average was only 10°. The maximum shear encountered in the 50 cases was 20°. These results would indicate that at least during the fall between sunrise and sunset the flow in the lowest 600 m can be reasonably well approximated by applying a logarithmic extrapolation from the 30 m speed and a correction of 10° to the right for heights above about 200 m.

Factors such as frontal systems, strong inversions, and topographic features will complicate the vertical structure of the flow (flight 29 in fig. 14). There were no tetroon flights at night to compare with windfield trajectories during inversion conditions; however, it is possible to investigate the vertical shear of the horizontal wind by using the wind data at the 266 and 444 m levels on the WKY tower.

To check the consistency of the wind data from the WKY tower with the wind data from the tetroons, we compared the speed and direction of all tetroons that passed within a 16-km radius of the tower with tower wind speed and direction interpolated to the tetroon height at its closest position to the tower (table 4). The minor bias toward a negative difference in the directions should not be considered serious because the directions from the tower data are 20-min average values read to the nearest 10°. For some reason, the anemometers on the tower generally report the speed slower than is indicated by the tetroon. The average difference is about 34 percent of the average speed differences shown between the tetroon trajectories and the windfield trajectories. This same type of speed difference has been found between the tower winds and those determined by pilot balloon. An investigation for a satisfactory explanation of this problem is still underway.

Table 4. Comparison of Tower Winds and Tetroon-Derived Winds. The values shown are obtained by subtracting tetroon data from tower data. Wind direction is the direction from which the wind was blowing.

Type of Difference	Number of Cases	Mean Direction Difference (°)	Number of Cases	Mean Speed Difference (m sec^{-1})
Positive	17	6	5	1.8
Negative	26	-7.4	35	-1.8
None	0	0	3	0
Total	43	-2	43	-1.2

In anticipation of an analysis of the vertical wind shear and the vertical oscillations exhibited by the tetroons, we developed a method of presenting the history of the temperature profile measured on the WKY tower. The 20-min averaged values of these temperature profiles were plotted on microfilm — three to a graph — with a time interval of 2 hr. The last profile on one plot was used as the first profile on the next; this allows the heating or cooling during a 2-hr interval to be examined continuously. Six plots were required to cover 1 day, and 2 days can be shown on one page. The history of the temperature profile on the WKY tower was plotted for September 27, 1971, through October 12, 1971. Examples are shown in figure 15.

Two contrasting histories have been selected for demonstration. The first series is for a day (September 28) that has been preceded by 2 days of southerly flow bringing warm moist air from the Gulf of Mexico. Clouds during the night prevented the formation of an inversion by radiative cooling and very little heating was required to bring about neutral stability by 1000 CDT. The second series is for a day that was preceded by 2 days of northerly flow, behind a passing cold front, bringing cold dry air from the midwest. Here a strong inversion is developing during the early morning; it is then strengthened by warming above 200 m between 0400 and 0800 CDT. The stability condition during this time contrasts sharply with that on September 28. The rapid heating of the lowest 200 m and cooling of the upper 300 m between 0800 and 1200 CDT on October 11 suggests turbulent heat transfer between these layers in addition to the normal heating for this period. This might be related to the breakup of a low-level jet, which was observed in the tower winds and is somewhat substantiated by some sporadic vertical oscillations in a tetroon trajectory between 0930 and 1000 CDT. The oscillations had an amplitude of 100 m and a period of

(a) 09/28/71

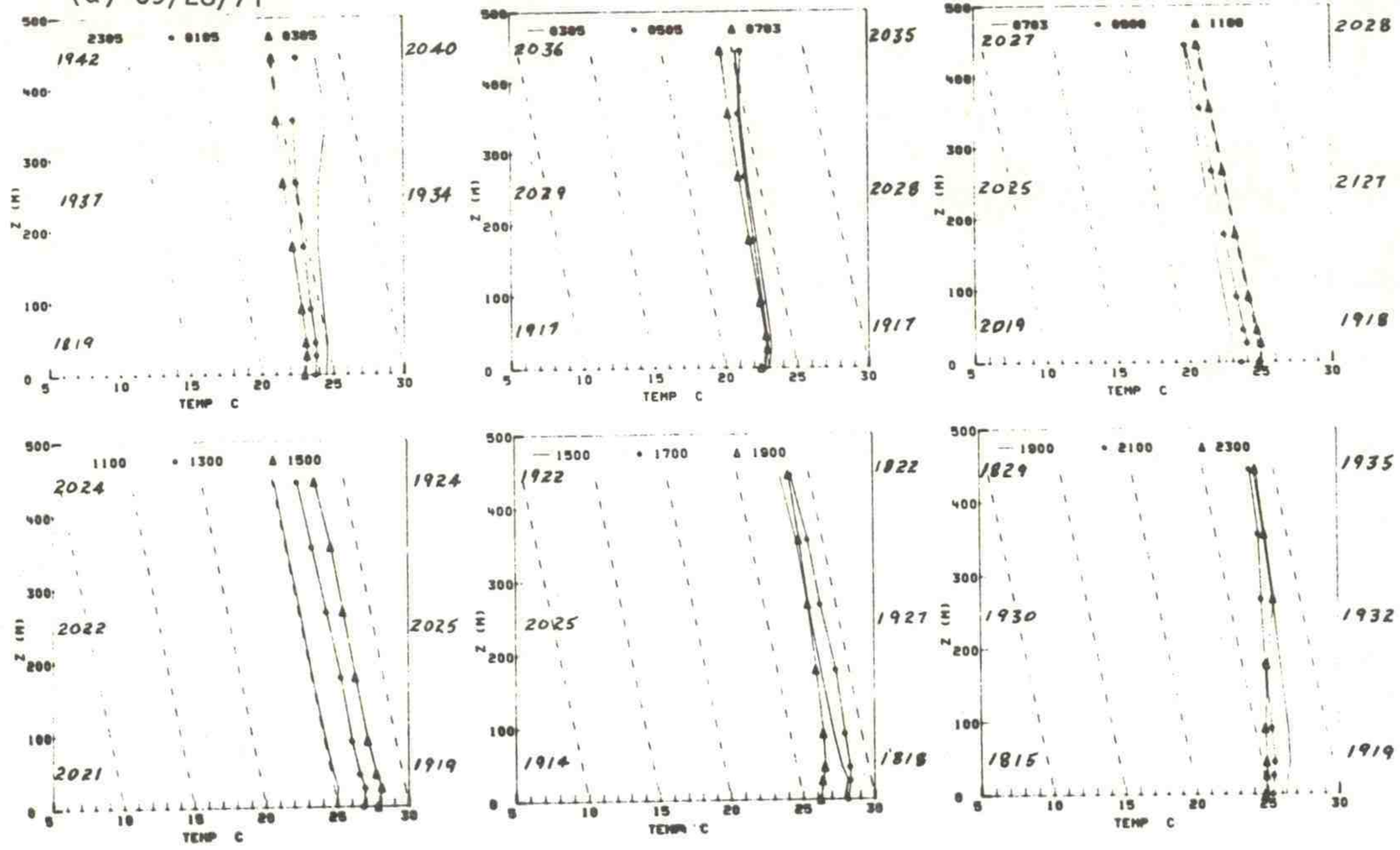

(b) 10/11/71

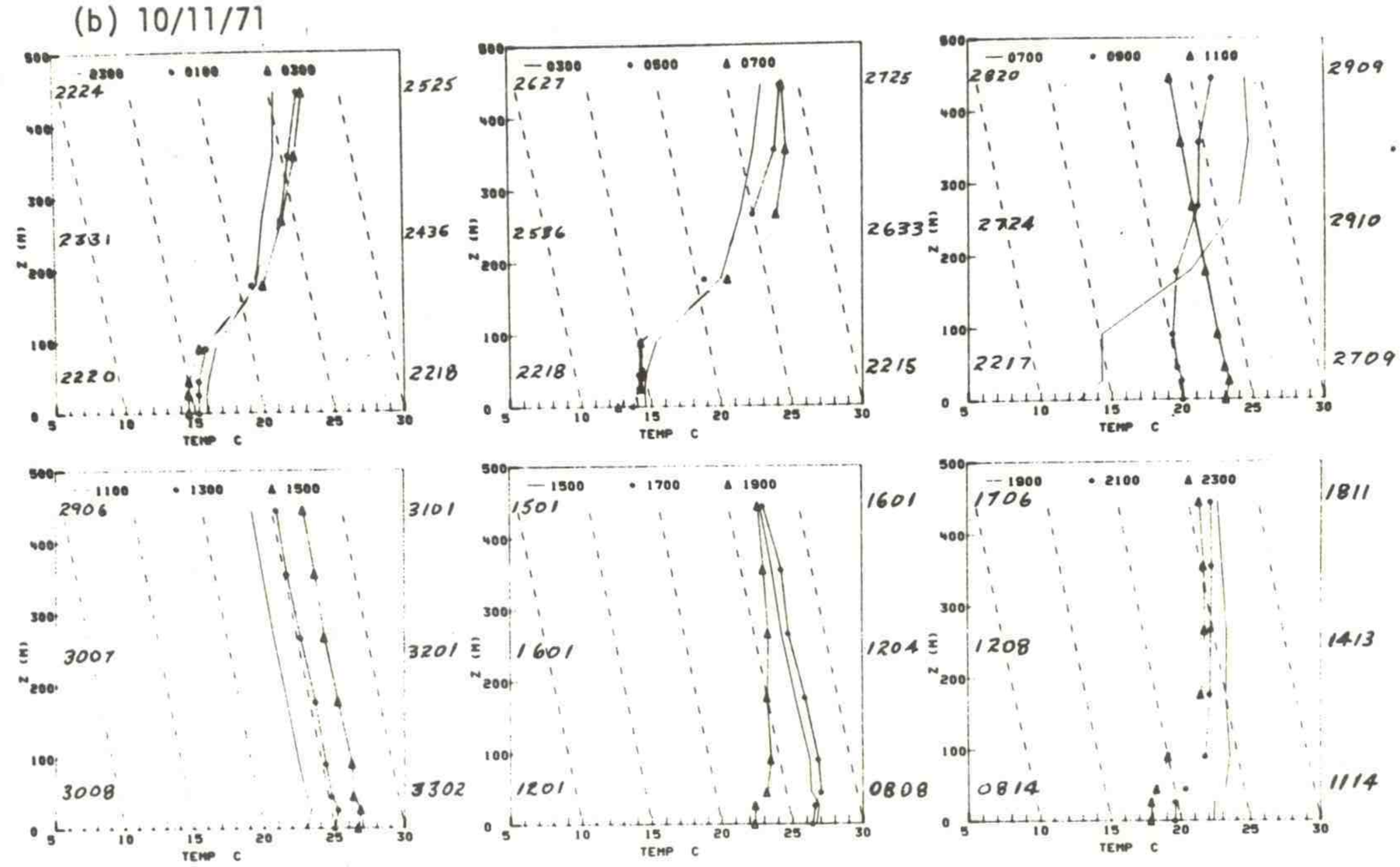

Figure 15. Temperature profile plots from the WKY tower in Oklahoma City. The identifying symbols and times are at the top of each graph. The slanted dashed lines are the dry adiabatic lapse rate. Wind direction and speed at three levels are shown for the second and third profiles of each plot. The first two digits are wind direction in tens of degrees and the last, wind speed in miles per hour.

about 7 min, which is greater than expected for the thermal stability that existed at the time.

In summarizing the results of the preliminary analysis of the data from the Oklahoma experiment, we must emphasize that the 3-week sample in the fall would probably not represent conditions in the extremes of winter or summer; however, the sample probably represents about 6 to 7 months of the year. The terrain could also be considered to be fairly representative of a large area of the central United States but not of the western and eastern portions of the country. The terrain appears to have a much less pronounced influence on the mesoscale flow patterns here than is observed at the NRTS. This suggests average transport might be reasonably well estimated from the source wind only. Trajectory pattern comparisons for both types of advection show the single-station advection does fairly well in covering the same area as the windfield advection for a 12-hr release. However, comparing individual trajectories shows differences becoming large for short-term unexpected releases. The 20 to 30° diurnal oscillation is southerly flow that shows up so dramatically in the trajectory plots is primarily a temporal variation, but an important phenomenon of which to be aware in terms of transport. The tetroon and windfield trajectory comparisons indicated that during daylight, a logarithmic extrapolation of tower speed and a 10° correction to the right of the 30-m wind direction will give a reasonable first guess of the transporting winds in the lowest 600 m of the atmosphere.

Further and more detailed analysis of the rest of this unique data set should provide valuable information in several areas. For example, the available surface synoptic data and upper air soundings should be used together with the mesonetwork, tetroon, and tower data to determine the worth of this routinely available data in the determining of the mesoscale transport in moderately populated areas. There can be significant differences in the wind representation between consecutive 20-min averages from strategically positioned sensors at 15 to 30 m and 1-min averaged dial readings once an hour from a sensor 3 to 6 m above an airport terminal. The temperature and wind data available on the WKY tower, along with the tetroon and synoptic weather data provide an opportunity to study their detailed behavior in variance stability conditions. This information should also provide a more accurate estimate of vertical wind shear for practical use.

2. PRELIMINARY WORK ON HASWELL, COLORADO, MESOSCALE STUDY

This experiment is being planned in conjunction with a series of experiments that will be conducted in August 1972 by the Wave Propagation Laboratory of ERL. Their experiments involve monitoring several atmospheric properties with sophisticated indirect measurement techniques. Our purpose is to collect supplementary and comparative information by direct techniques and also the benefit of the data gathered by the indirect methods. The experiment will also provide an opportunity to study mesoscale

wind patterns and transport in an area having topographic characteristics somewhere between those of the NRTS in Idaho and those of central Oklahoma. The site of the WPL experiment is within a few kilometers' radius of their 154-m tower, about 6 km south of Haswell, Colorado. The 80- by 80-km mesogrid for this study is centered on the WPL tower and is shown in figure 16 along with the NRTS, Oklahoma, and Los Angeles grids.

The mesoscale wind network was set up in late May 1972 to provide a longer data sample than would have been available during the 2-week WPL experiment in August. Because of the sparse population in southeastern Colorado, existing towers could not be counted on to provide positions for elevated sensors. For this reason, enough tower sections for nine stations, along with the sensors and recorders, were taken to the site of the experiment. Techniques developed for efficient erection of 15-m towers and experience in sensor and recorder installation gained in Oklahoma accounted for the rapid deployment of nine wind stations over a 6400-km^2 area, plus

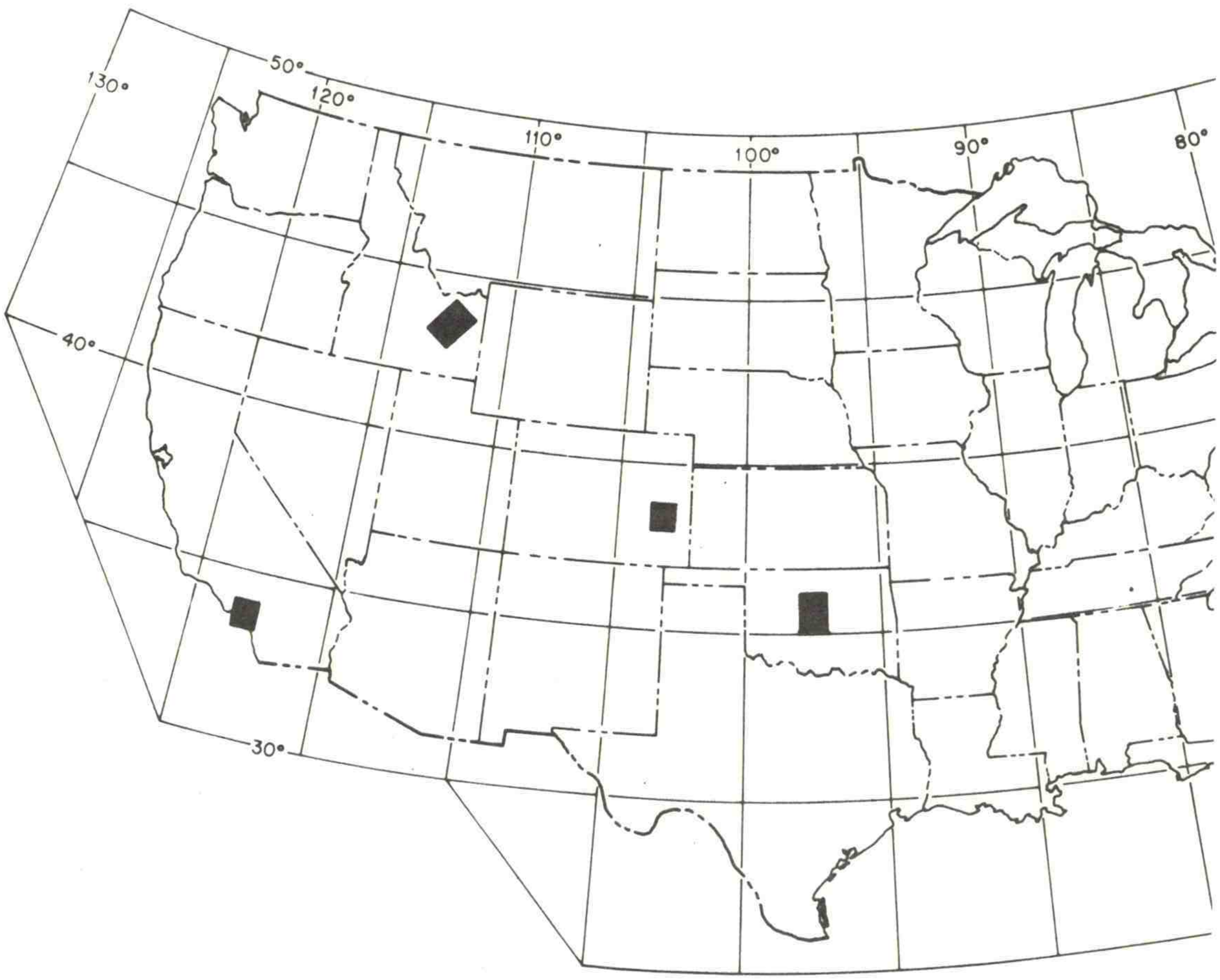

Figure 16. Relative size and location of mesoscale networks in which transport has been studied from using network winds in conjunction with tetroon flights.

a sensor atop the 150-m WPL tower. Site location and installation by a five-man crew required 7 days for the entire network.

The size of this network and the configuration of the stations were designed to provide better support to the WPL program than would have been provided by the type of network used in Oklahoma. The station locations and three crude height contours over the grid are shown in figure 17. The mean slope between the lowest and highest points on the grid is 4.3×10^{-3}, which is about twice that found for the Oklahoma grid and half the value for the NRTS grid. In terms of the height variation over short distances, the Colorado grid is quite smooth compared with the Oklahoma grid. The major terrain features over the Colorado grid are the general downward slope from the northwest resulting in a broad ridge. The southern boundary of the grid lies in the Arkansas River Valley with a moderate amount of trees, grass, and farm crops while the northern boundary lies in dry, almost barren country with meager vegetation and pasture land.

The wind station data, including the 15- and 150-m levels on the WPL tower, are recorded in the same format as for the Oklahoma data. The data from the strip charts were again averaged over 20-min intervals. Temperature profiles on the WPL tower will be available for only the 2-week period of this experiment. We will fly tetroons in pairs during this period, and this should provide even more information on the vertical structure of the flow than the individual flights in Oklahoma.

Some of the wind data taken in early June have been read, edited and punched on cards. A sample of the windfield plots for the data is shown in figure 18, and a sample of the trajectory plots is shown in figure 19. Three terrain contours have been included with each plot to aid in correlating variability in the wind pattern with terrain features. For the

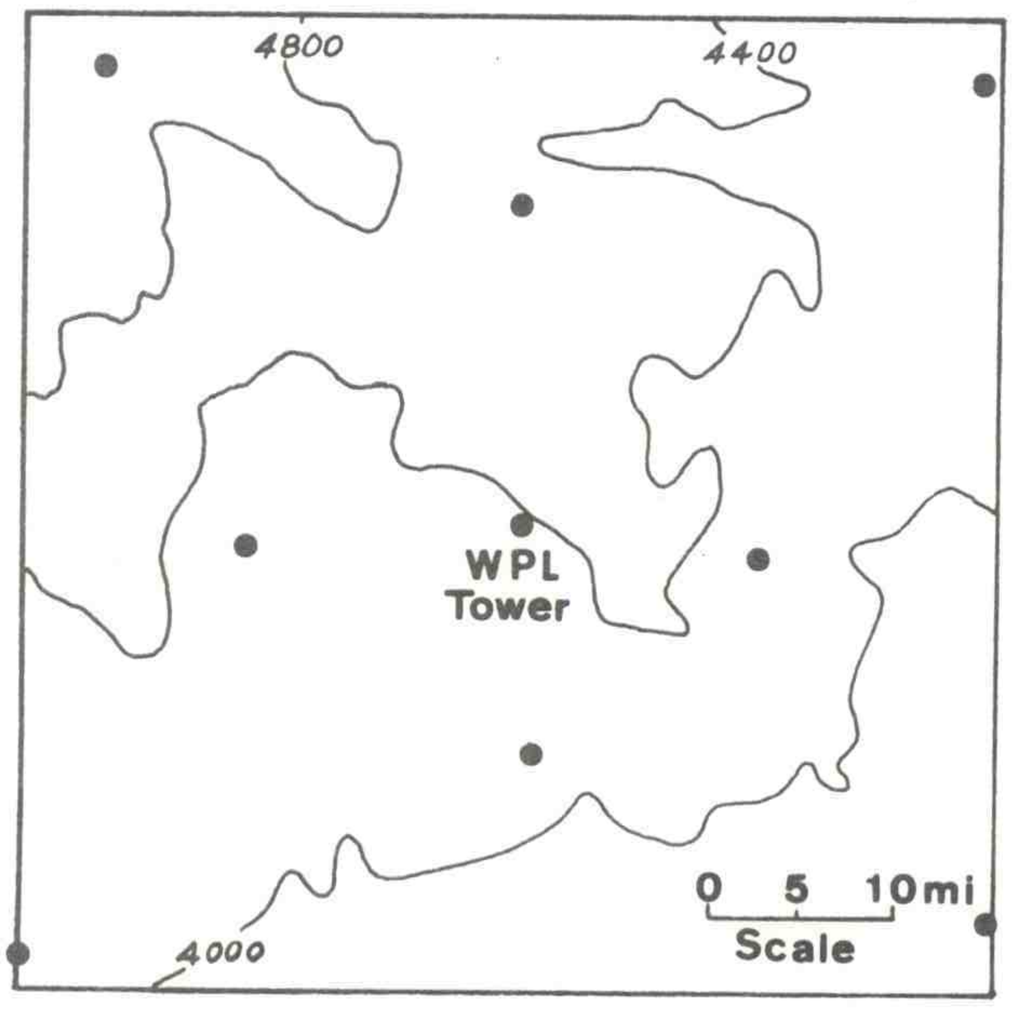

Figure 17. Wind station network configuration for Colorado study. The contour elevation is shown in feet.

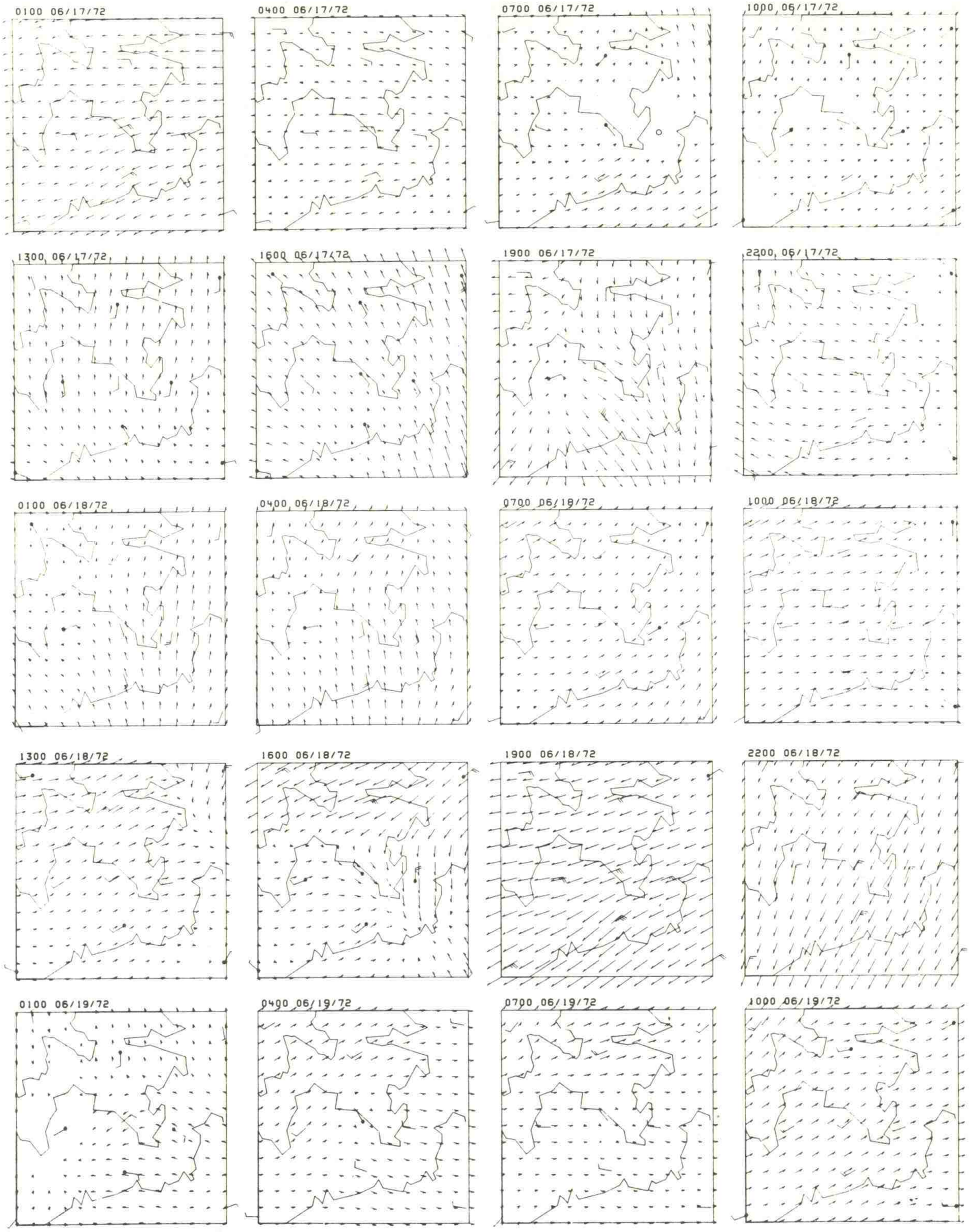

Figure 18. Three hourly windfield plots from Colorado mesonetwork. Grid spacing is 6.5 km. The scaling for the wind vectors is 11 m sec^{-1} for one grid unit.

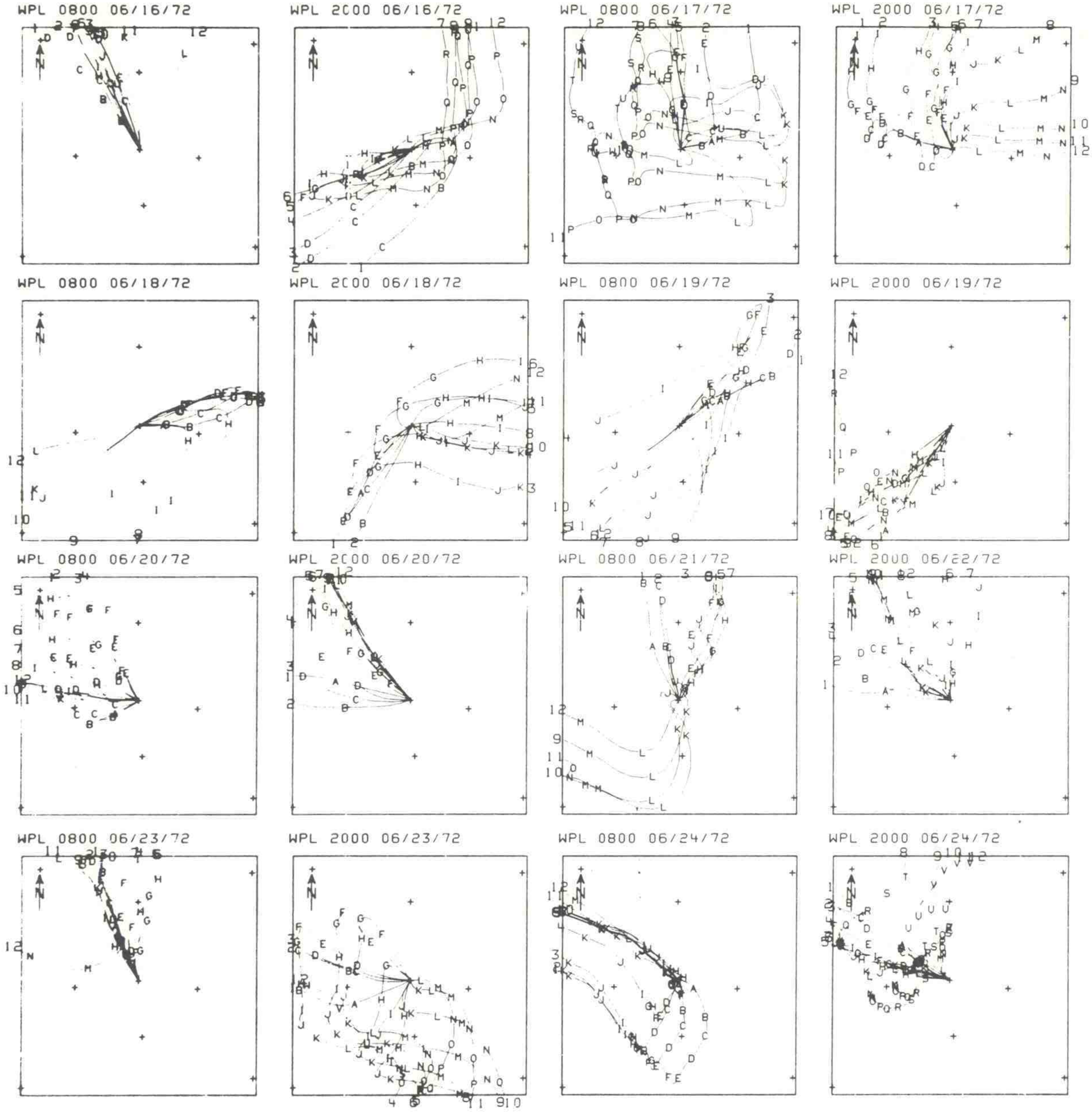

Figure 19. Trajectory plots from Colorado data. See figure 10 for details.

brief period shown, there seems to be more spatial and temporal variability in the flow than any period of similar length in the Oklahoma data sample. However, the time of year is not the same and the entire Oklahoma sample was quite short. As the Colorado data sample extends into the autumn and the supplementary tower and tetroon data become available, a comprehensive comparison should be possible.

3. CONVERSION OF THE NRTS NETWORK TO RADIOTELEMETRY

The telemetered wind stations have been strategically located on a rectangular grid 220 x 100 km orientated NE to SW in the upper Snake River Plain. Seven stations are within the boundary of the NRTS and 17 are off-site installations. Temperature sensors are also to be installed at many of these locations.

Each station within the network is scanned at 6-min intervals for wind, radiation, and temperature data. A PDPB/S computer interfaced with a Kennedy tape recorder records the sequence on magnetic tape. Each 6-min sequence composes one physical record of information written on the magnetic tape in ASCII (American Standard Code for Information Interchange) code. An on-line teletype can also be activated to monitor the network during sequencing.

Seven-track tapes (200 BPI) that record the telemetered data are changed on a routine basis and processed by the IBM 360-75 computer through the remote input terminal located at Central Facilities. Approximately 40 m of tape is used daily, however, the tapes are changed three times a week as a precautionary measure against equipment failure. The FORTRAN program for processing the telemetered wind and temperature data has been compiled to machine language and these instructions have been written for disk for direct access to the IBM 360-75.

Contents of the data tape are transmitted via telephone wires from the remote input terminal directly to a disk pack at the computer center, using a special tape READ routine. This routine (MR61) is accessed by Job Control Language (JCL). Upon execution of the job step, the telemetered data residing on disk are converted from ASCII to binary representation, one record (6-min sequence) for each read instruction.

A search is then made to locate the Julian date group. The Julian date will be the first three digits with values of 1 59 9 in the record. All other characters (alphabetic) will have a code other than 1 to 9. The time that the sequence was initiated is determined by the identification of a colon (:) between the hour and minute.

Character scanning now identifies station call letters, which are coded as three unique alphabetic characters preceding the data channels. The translated characters are compared with a set of numbers that have been read in before execution to determine which station call letters have been identified. The next step after station identification is to check by a pre-read code for the station read-in by control cards, what data the station should be transmitting and which channels these data are in. If any characters other than 1 through 9 appear as any digit in the data channel, the channel is considered missing. However, if the character is alphabetic, the program checks for another set of call letters. When no station call letters can be identified, the search is continued for the

next data channel of the previously identified station. The three numeric digits from each data channel are packed, checked for values between 1 and 998, and stored for further use.

The u and v wind components, extracted from the data channels, are summed separately until the end of the hour, when the hourly average wind direction and velocity will be computed. Hourly averaged wind direction and velocity are computed as follows,

$$\overline{u} = \Sigma(u-500)/N \tag{1}$$

$$\overline{v} = \Sigma(v-500)/N \tag{2}$$

by use of ATANZ and SORT subroutines from the system library

$$D = 57.29578*ATANZ(\overline{V},\overline{U}) \tag{3}$$

$$S = SQRT(\overline{u}**2+\overline{v}**2)/5.0 \quad . \tag{4}$$

The telemetered values of u and v have been multiplied by 5 for greater resolution, and 500 was added to avoid negative numbers. The 6-min integrated values of temperature, u, and v are stored in an array during processing, and at the end of each hour the array is written to disk to be later merged with previous data. The hourly averaged wind directions and speeds are printer listed and retained for reference.

Hourly averaged wind directions and speeds are plotted by a Calcomp plotter at 3-hr intervals. The rectangular grid is scaled from 220 x 100 km to 11 x 5 cm. Four maps are plotted for each 22 x 28 cm area of plotter paper. The sheets may then be cut to page size. The NRTS site boundary is plotted within the grid with date and time labeled above the grid. Wind direction is illustrated by drawing lines from the scaled station location toward the direction from which the wind is blowing. Barbs are drawn at 95° perpendicular to the direction shaft for each 5 m sec^{-1} of wind speed. Speeds less than 5 are represented by barbs of corresponding smaller length.

4. THE EFFECT OF SAMPLING INTERVAL ON TURBULENT ENERGY SPECTRA

When collecting experimental data, it is advantageous to use as long a sampling interval as possible in order to reduce the volume of data that must be processed. One must use care in selecting a sampling interval, however, to insure that the data will be meaningful.

To examine the effects of sampling interval on speed and velocity spectra calculated from bivane data, we studied data from a bivane located 4 m above the ground when the wind speed averaged 2.5 m sec^{-1}. The data

were sampled at an interval of 0.58 sec for a period of 79.2 min; but by using every other data point or every fourth data point, we could compare data with sampling intervals of 1.16 and 2.32 sec, respectively.

Means, variances, and spectra were calculated for the wind speed and the three velocity components using all three sampling intervals. For the intervals chosen, no appreciable differences existed in the means or the variances; as can be seen from figures 20 through 25, the speed (S) and horizontal velocity components (u and v) are similar except at the high frequency ends where the effects of aliasing can be seen. Our experience has been that good vertical velocity (w) spectra cannot be obtained from bivane data, especially when the bivanes are at lower elevations. The w spectra calculated in this study are no exception to the rule.

If we use the spectra calculated with Δt = 0.58 sec as a standard, we see that for the U and S spectra aliasing begins to appear at about 0.3 Hz for Δt = 1.16 sec, and about 0.07 Hz for Δt = 2.32 sec. For the v component spectra, the effects of aliasing began to appear at about 0.1 Hz for Δt = 1.16 sec, and about 0.07 Hz for Δt = 2.32 sec.

This study would seem to indicate that unless we were interested in the higher frequencies, the data measured at intervals of 2.32 sec would be almost as good as that measured at 0.58 sec intervals.

5. SITE EVALUATION PROGRAM

5.1 Introduction

A computerized model has been programmed to calculate simulated accident and annual average atmospheric dilution factors. This program makes it possible to rapidly evaluate potential nuclear power station sites in a consistent manner.

For input to the program, the applicant must provide a joint frequency distribution of wind speed and stability classes for each directional sector from a representative 12-month period. In most cases, periods of calm are included separately as the number of calms occurring for each stability class. The program assigns the calms to the various sectors in the same ratio as the lowest wind speed class and adds them to that category. Also included as input to the program are the distances to the site boundary for each sector, the cross-sectional area and height of the reactor building, and the distance to the nearest population center. If the reactor has a stack, the applicant also includes the height and diameter of the stack and the exit velocity of effluent, the distance and bearing of the stack from the reactor, the distances from the stack to the site boundaries for each sector, and information on terrain. Terrain heights and distances are read into the program for each sector; the program performs a linear interpolation to obtain the terrain height at any needed location. Plume rise is determined by the formulas developed by Briggs (1969).

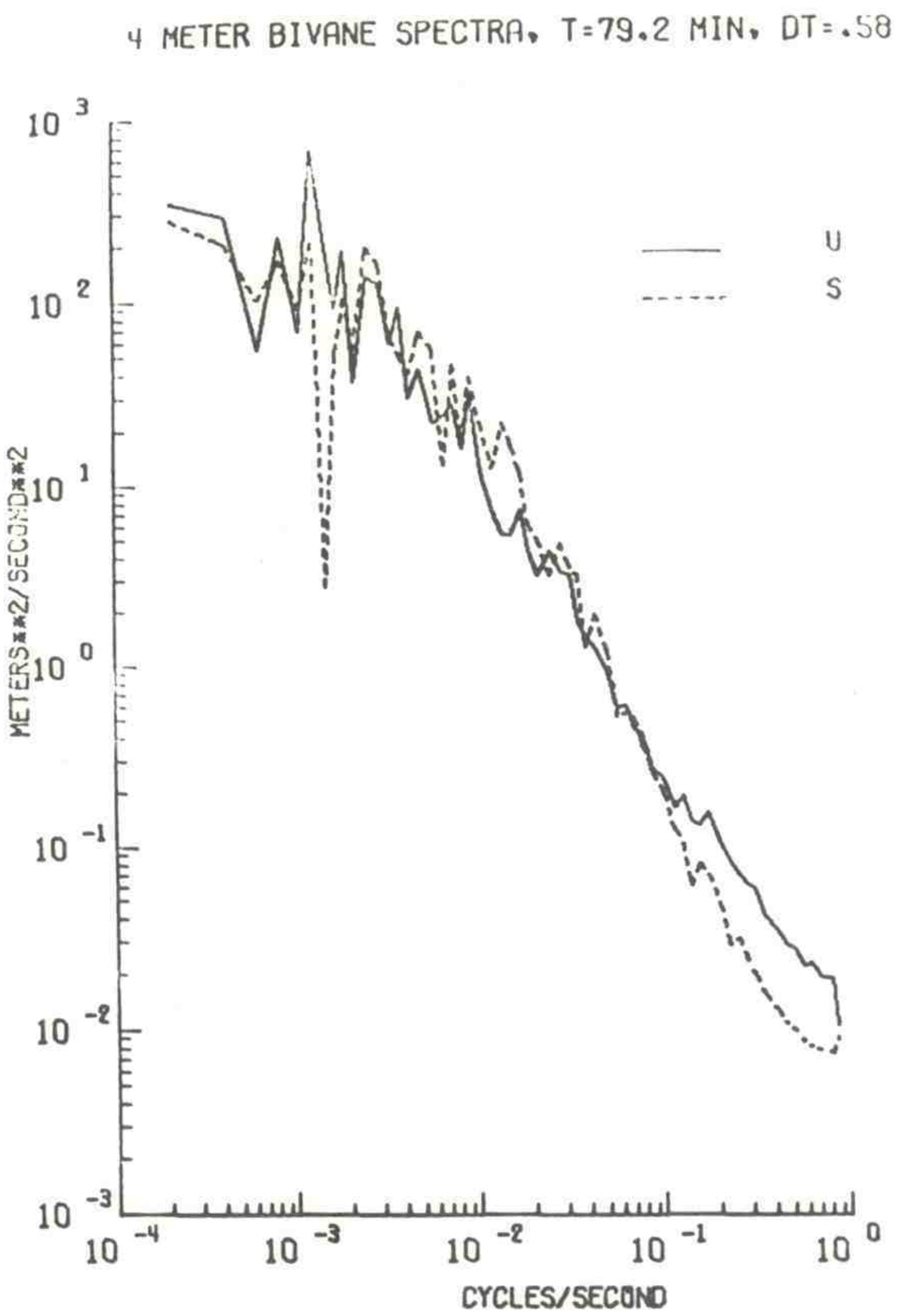

Figure 20. u and S spectra sampling interval - 0.58 sec.

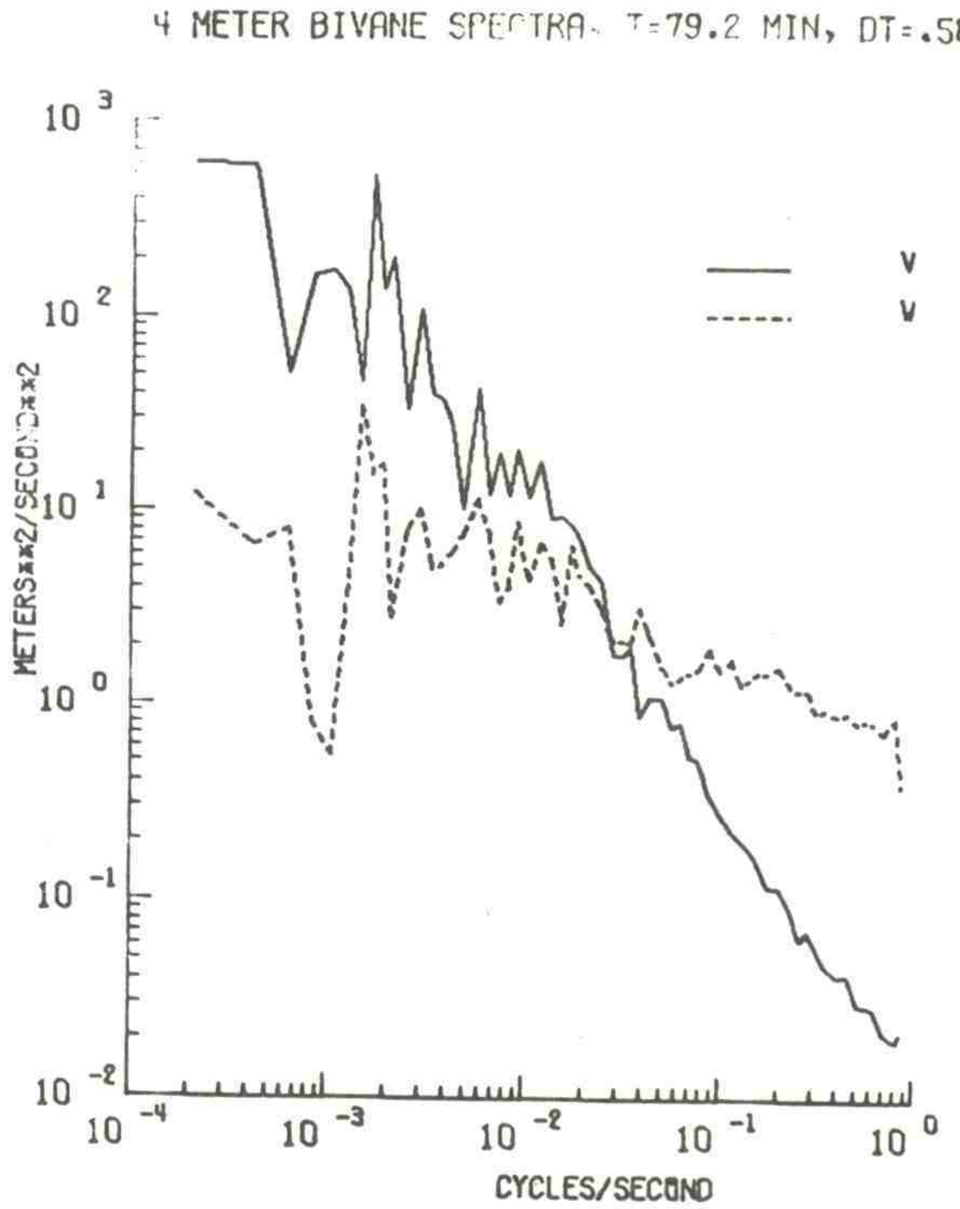

Figure 21. v and w spectra sampling interval = 0.58 sec.

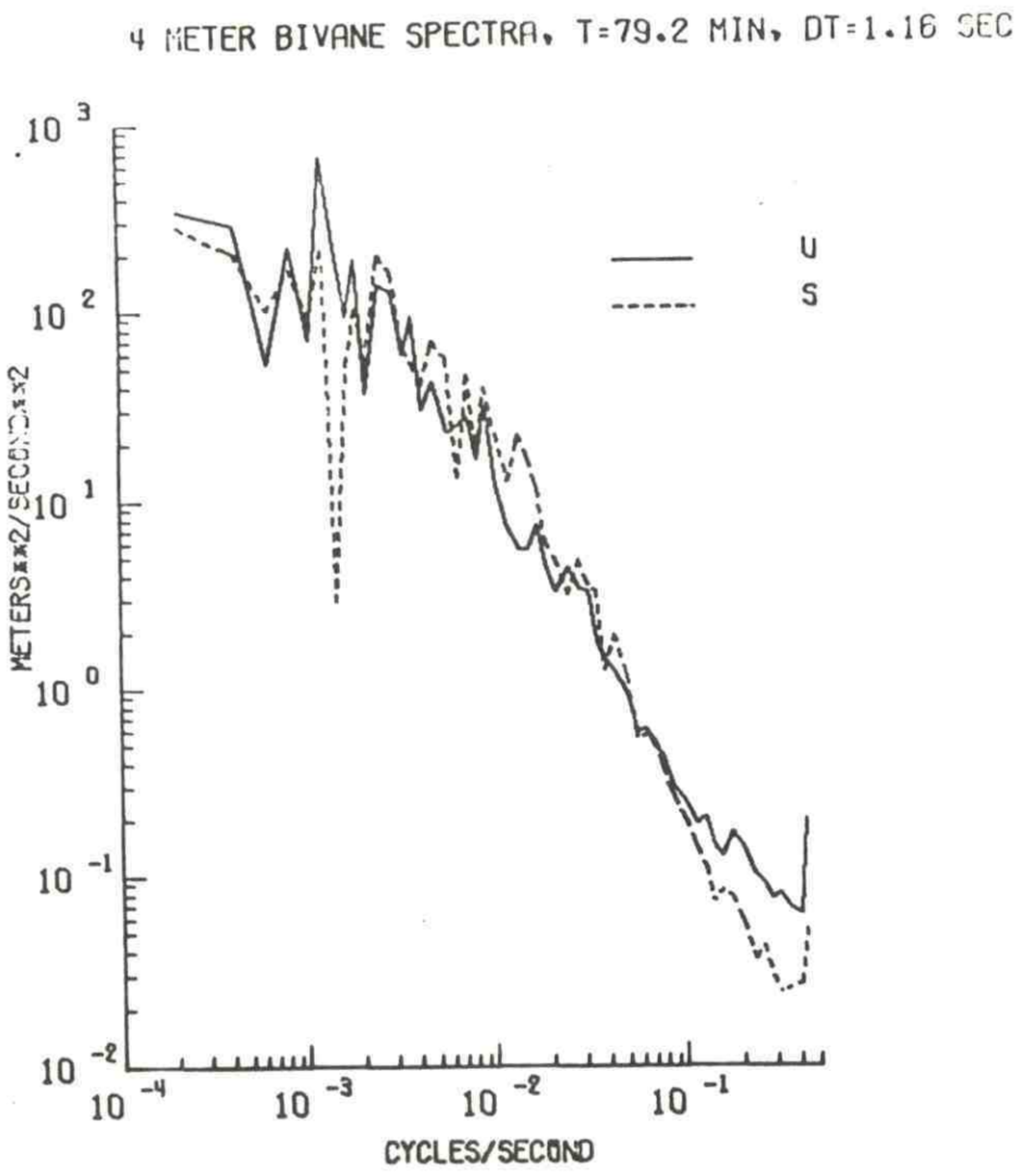

Figure 22. u and S spectra sampling interval = 1.16 sec.

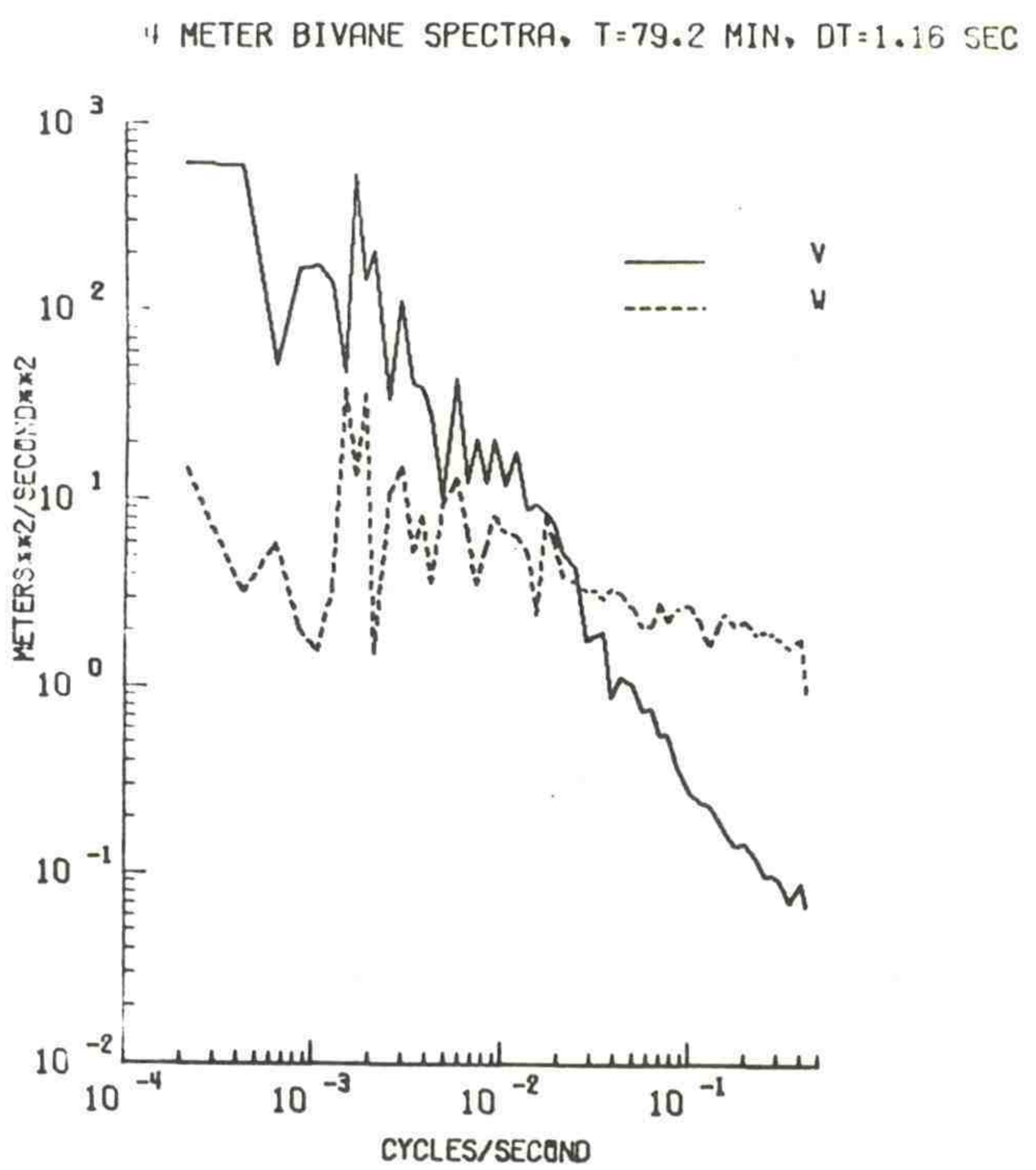

Figure 23. v and w spectra sampling interval = 1.16 sec.

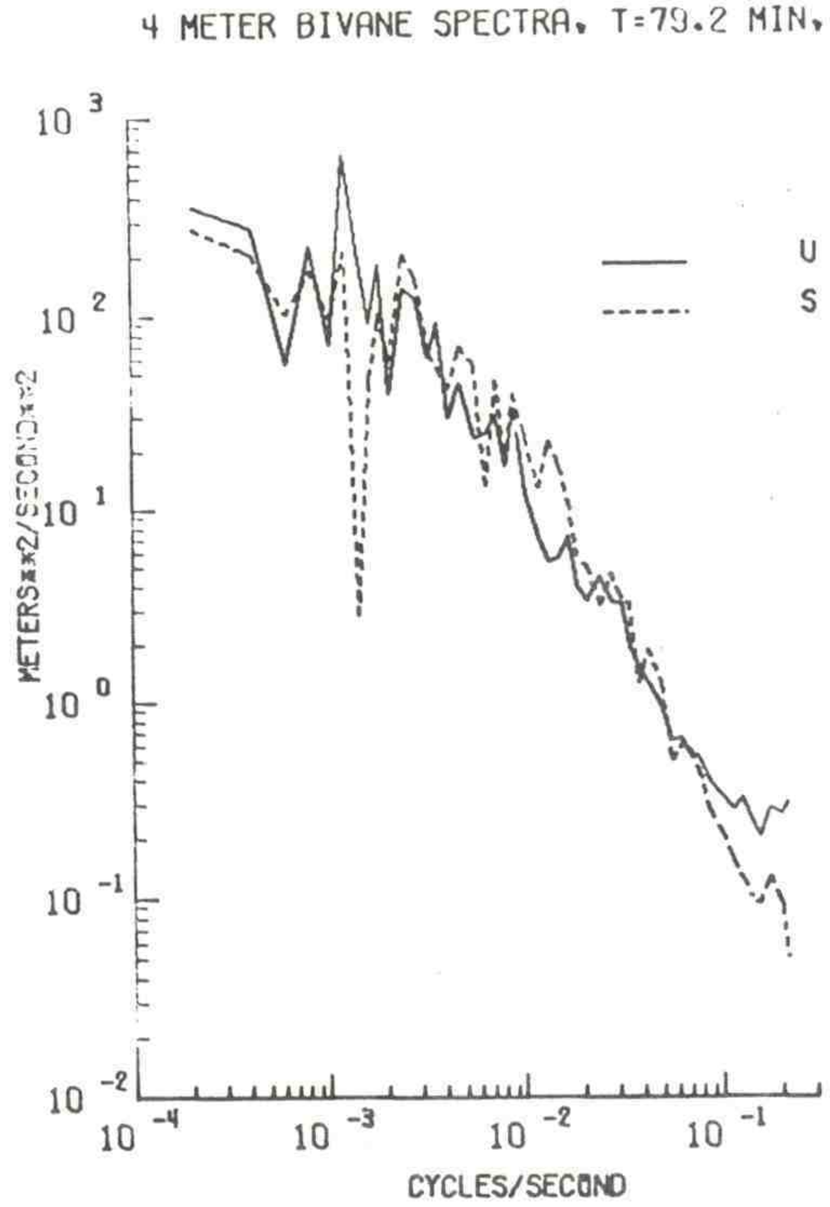

Figure 24. u and S spectra sampling interval = 2.32 sec.

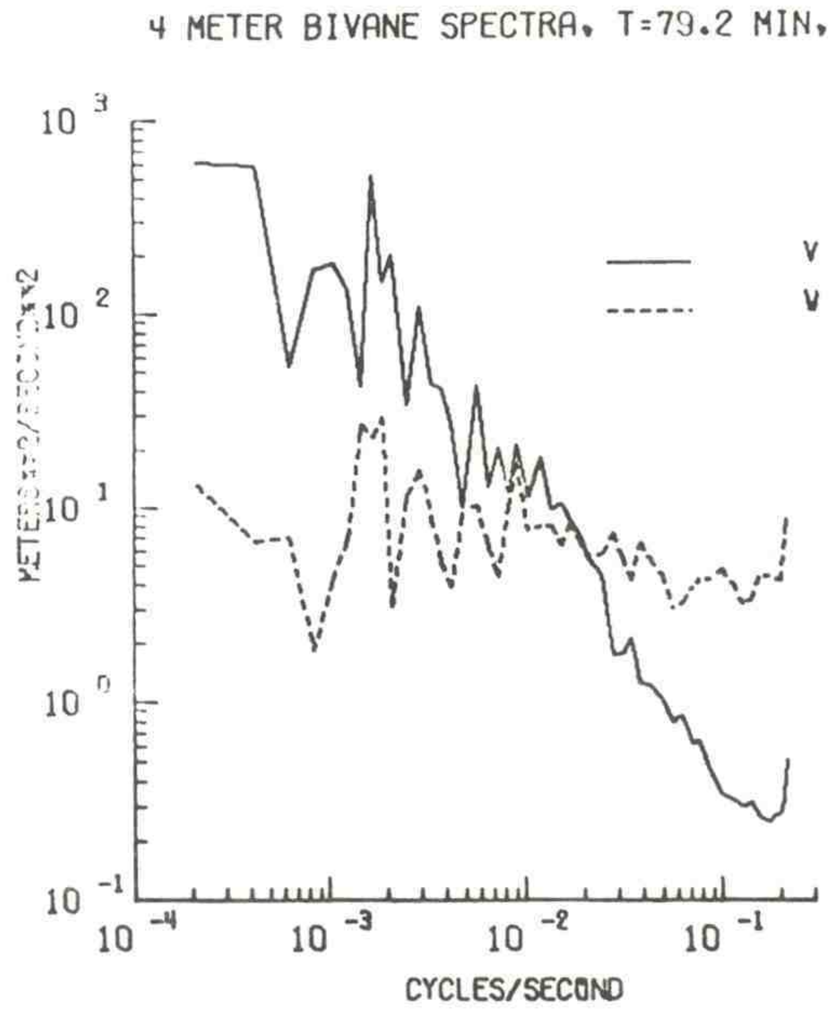

Figure 25. v and w spectra sampling interval = 2.32 sec.

5.2 Design Basis Accident Model

Accident meteorology is defined as the value of χ/Q that is exceeded 5 percent of the time during a year of "typical" weather conditions. The program has the option to make calculations for either a ground-level or elevated source. The equations used are as follows:

$$\chi/Q = 1/U_m(\pi\sigma_y\sigma_z + CA) \geq 1/3\overline{U}\pi\sigma_y\sigma_z \quad \text{(ground-level source)}, \qquad (5)$$

$$\chi/Q = e^{-\frac{1}{2}\left(\frac{h}{\sigma_z}\right)^2}/U_m\pi\sigma_y\sigma_z \quad \text{(elevated source)}, \qquad (6)$$

U_m = the upper limit of the wind speed class,

$\sigma_y\sigma_z$ = the standard deviations of material in the plume in the y and z directions ,

C = a constant equal to 0.5 ,

A = the cross-sectional area of the reactor building ,

h = stack height + plume rise - terrain elevation.

For each combination of wind speed and stability class, χ/Q is calculated and the results are stored along with the associated probability of occurrence as determined from the joint frequency distribution. For a ground-level source, three methods are used to determine the distance at which to make the calculations:

1. The distance from the reactor to the nearest site boundary (minimum site boundary).

2. The distance to the nearest population center (low population zone).

3. The actual distance to the site boundary for each directional sector.

For an elevated source, the problem becomes somewhat more complicated. The same three procedures are used for determining distances, except that they are measured from the stack rather than the reactor; furthermore, since the maximum value of χ/Q may occur beyond the given distance, a searching procedure finds the maximum value of χ/Q at or beyond the given distance.

The array of χ/Q values is ordered from the greatest to the least, and the cumulative probabilities associated with them are summed. A curve then is fit to the data points by the least-squares method. A plotting routine has been developed to plot the data points and curve on a log-probability graph (fig. 26) so that both graphical and tabular forms of output are possible.

5.3 Average Annual Model

In this model, a long-term continuous release is assumed. The program may optionally calculate a ground level, elevated, or mixed release.

The basic equation used is

$$(\chi/Q)_{Avg} = \frac{(2/\pi)^{\frac{1}{2}}}{r\theta} \Sigma \frac{f_{ijk} \exp(-h^2_{ijk}/2\sigma^2_{z,j})}{\overline{U}_i(\sigma^2_{z,j} + CD^2_z/\pi)^{\frac{1}{2}}}$$

$$\geq \frac{(2\pi)^{\frac{1}{2}}}{r\theta\sqrt{3}} \Sigma \frac{f_{ijk} \exp(h^2_{ijk}/2\sigma^2_{zj})}{\overline{U}_i \sigma_z} , \qquad (7)$$

$\overline{U}_i$ = the average wind speed in the ith wind speed category ,

σ_{zj} = the standard deviation of plume material in the jth stability category,

f_{ijk} = the joint probability,

h_{ijk} = the effective stack height,

C = a constant equal to 0.5,

D_z = the height of the building,

r = the distance ,

θ = sector width in radians.

Values of (χ/Q) are calculated for the site boundary in each sector and for a number of distances out to 80 km. In making use of these results, however, keep in mind the uncertainty of values calculated at these distances. Each sector is divided into a number of segments, and an average value of (χ/Q) is calculated for each segment.

The values of (χ/Q) average for each segment may be further smoothed by averaging them with neighboring sectors. If desired, we may also obtain segment averages over all segments at a given distance from the reactor. Output from the annual average portion of the program is both tabular and graphical. The graphs include plots of (χ/Q) average versus distances for each sector (fig. 27) and contour maps depicting isopleths of (χ/Q) average surrounding the site area (fig. 28).

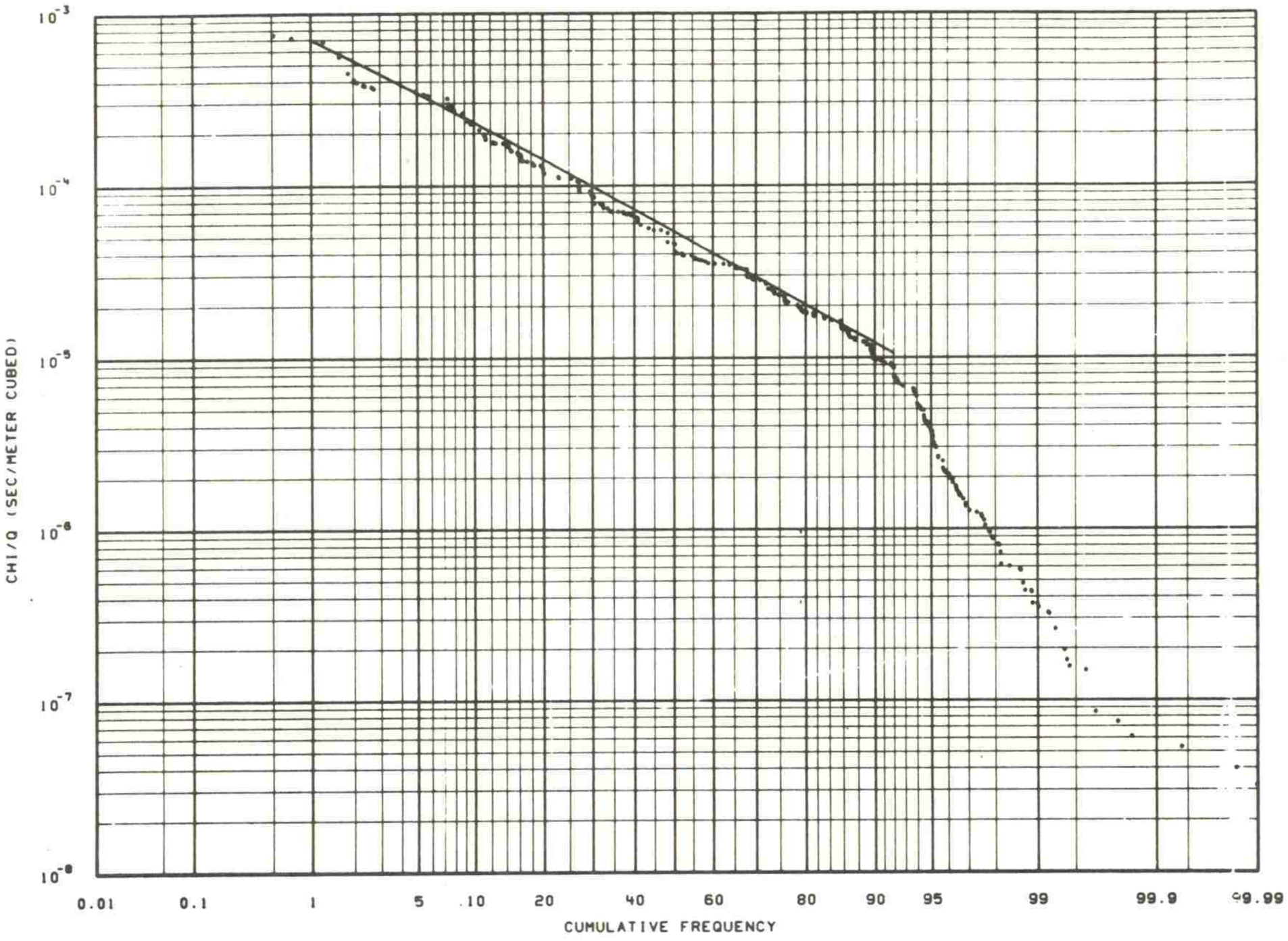

Figure 26. Design basis accident plot of χ/Q versus cumulative probability for the Forked River Nuclear Power Station.

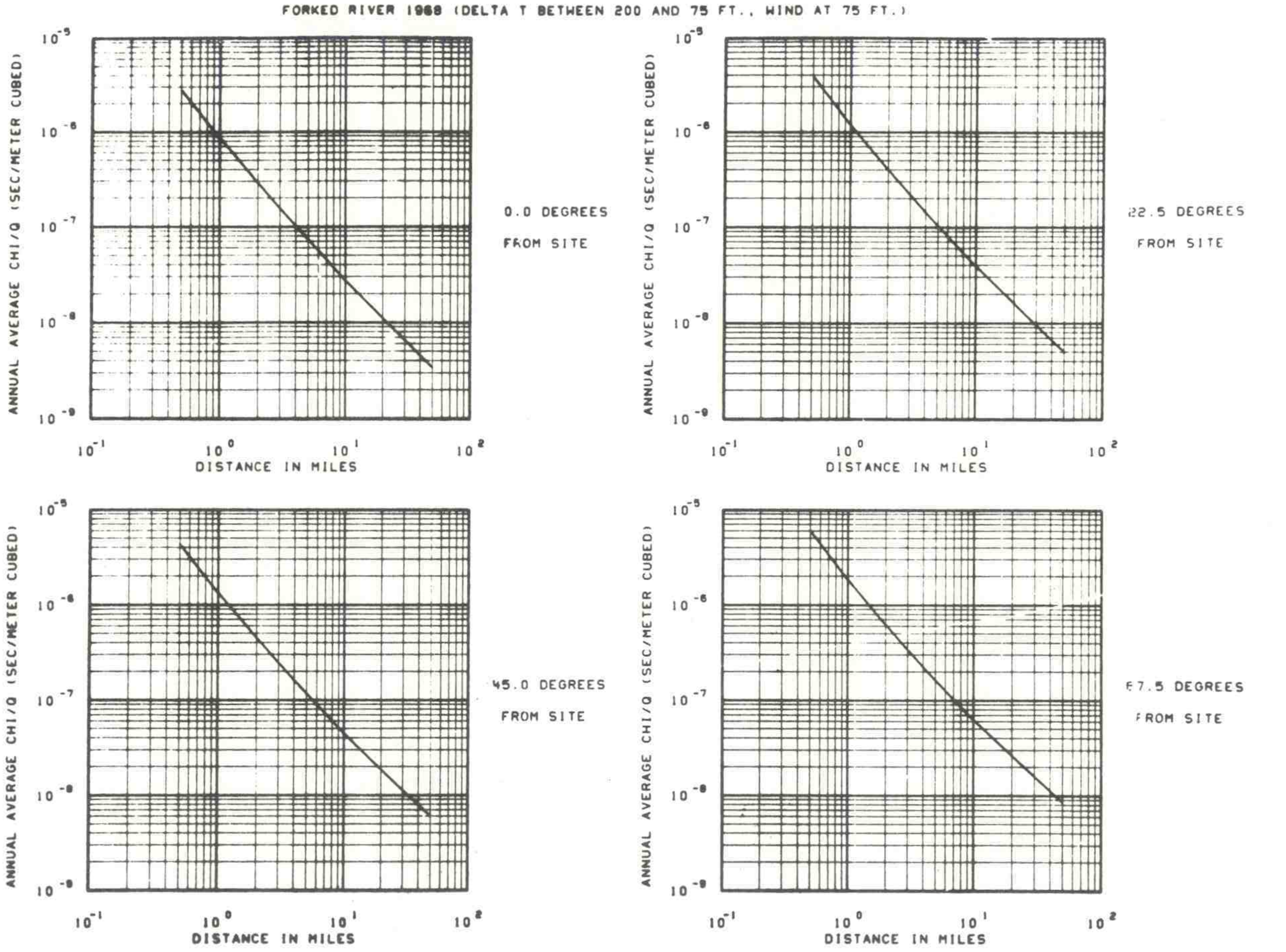

Figure 27. Examples of annual average plots of χ/Q versus distance for each directional sector for the Forked River site.

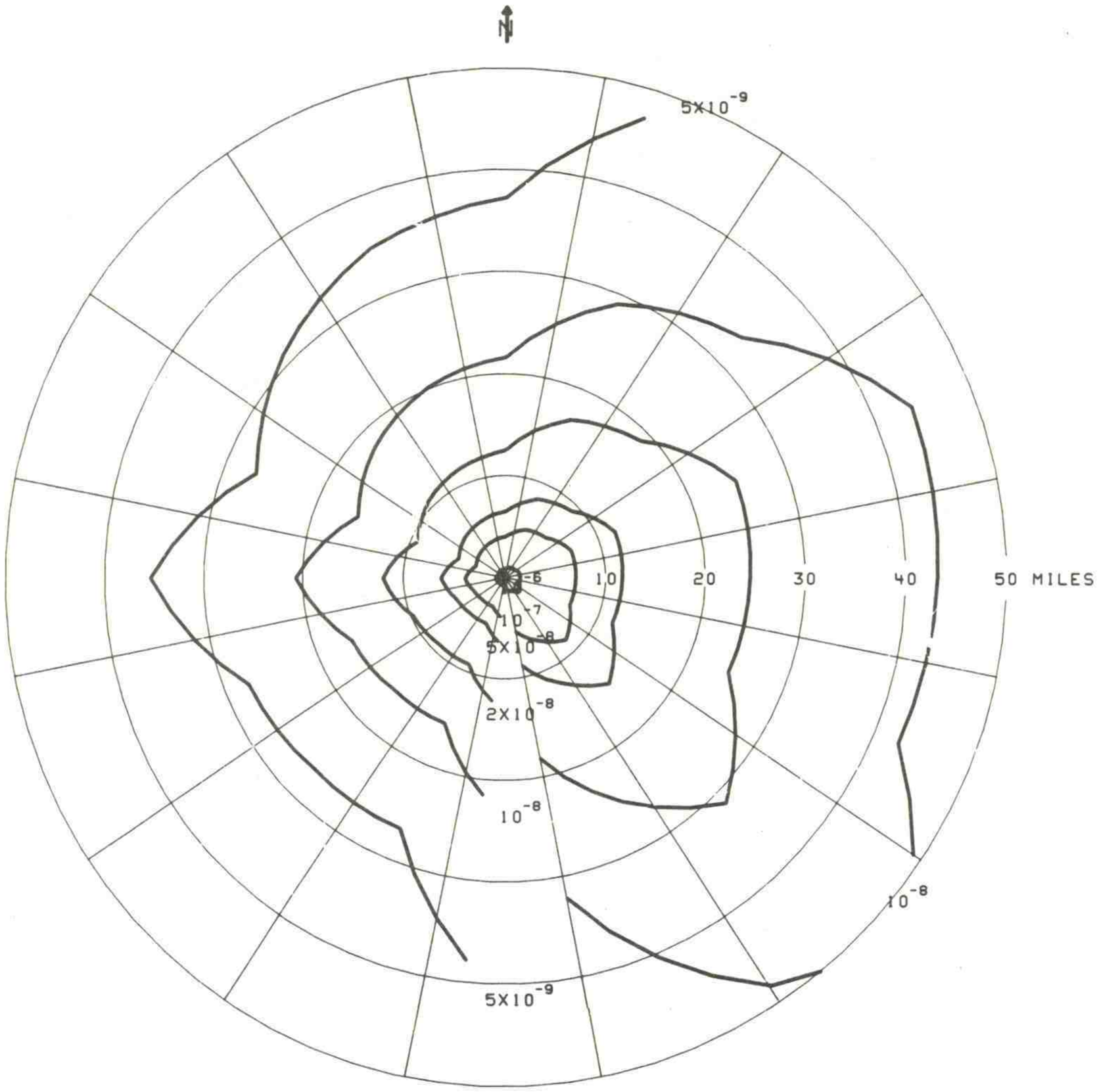

CONTOURS OF ANNUAL AVERAGE CHI/Q (SEC/METER CUBED)

FORKED RIVER 1968 (DELTA T BETWEEN 200 AND 75 FT., WIND AT 75 FT.)

Figure 28. Contour map of annual average χ/Q for the Forked River site.

6. DIRECTIONAL WIND SHEAR UNDER LOW WIND SPEED CONDITIONS

An interesting phenomena noted during the initial Building Wake Studies was the frequent occurrence of strong directional wind shear in the vertical. During conditions of a stable temperature, lapse rate, and low wind speeds, the winds at the 4-m level of the Grid III tower were often flowing in almost the opposite direction from those at the 61-m level. An example of this phenomena (fig. 29) shows smoke being released at three different levels on the Grid III tower. At each level, the wind is blowing in a different direction. Figure 30 is an episode that occurred the morning of July 8, 1971, in which the long vectors represent the winds at the 61-m level, and the short vectors are the winds at the 4-m level. Immediately above each pair of vectors are two numbers. The lower number represents Mountain Daylight Time (MDT), and the other is the temperature gradient (°F/100 ft) as measured between the 61- and 4-m levels. This figure, then, is a series showing wind shear at 10-min intervals with the corresponding temperature lapse rate printed for each plot. The wind speeds at the top of the tower varied from 3 to 6 m sec^{-1}, and at the bottom from 0.5 to 3 m sec^{-1}. From 0555 to 0735 MDT, stable conditions existed. The wind at the top of the tower was fairly steady from

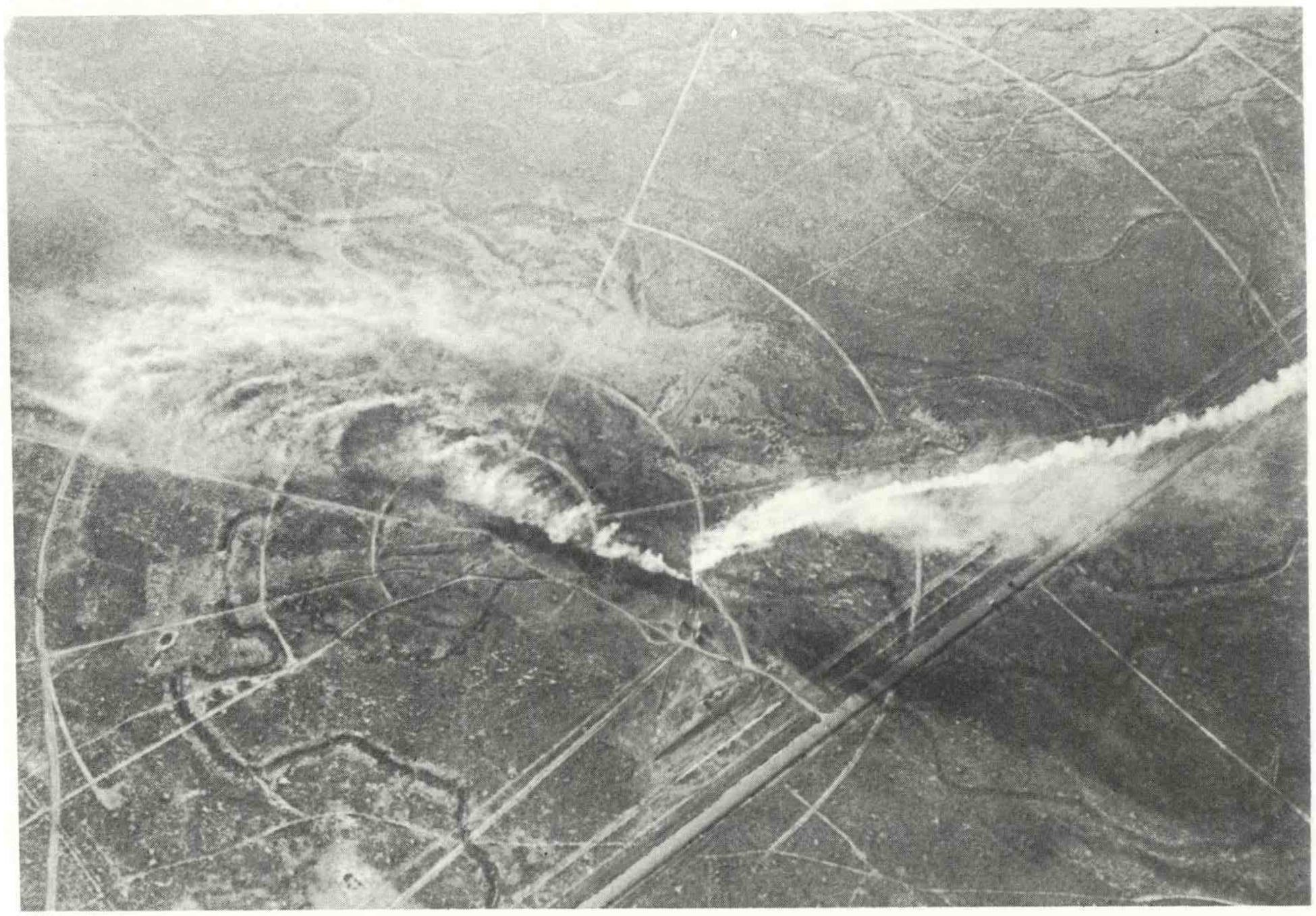

Figure 29. Aerial photograph showing smoke being released from the surface, 25 m, and 61 m on the Grid III tower.

out of the north or northeast at about 5 to 6 m sec^{-1}, while at the bottom the wind was meandering at about 1 m sec^{-1}. From 0635 to 0655 MDT and again at 0735, the directional shear was about 180°. After 0745 MDT, lapse conditions existed and the mixing from above brought the lower level winds more in line with those at the top of the tower. Under these stable conditions, the air apparently became stratified and the lower level winds became uncoupled from those farther up the tower.

When examining the topography of the upper Snake River Valley, we find the plain rises from the SW to the NE. Near the Grid III tower, however, there is a smaller scale slope in the opposite direction. On this morning, we were probably witnessing a downslope wind at the top of the tower that was governed by the large-scale valley slope, while the winds at the bottom of the tower were following the smaller scale slope on a local level.

Studies comparing speed spectra with u and v spectra from the upper and lower levels on the nearby CFA tower have also demonstrated this uncoupling effect; they showed a diurnal wind reversal at the top of the tower that did not exist at the bottom.

To determine how frequent and under what conditions this phenomena occurs, we instrumented the 61-m tower at Grid III to measure wind velocity (10-sec intervals) at the 4, 16, 32, and 61 m levels and temperature (1-min intervals) at the 1, 2, 4, 8, 16, 32, and 64 m levels. The data, taken for about 3 weeks, have been stored on magnetic tape, and 10-min means and standard deviations have been computed. The 10-min average temperature gradients have been plotted for each 10-min period, and the wind speeds and directions have been superimposed on the plots to aid in the selection of data cases. Further analysis of the data has not yet taken place, and at this point all we can say is that under stable atmospheric conditions the winds near the surface sometimes become uncoupled from those above. The character of the diffusion in the different layers would obviously be very different under these conditions. A study of the meandering nature of the surface wind during low wind speed conditions would probably contribute to the explanation of low wind speed diffusion.

7. APPLICABILITY OF GEOSTROPHIC WINDS TO MESOSCALE TRANSPORT

There are two primary motivations for evaluating the surface geostrophic winds. First, we are interested in determining transport statistics by using winds dynamically derived from the historical series of meteorological charts and data. If such an approach should have any merit, it would certainly be true at a Plains location such as Oklahoma City. Second, we are interested in determining which elevation above ground the geostrophic winds might best be applied. The presence of the 458 m WKY tower in this study serves the purpose.

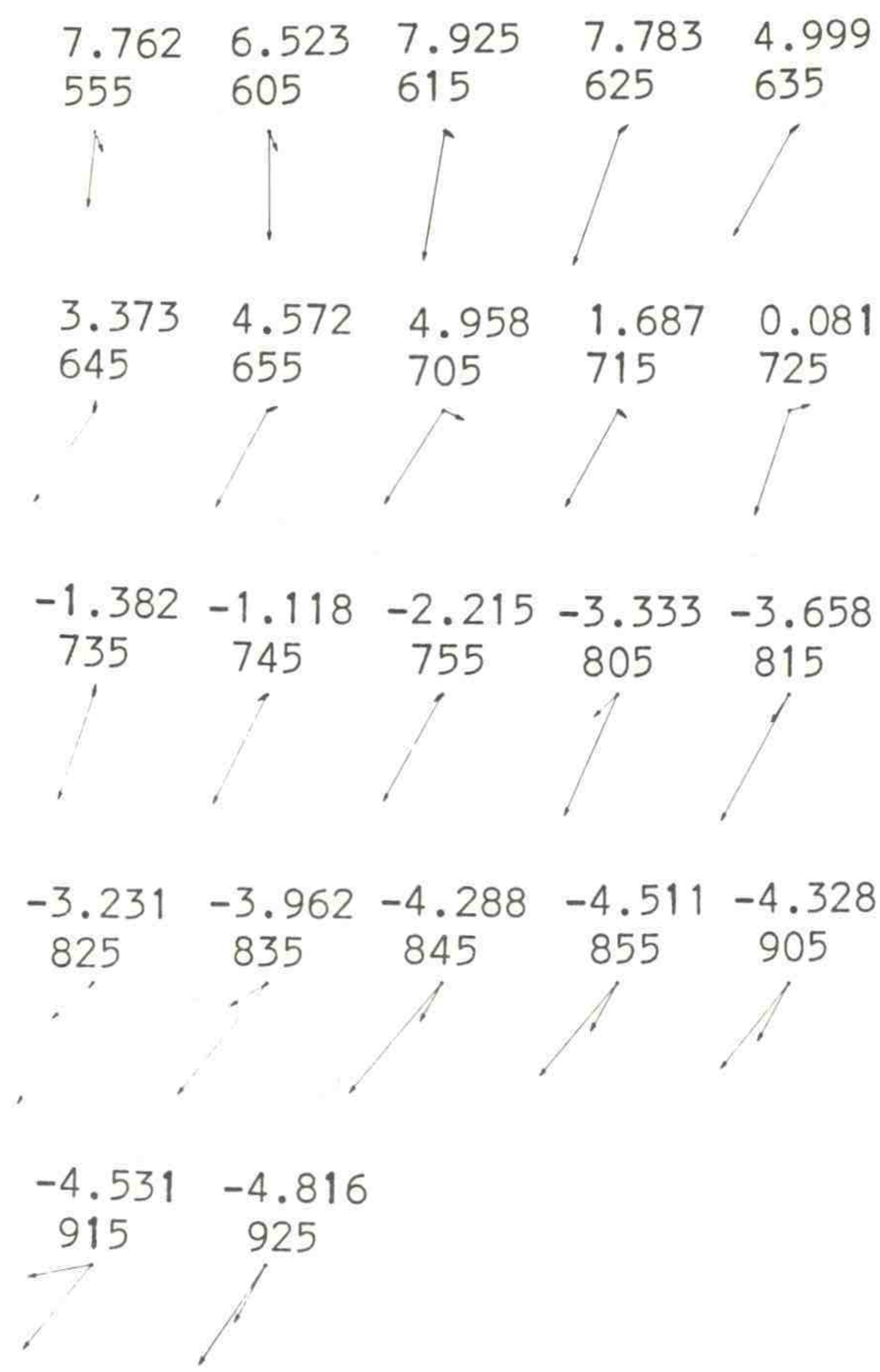

Figure 30. Directional wind shear in time.

Because of the much denser network of airway observation stations, the geostrophic winds were calculated from observed altimeter settings and temperatures rather than computing them from radiosonde observations of the geopotential of a near-surface constant pressure level. Using the altimeter correction system of Bellamy (1945), we may write the geostrophic component equations as

$$U_g = -\frac{g}{f}(1 + S^*)\frac{\partial D}{\partial y} + \frac{g}{f} S^* \frac{\partial z}{\partial y} \qquad (8)$$

$$V_g = \frac{g}{f}(1 + S^*)\frac{\partial D}{\partial x} - \frac{g}{f} S^* \frac{\partial z}{\partial y} , \qquad (9)$$

where D is the height difference from sea level of the standard atmospheric altitude corresponding to the observed altimeter setting, z is the terrain height, and

$$S^* = \frac{T_v - T_p}{T_p} , \qquad (10)$$

where T_v is the observed virtual temperature, and T_p is the temperature corresponding to the station pressure altitude in the standard atmosphere.

The 1° latitude by 1-1/4° longitude computational grid, and locations and altitudes of the 10 observing stations are shown in figure 31 and table 5. D, z, and S* values were interpolated to grid points according to the inverse-square weighting of the observations of the corresponding variables evaluated at the nearest four stations.

Because of the critical dependence of the derived winds upon the computed gradients, the S_1 scores (Tweles and Wobus, 1954) were computed for the inverse square and inverse linear derived gradients of D against a careful hand analysis, where

$$S_1 = \left| \frac{(F-\phi)}{MAX(F,\phi)} \right| /n \quad , \tag{11}$$

n is the number of gradient measurements on a map, F is the gradient from the objective analysis, ϕ is the gradient from the hand analysis, and $MAX(F,\phi)$ is the maximum of the values F and ϕ. Scores were computed for four map times, 0200 and 1300 CDT of both October 1 and October 9. There was no statistically significant difference between the inverse square and inverse linear methods of objective analysis. The S_1 scores were all within 0.305 to 0.435, and the maximum difference between inverse square and inverse linear for any one map time was 0.018. At the interior of the grid, and particularly the grid points surrounding Oklahoma City, the differences between objectively and subjectively derived gradients,

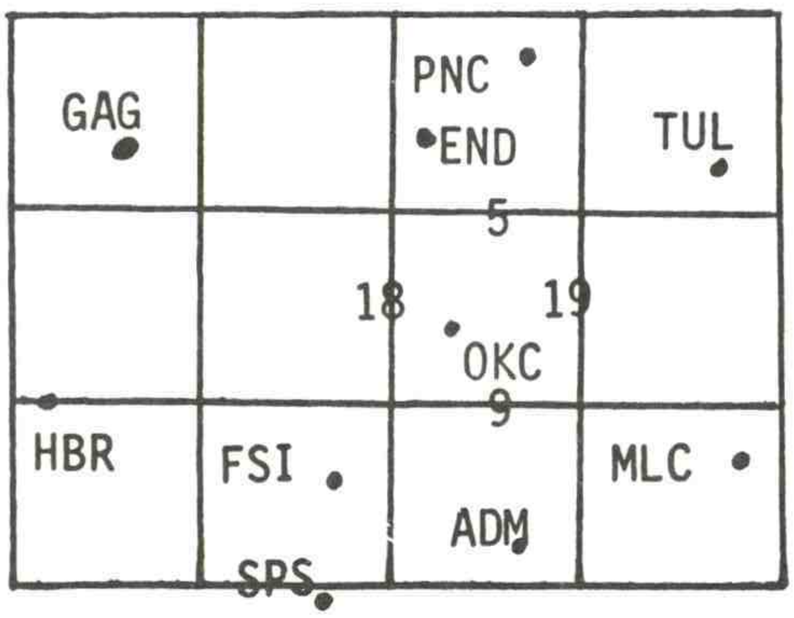

Figure 31. Computational grid for geostrophic winds in Oklahoma. The grid squares are 1° latitude by 1.25° longitude. The numbers are identifiers of gradients.

Table 5. The Stations' Observations the Grid Point Values of D, z, and S were Interpolated From.*

Station Name	Latitude (°N)	Longitude (°N)	Altitude (CM)	Coordinate x	Coordinate y
Gage, Okla. (GAG)	36.30	99.77	680	3.42	2.30
Enid, Okla. (END)	36.38	97.80	360	1.84	2.38
Ponca City, Okla.(PNC)	36.73	97.10	308	1.28	2.73
Tulsa, Okla. (TUL)	36.20	95.90	206	0.32	2.20
Oklahoma City, Okla. (OKC)	35.40	97.60	392	1.67	1.40
Hobart, Okla. (HBR)	35.00	99.05	477	3.84	1.00
Fort Sill, Okla. (FSI)	34.60	98.40	362	2.32	0.60
Ardmore, Okla. (ADM)	34.30	97.02	238	1.22	0.30
McAllestor, Tex. (MLC)	34.88	95.78	229	0.22	0.80
Wichita Falls, Tex. (SPS)	33.97	98.48	310	2.38	-0.03

$\frac{\partial z}{\partial x}$ and $\frac{\partial z}{\partial y}$, was generally less than 3 m per grid interval (approximately 108 km).

The initial test was conducted by evaluating the geostrophic wind at Oklahoma City by interpolation of U_g determined from gradients 18 and 19 and V_g determined from gradients 5 ^{g} and 9; figure 31 shows the referenced gradients. The winds observed on the WKY tower and the geostrophic winds derived by the inverse square interpolation are shown in table 6. Difference between the geostrophic winds and the OKC surface winds is depicted in figure 32.

In the south wind situation of October 1, the nocturnal low-level jet was producing supergeostrophic winds after 0600 CDT at the middle level, and after 1000 CDT at the top of the tower. On October 9, a cold front passed the WKY tower shortly after 0400 CDT. This front was responsible for considerable mesoscale departure of the local pressure gradients at the WKY tower as opposed to those derived using Oklahoma City and Ponca City to the north. (Enid was missing until 0900 CDT.) The directional difference between the geostrophic wind is generally 30 to 40° in the south

Table 6. Observed Winds on the Hour at Three Levels of the WKY Tower and the Computed Geostrophic Wind.

Time (CDT)	WKY Tower 90 m	WKY Tower 266 m	WKY Tower 450 m	Geostrophic Wind
		October 1, 1971		
0200	1715*	1835	1742	2020
0300	1817	1835	1843	2121
0400	1819	1831	1842	2123
0500	1815	1836	1842	2025
0600	1816	1934	1942	2232
0700	1716	1928	1934	2233
0800	1815	1828	1944	2235
0900	1817	1830	1935	2234
1000	1918	1827	1936	2235
1100	1920	1825	1929	2139
1200	1819	1923	1925	2239
1300	1720	1924	1822	2238
		October 9, 1971		
0200	0000	0102	3603	0113
0300	0000	3402	3307	0115
0400	2603	3006	3211	0318
0500	3112	3216	3218	0422
0600	3413	0323	0118	0322
0700	3512	0223	0122	0425
0800	3412	0221	0119	0424
0900	3414	0220	3621	0328
1000	3411	0124	3619	0221
1100	3510	0123	0119	0221
1200	3609	0111	3612	0119
1300	3514	3515	3514	0117

* Direction, 170° and speed, 15 kt.

wind case, and generally 00 to 20° in the north wind case when comparing with the observed winds at the 266-m level of the tower.

During the period of the low-level nocturnal jet, the lowest level of the tower was in best agreement with the geostrophic winds, otherwise the top level was in best agreement during the south wind period. There was no significant difference between the agreements of the middle and top levels with computed surface geostrophic winds for the north wind case.

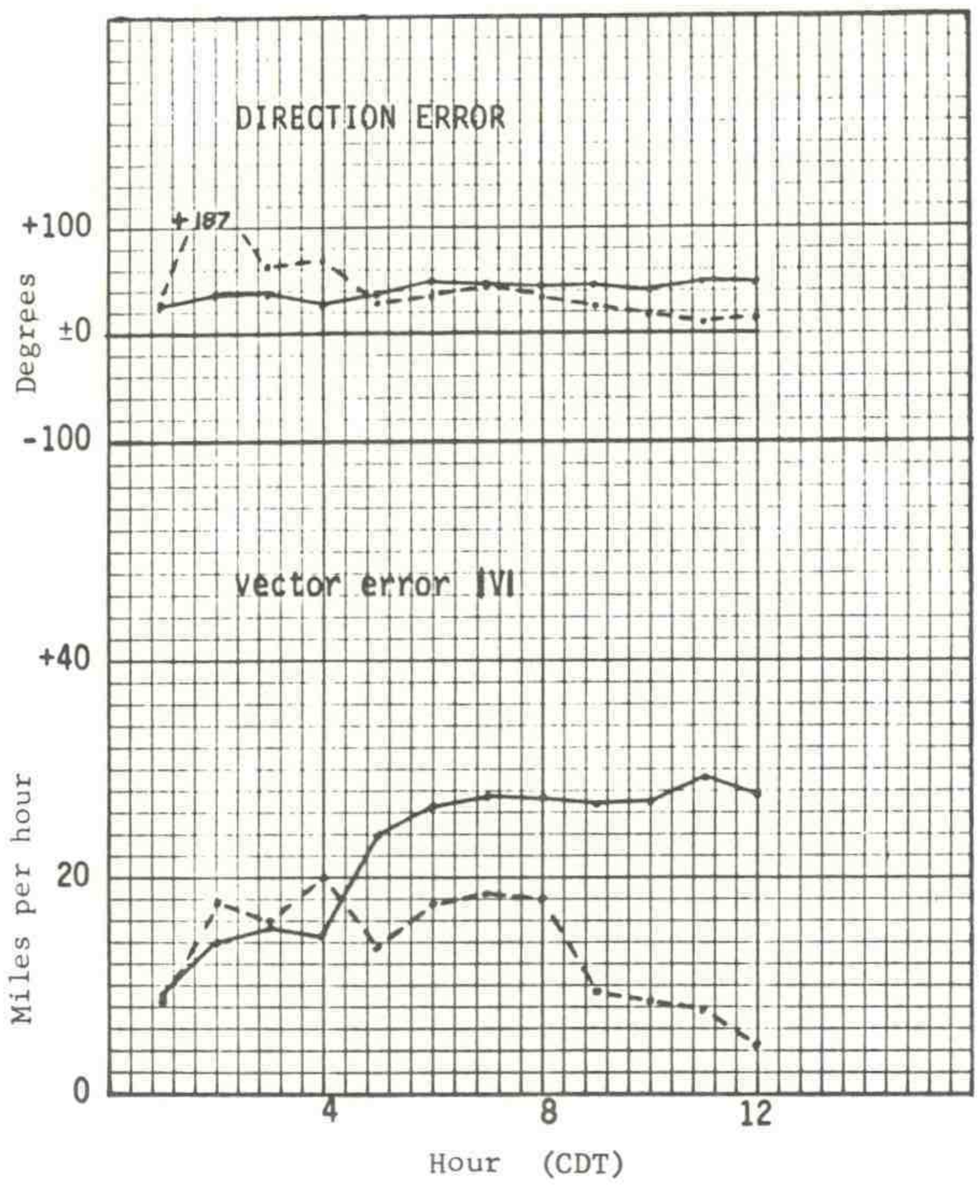

Figure 32. Difference of computed geostrophic wind from observed wind at Oklahoma City ($V_g - V_{Obs}$). Solid line — Oct. 1; dashed line — Oct. 9.

Certainly the data sample is very small, consisting of only two random cases, therefore, conclusions must be drawn with reservation. These results show large differences between geostrophic and observed winds and tend to confirm the intuitive suspicion that derived geostrophic winds are greatly different from derived mesoscale windfields for determining transport of material in the atmosphere. An important consideration in deriving transport is the grid interval of computation. In the mesoscale windfield studies, the interval was 8 km whereas, the interval for geostrophic winds was approximately 110 km. The large computational interval for the geostrophic winds precludes determining fine detail of the characteristic transport in the mesoscale. The differences in direction and speed of geostrophic winds when compared with the observed winds are almost certainly greater than the same differences with the mesoscale-derived windfield, even for grid points that are in juxtaposition. For the effort involved, and the degree of accuracy attainable, computed geostrophic winds appear to be an unadvisable approach to determining transport of material over a region only a few tens of kilometers square. Actual wind records from a single station, though inferior to a windfield derived from many wind stations, are of at least equal value to computed geostrophic winds in determining transport in the mesoscale.

8. AN APPLICATION OF THE MESOSCALE WINDFIELD METHOD

An historical data set of hourly wind records from several stations in a mesoscale area may be used to answer a number of questions. As an example, it may be desirable to determine how often air may move from a source 'S' to a small receptor area 'B' in 6 hr. At the NRTS, it was necessary to know how often mid-September daytime winds would move air northeastward from the CPP facility so that it would cross each of four 30° tracer-sampling arcs (the outermost arc being 100 km from the source). This must continue to do so for 6 hr and end by sunset. It was also necessary to know whether such successful cases are predictable 12 to 36 hr in advance for tracer-test planning, and whether prediction with almost certainty 1 hr in advance was possible for the initiation of the tracer release.

For the period of concern (September 11 to 22), frequencies of successful cases were determined by plotting daytime hourly trajectories for a 3-year sample for September 10 to 25. The first part of the 1969 sample is shown in figure 33. There were seven successful cases of a possible 48 in the 3-year sample.

Whether or not these successful cases could be predicted on the planning scale, that is, 12 to 36 hr in advance, required an examination of the synoptic weather charts associated with each case. Figure 34 is a composite of the 1200 GMT 500-mb charts on the days of success. The 41 remaining 500-mb charts were then scanned to see if any were highly correlated to the composite. This would not be a reasonable thing to do in every such experiment; however, the seven charts that were composited showed amazingly little diversity between them, and all appeared to belong to a definite pattern typified by the composite. The pattern was basically a zonal flow with the trough line somewhere between 120°W and 130°W. Five cases were found where the 500-mb chart was well correlated (by visual inspection) to the composite chart. In fact, the map of September 19, 1970, looks almost identical to the composite chart but was an unsuccessful case. The problem is to see whether the surface chart is able to be used as a discriminator between successful and unsuccessful cases where the 500-mb chart is well correlated to the composite chart of successful cases. It would consume much space for discussion and figures showing the 12 surface charts associated with the 500-mb charts of the composite 500-mb pattern and those that are well-correlated but belonging to unsuccessful cases. Suffice it to say, therefore, that pre-frontal; post-frontal; surface low pressure centers to the NE, E, SE, and S; and high pressure moving in from the NW, W, and SW were all connected with both the successful and unsuccessful 12 cases of well-correlated 500-mb charts. It appears that with the use of prognostic 500-mb charts, it is possible to give alerts 12 to 36 hr in advance for very nearly all successful cases; however, nearly 50 percent of the alerts will not materialize as successful cases.

The final step, namely the ability to accurately predict in the last 1 or 2 hr preceding its onset, whether or not a case will be successful

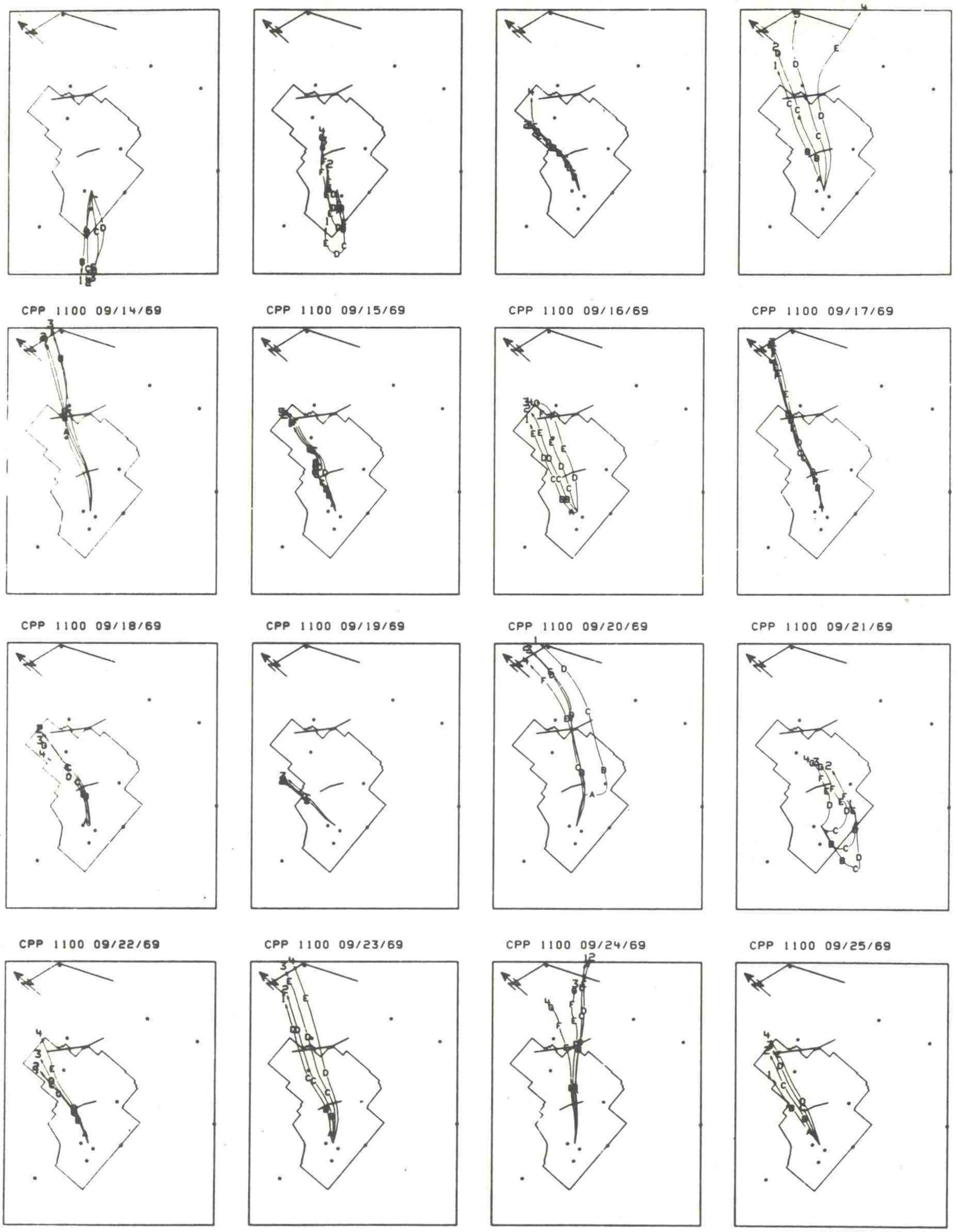

Figure 33. Series of four trajectories beginning from CPP at dates and times shown.

becomes essentially an ability to assess the persistence of the existing wind condition as shown by the mesoscale windfield.

Once the basic SW flow begins, the subsynoptic scale pressure gradients appear to be quite well correlated to the variations between S and W components. If pressures are quite low in SW Idaho relative to the upper Snake River Plains, the wind will invariably have too much southerly component to cross the arcs, as on September 18, 1969 (fig. 35). September 19, 1968, shown in figure 36, is a typical case of too much westerly component because of high pressure to the north. The final determination for the 1-hr prediction of success still depends upon having both a favorable flow pattern and an ability to monitor the mesoscale windfield.

In this study, we see the mesoscale windfield being used to determine successful and unsuccessful cases in a data sample, and finally being used in real time for subjective decisions.

9. LONG-TERM TRAJECTORIES DETERMINED FROM SINGLE- AND MULTI-STATION MODELS

Considerable effort has been expended to standardize the required calculations of environmental hazards for the safety analysis reports of proposed nuclear reactors, and to prepare environmental impact statements about industrial sources of a variety of atmospheric pollutants. Though models using all available wind records do exist, the standard calculations use a wind rose from a single station to determine frequency of transport in the various directions from a source. Because of characteristic turnings in the windfield and diurnal changes in the wind's character, the adequacy of a single wind record is rather limited. This study compares the long-term, two-dimensional distribution patterns of trajectories derived by the wind rose with the windfield determined from many stations. An earlier study (NOAA Tech. Memo. ERL ARL-32, 1971) lacked the needed data from a plains station and did not allow recirculation or extended dwell of air parcels being moved in the windfield. However, an idea of the divergence between the distribution patterns obtained from single station versus those of multi-station was established.

Simulated trajectories are derived on a computer from one release point in each of three geographically diverse regions: the NRTS, Los Angeles, and Oklahoma City. The method of determining the trajectory is that developed by Wendell (1972). In each of the three studies, one particle is released at the beginning of each hour, and advected for 12 hr, or until the trajectory leaves the grid, whichever comes first. The data samples were for September 1 to October 1, 1969, at Los Angeles; September 21 to October 12, 1971, at Oklahoma City; and 1969 at the NRTS.

The y-x computational grid units were 30 x 20 at the NRTS, 13 x 13 at Los Angeles, and 16 x 11 at Oklahoma City. The grid interval was 4.3 km at the NRTS, 5 km at Los Angeles, and 8 km at Oklahoma City. Smaller details may be resolved on smaller grids; however, the disparity in the

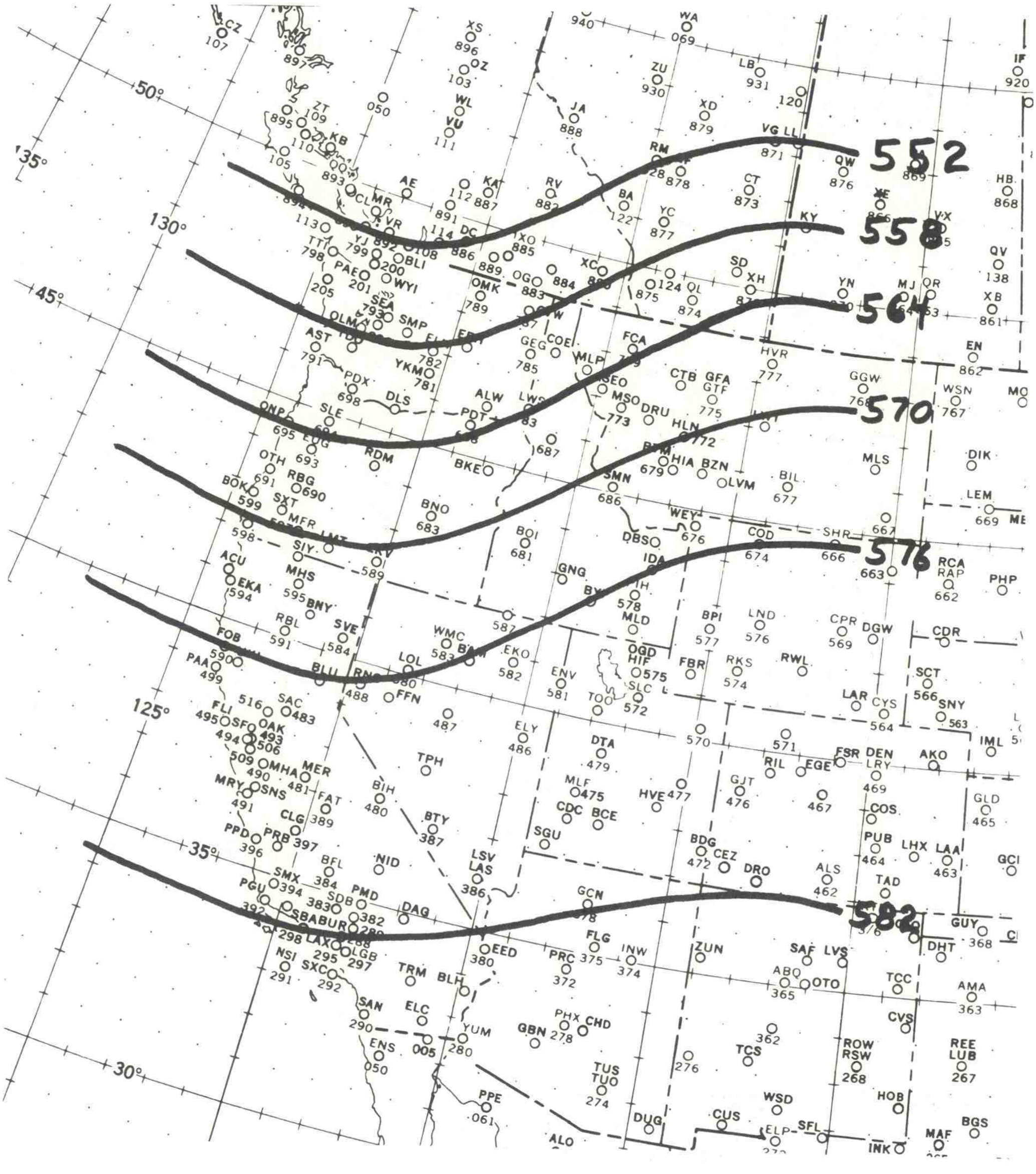

Figure 34. Composite 500-mb chart of 7 days resulting in favorable SW winds for testing on the long range diffusion test grids.

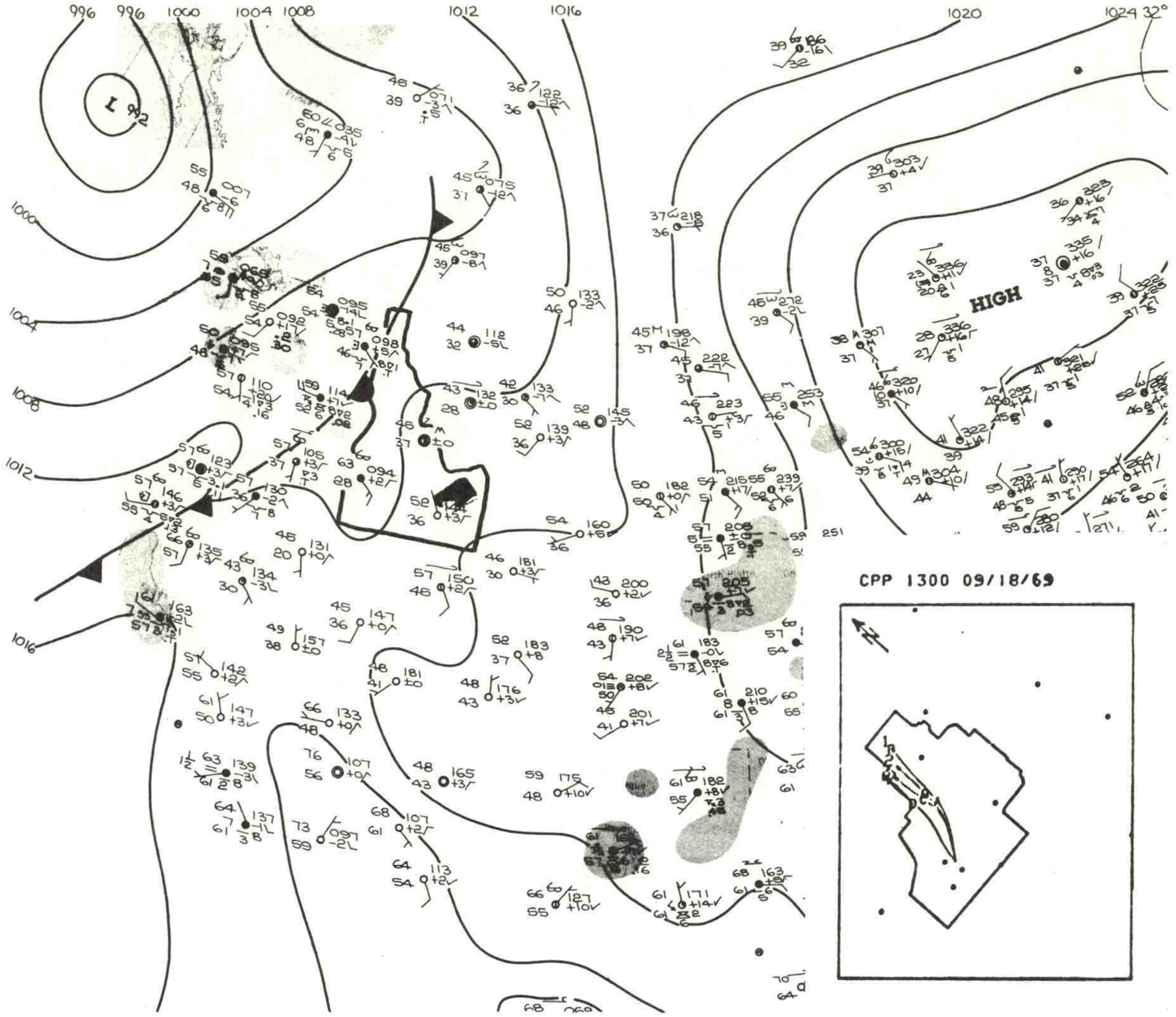

Figure 35. Surface chart analysis for 1200 GMT, Sept. 18, 1969, and associated set of four trajectories released from CPP starting at 1300 on the same day.

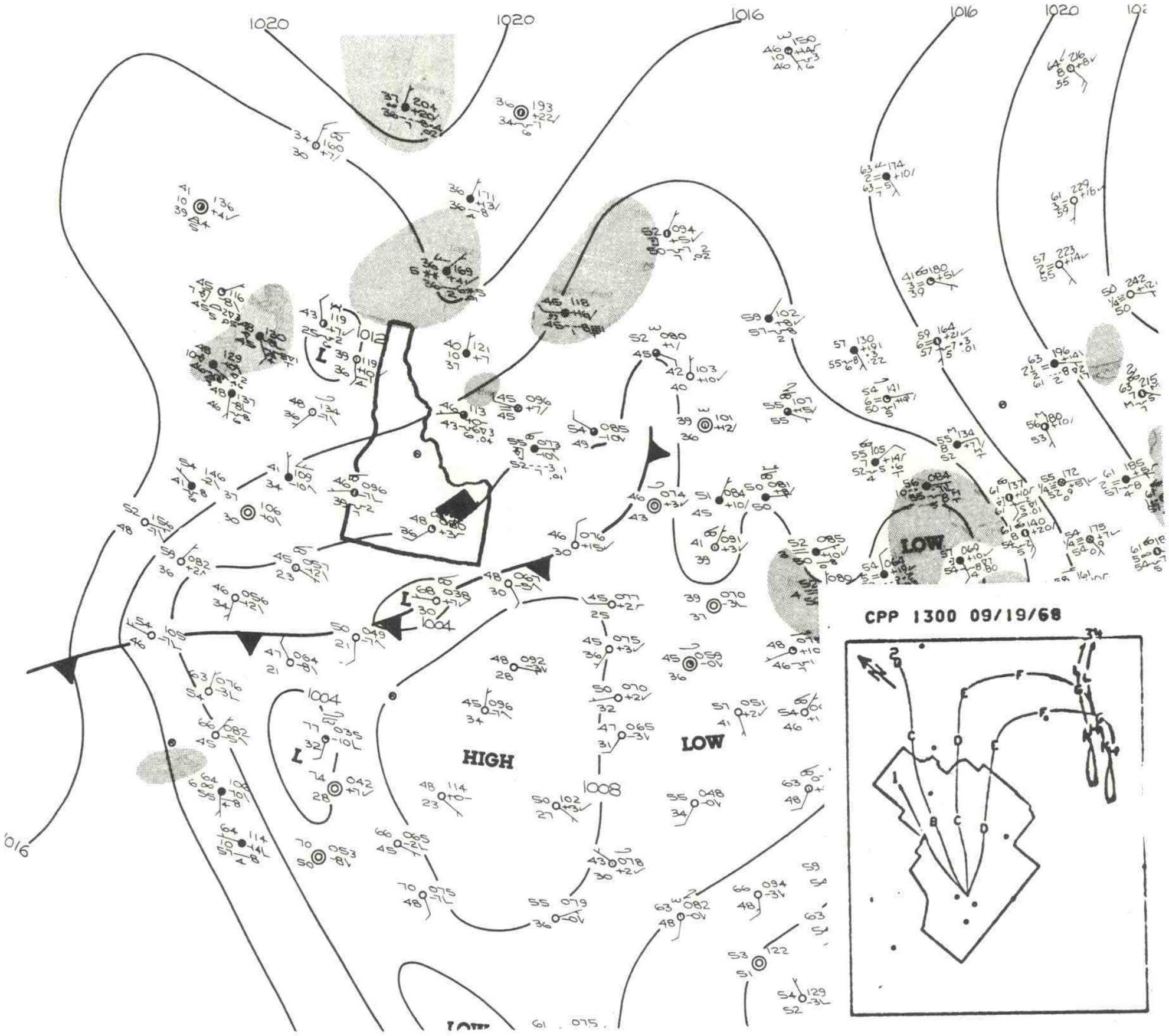

Figure 36. Same as fig. 35, except date is Sept. 19, 1968.

computational grids is insufficient to make any significant difference in the basic patterns of the transport statistics.

Two basic transport statistics are computed to compare the results of the contemporary "single-station" long-term dosage calculations with the same calculations using a windfield for transport. The single-station calculations of transport statistics are drawn from a wind rose that is composed of winds averaged over an hour for the period of record, while the windfield transport statistics are drawn from the derived trajectories. Note that what is being computed are "transport statistics" and not "dosage statistics," since no time-dependent function of dosage rate was used once the hypothetical particles were released.

Transport statistics using a wind rose are computed two ways. The first, called "wind rose transport statistics," is to simply determine the proportions of each direction ray that are intercepted by each grid square, and multiply the nonzero proportions by the frequencies for those rays. Figure 37 shows a typical grid square intercepting parts of two direction rays, about 50 percent of the 240° ray, which includes angles from 235° to 245° and about 40 percent of the 250° ray, which includes angles from 245° to 255°.

The frequencies are adjusted to account for winds too weak to advect particles as far out as a given grid square within the given time limit. For the advection time limit of 12 hr, a grid square whose center is more than 22 km from the source will not include 0.5 m sec^{-1} winds in the wind rose frequencies.

Before discussing the second approach to using the wind rose, the "windfield transport statistics" method should be explained. The windfield derived trajectories were interpolated for each 10-min time step exactly as in the studies already cited. For each 10-min segment of each trajectory, each grid square crossed or entered was given an incremental count. This method is only a step from computing dosage, because the final statistics reflect the total dwell time of trajectories over grid squares.

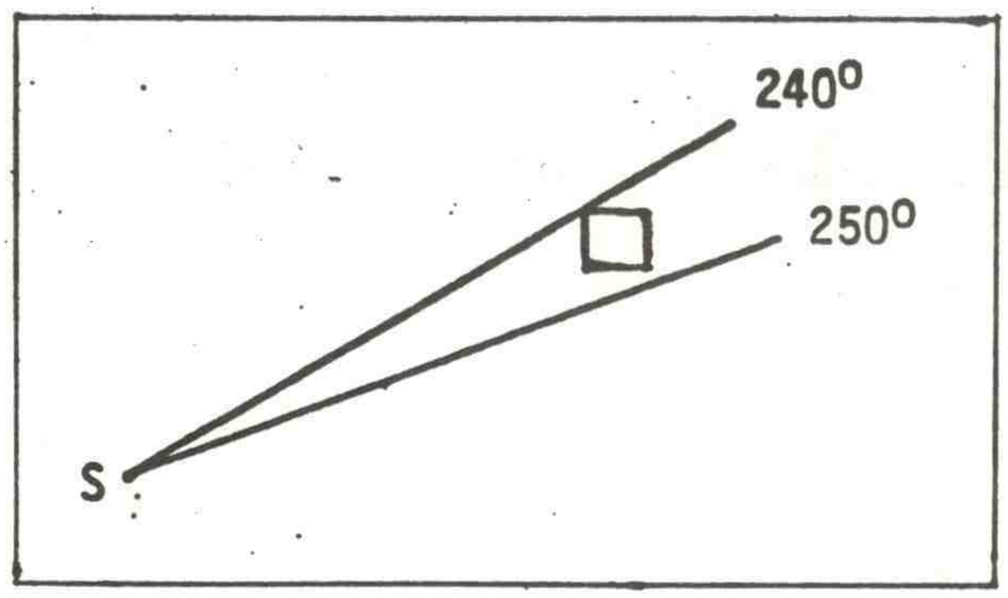

Figure 37. Grid square intercepting parts of two direction rays of a wind rose.

The second wind rose method is analogous to the windfield method in that it considers the total dwell time of a trajectory over a grid square. The wind rose was an s x d matrix, $_{s}WR_{d}$, where 's' is the number of speed classes and 'd' is the number of direction classes. The latter was 36 at the NRTS and Oklahoma City, but only 16 at Los Angeles. The number of speed classes was taken as 40, a class for each unit increment of speed in miles per hour up to 40 mph. All the cases belonging to a speed and direction class were advected simultaneously in 10-min steps, as with the windfield trajectories. To get a smoother contour pattern, the trajectories of each direction class were divided evenly over 1° sub-intervals and advections made for each of the 360 sub-intervals. Trajectory frequency was counted the same way as with the windfield. The method shall be called "wind rose - total hits analogy."

There is a boundary problem with the windfield computed statistics that results in an unfavorable comparison to wind rose computed statistics. The nearer the boundary, the larger the number of trajectories that in reality should have been recirculated over the grid, but could not be because they had been advected off the grid before the recirculation began. This results in a negative bias of counts in the windfield computed statistics; this is least near the center of the grid but may be very sizable near the boundaries, particularly if diurnal wind shifts are characteristic.

For each of the three geographical areas, five matrices of transport statistics were derived; windfield (WF), wind rose (WR), wind rose - total hits analogy (WRTHA), the ratio WR/WF, and the ratio WRTHA/WF. The two ratio matrices were normalized and smoothed before entering the computer contour plotting routine. Normalizing was accomplished by multiplying all matrix elements by the inverse of the value of the matrix element representing the pollutant source. The smoothing was accomplished with the operator $\phi_f = \phi_o + \alpha\nabla^2\phi_o$ (Dingle and Young, 1965). By repeated applications of different values of α, a very selective damping of short wave "noise" and nonamplification of longer waves may be accomplished. For this test, α was set equal to 1/8 and given only one pass. The resulting damping curve is shown in figure 38.

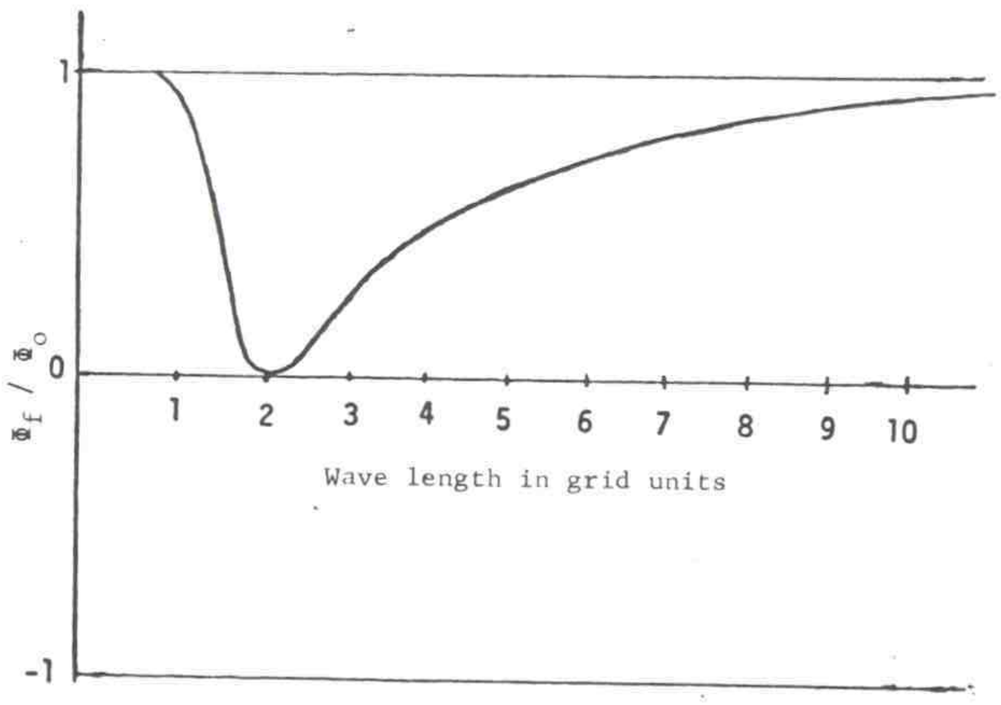

Figure 38. The damping curve for $\alpha = 1/8$ in the operator $\Phi_f = \Phi_o + \alpha\nabla^2\phi_o$.

The transport statistics matrices were then computer contoured with an overlying geography to give orientation and geographical references. The dimensions of the borders are 96 x 132 km at Oklahoma City, 68 x 68 km at Los Angeles, and 45 x 135 km at the NRTS.

The contoured patterns are shown in figures 39 to 41. Oklahoma City, centered on the WKY tower, is shown first because of the relatively good

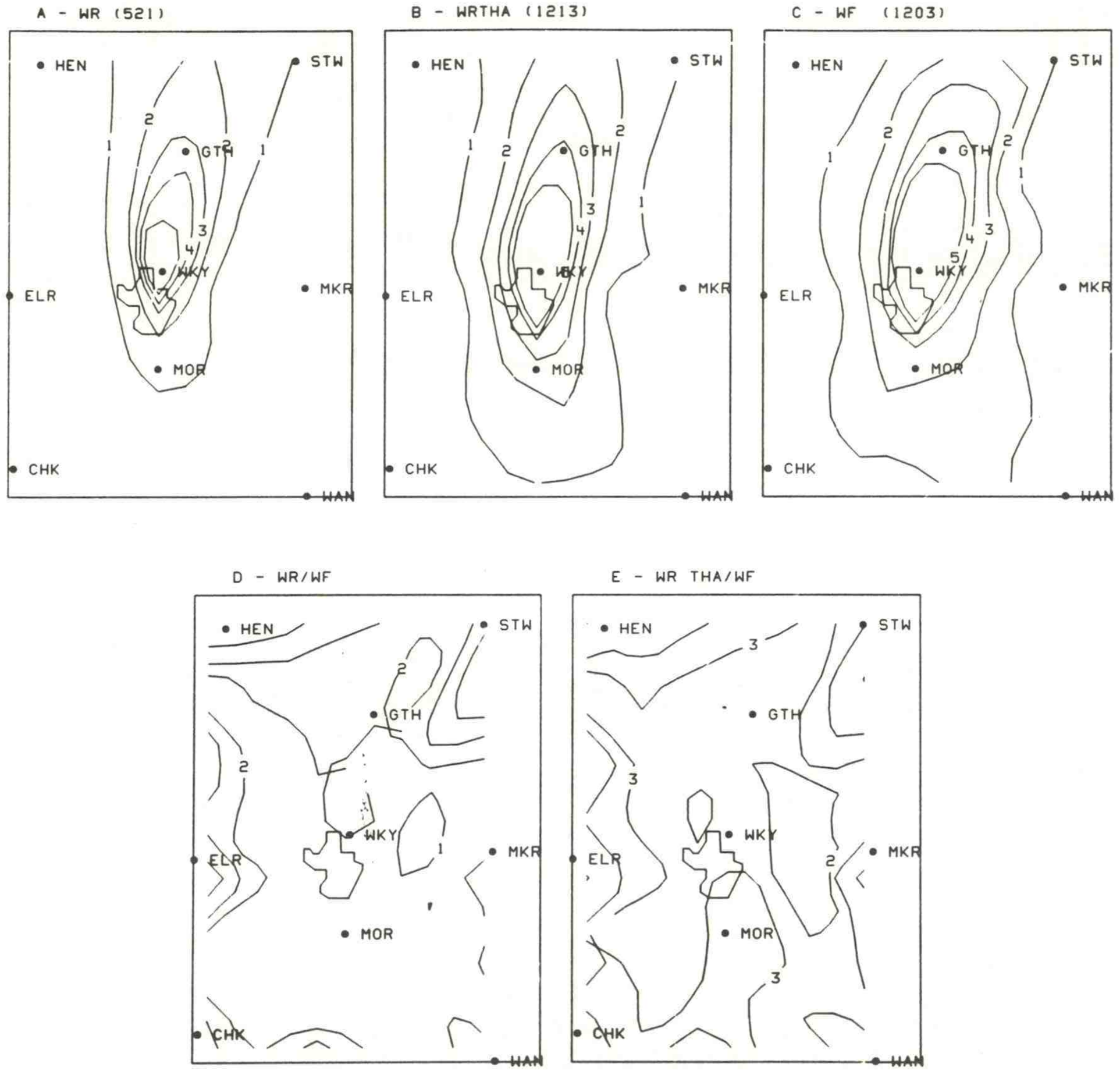

Figure 39. Total hits analysis for Oklahoma City. Advection is by WR - wind rose; WRTHA - wind rose total hits analogy; and WF - windfield. Panels D and E are the indicated ratios. The numbers in parentheses in panels A, B, and C are the values for the release square. The contours represent 5 to 25 percent in 5 percent increments of the release square value.

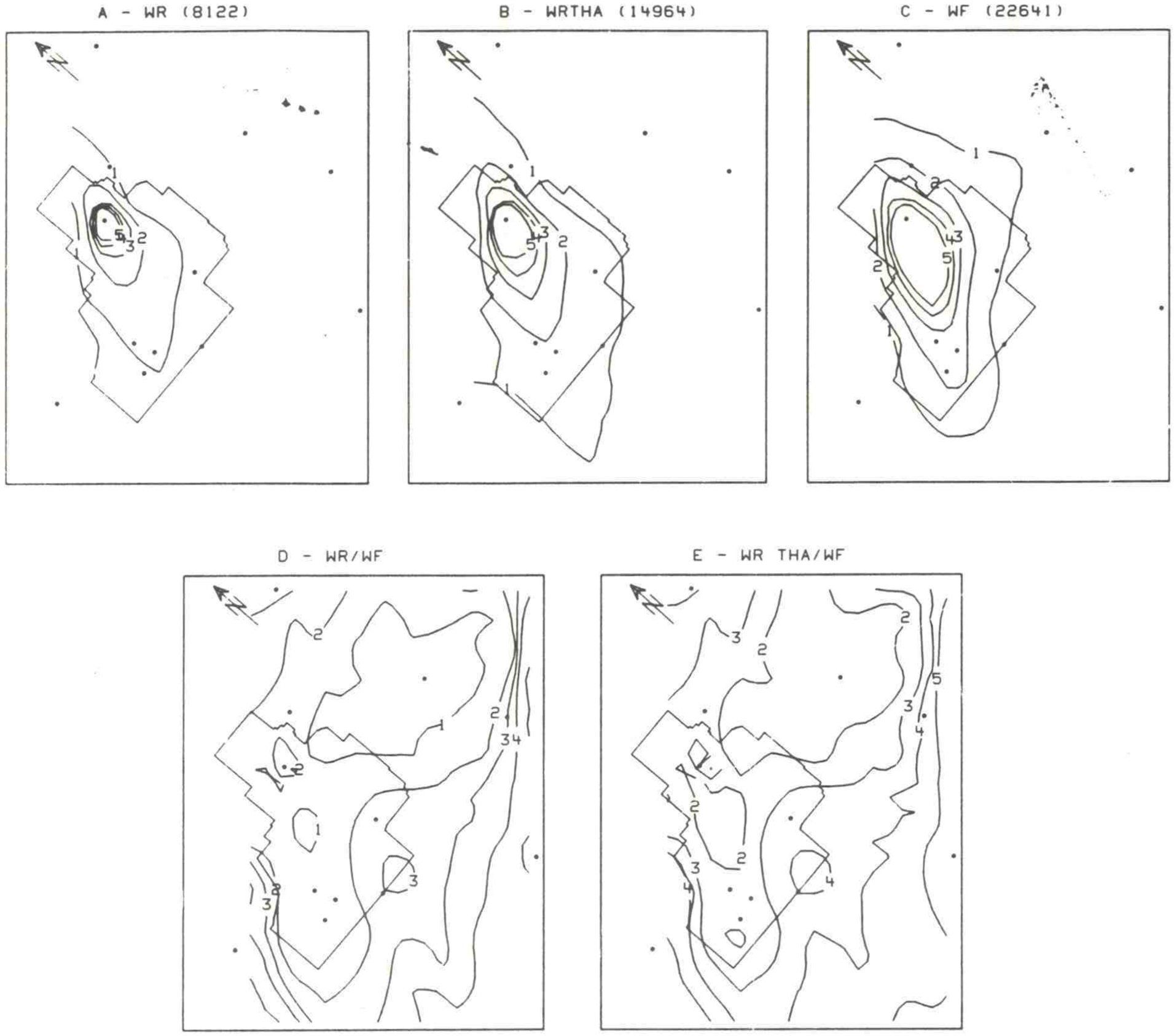

Figure 40. Same as fig. 30, except for release from LOFT at the NRTS.

correlation between patterns derived by single-station (wind rose) records and patterns derived by multiple station (windfield) records. The NRTS (fig. 40) centered on LOFT in the north, shows quite good correlation of single-station and multi-station results except for certain areas of characteristic events in the mesoscale windfield. The final set (fig. 41) shows the Los Angeles results centered on "F" near Long Beach where correlations of single-station and multi-station transport statistics are extremely poor.

If one inspects the trajectory patterns for an entire period of record, as done at the NRTS (Wendell, 1970), it is surprising that with the large number of individual cases that show characteristic turnings and recirculation, the wind rose transport patterns compare with windfield transport patterns as well as they do. Inspection of the daily sets of trajectories at Oklahoma City revealed a large percentage of days when trajectories had

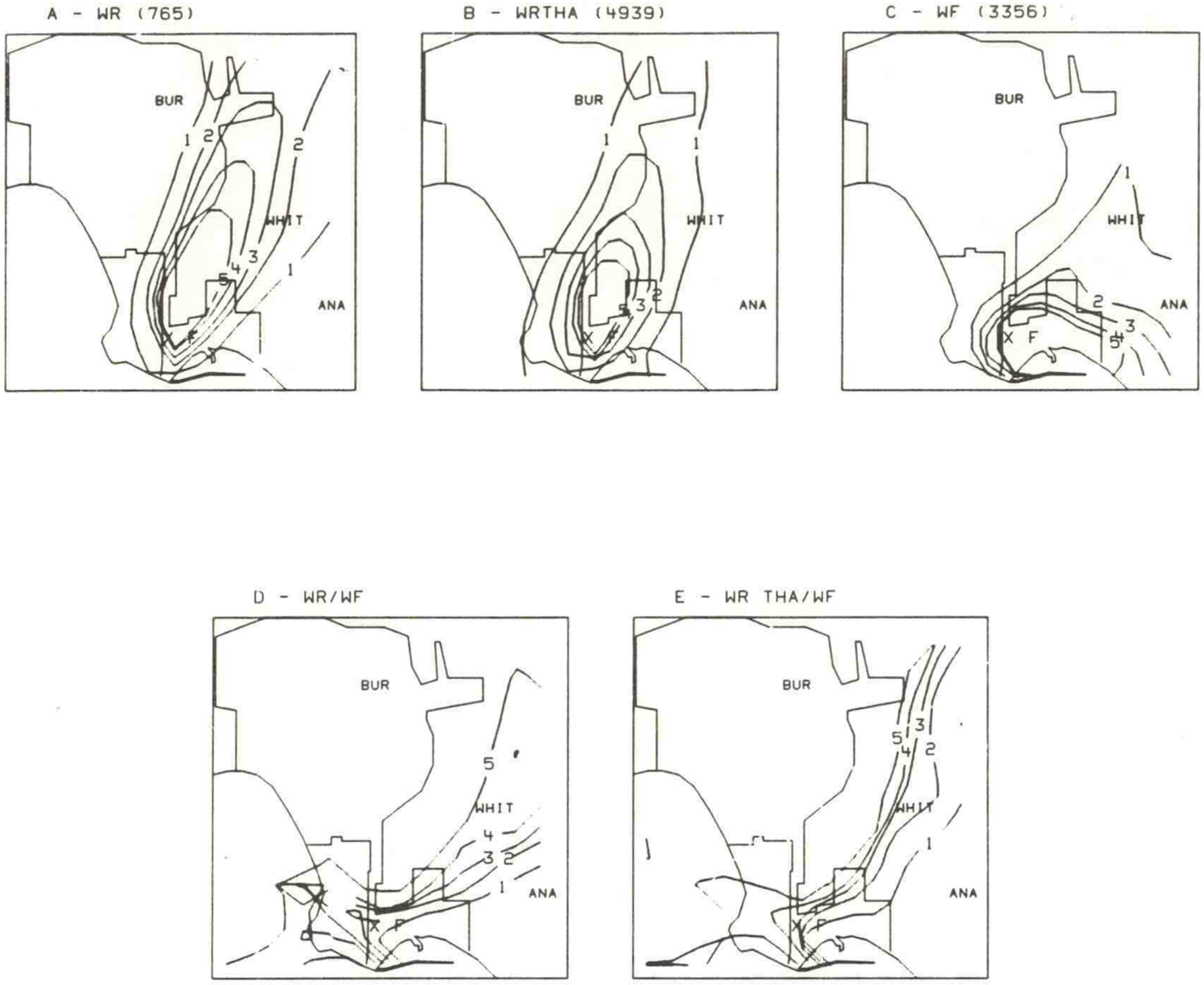

Figure 41. Same as fig. 30, except for release from 'point F' at Los Angeles.

curved patterns rather than straight. Apparently a strong tendency exists for veering, backing, or even direction-reversing trajectories to be replaced along their initial straight-line path by trajectories that started in other directions. Consequently, though large numbers of individual case studies show complex patterns of trajectory meanderings, there is a long-term statistical averaging of trajectories that reflects only characteristic perturbations in the mesoscale windfield.

At Oklahoma City, the model wind directions are SSW and NNW with nearly normal frequency distributions in the SSE through SW, and NNE through NNW. There are minor maximums for ESE and W winds. The southerly winds have the greatest average velocity, as noted by the shrunken contours to the north of the WKY tower on the WRTHA plot as compared with the WR plot. These shrunken contours would indicate either less dwell time, or higher velocities. The windfield plot shows the maximums at the north and south borders to be farther east than with the wind rose plots. A significant maximum also exists at the border directly east from WKY. This maximum is only vaguely suggested on the wind rose plots. The frequency minimum to

the NE of WKY on the windfield plot would indicate a tendency for SW winds to lack persistency, and shift more to southerly at times, or to shift from S through W to N with front passages.

The ratio patterns reveal how well the single-station patterns depict the windfield patterns. The WRTHA/WF ratio is the best of the two ratio patterns by reason of the use of "dwell time" in the computations of WRTHA. Ratios ranged from 80 to 120 percent within about 11 km of the WKY tower release point. Along the directions of primary flow, the ratios remained within 20 percent of unity all the way to the border. In the easterly directions from WKY, the ratios fell to as low as 40 percent at 16 km. This area was affected by several wind reversals. It means that at one point about 16 km east of WKY, the actual probability of hit or actual long-term dosage is at least twice as often as would be determined from a wind rose.

The NRTS transport frequency patterns show two particularly interesting features. The range of directions for N to E winds at LOFT is fairly uniform and results in a well-spread WRTHA pattern in the SW part of the grid. In reality, a strong channeling tendency exists that yields the narrower pattern seen on the windfield plot. The WRTHA/WF ratios are only 45 to 75 percent along the axis of the actual flow and become 150 to 200 percent — 8.24 km either side of the axis from the south part of the NRTS and continuing south. The second area of special significance is east of the NRTS boundary, at the latitude of LOFT, which is a known stagnation area in the middle of a converging counterclockwise circulation, which is typified by the windfield series shown in figure 42. The area affected is in the direction of a minimum in wind rose frequencies, while the stagnation effect is clearly shown in the windfield pattern as a pronounced maximum. The area about 24 km directly east of LOFT is characterized by WRTHA/WF ratios on the order of 33 to 45 percent. The area of ratios less than two-thirds extends nearly 65 km east of LOFT.

The diurnal wind reversals at the NRTS occur with such frequency that a major proportion of trajectories crossing any part of the upper Snake River Plain are what we call recirculated trajectories; that is, they have experienced a wind reversal. Hence, the boundary effect, which was discussed earlier, is especially critical at the NRTS and explains the rapid change in the ratios near the boundaries, especially the eastern and western boundaries which are not along the primary axis of flow.

The Los Angeles study is unique in that the chosen release point 'F' is 11 km WSW from the nearest wind station. In a plains location like Oklahoma City, this remoteness of the wind station from the release point would not be so serious so that wind rose frequency statistics could be calculated as though wind station and release point were in juxtaposition. At Los Angeles, it depends upon whether or not the remoteness means the two positions are in differently oriented parts of a characteristically curving flow. The release point 'F' is in the eddy behind the Palos Verdes hills that lie to the west. The characteristic on-shore flow at point 'F' is from the WNW-WSW, while the wind station 11 km to the ENE is

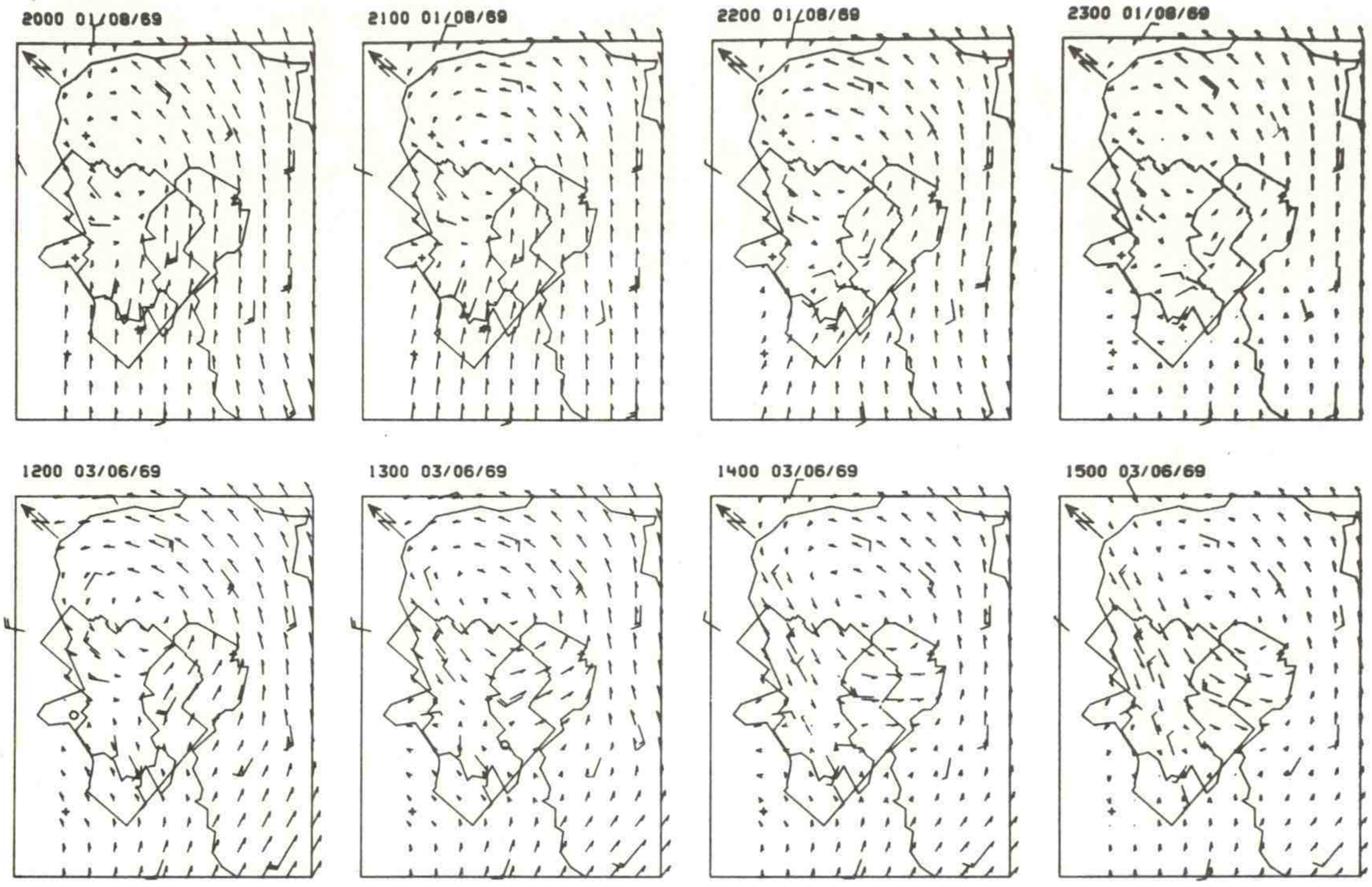

Figure 42. Series of windfield plots showing formation of large eddy, 2000 through 2300 MST, Feb. 9, 1969.

in the SSW sea breeze. The resulting wind rose is not representative of the prevailing winds at the release point, and consequently the ratios of wind rose and windfield statistics are almost exclusively very large or very small, and the wind rose transport statistics are misleading even within the first kilometer from the release point. This is an excellent demonstration of using an available wind record for a transport frequency study that is not only a poor guide, but also a completely misleading one.

There are some important conclusions that may be drawn from the investigations of wind rose versus windfield transport statistics at the NRTS, Oklahoma City, and Los Angeles.

1. In a real accident or emergency situation, the use of a single-station wind record for distances greater than those involving site evacuation should be in the hands of personnel experienced in boundary layer and small-scale flow. This is because the pollutant is being transported by a turbulent fluid with vertical as well as horizontal inhomogeneities and perturbations.

2. For estimates of maximum probability of hit in event of an accident, and for estimates of maximum long-term dosage, the wind rose may be a reliable indicator for distances to something like 80 km, providing no geographical features are encountered

that would induce characteristic changes in wind direction. There is likely to be a slight difference in direction between reality and the wind rose, as was the case at Oklahoma City, so that at 80 km the uncertainty in the position of the maximum is 32 km in either direction along the arc; 32 km represents about 20° in direction from the source at the 84-km arc.

3. For general estimates of probabilities of hit during an accident and for long-term dosages, there are so many uncertainties in geographical effects and characteristic small-scale meteorological features that reliable distributions may be estimated to only something like 24 km at a plains station, and only a couple of kilometers for a station near a barrier or seashore, which could cause great horizontal discontinuities in wind direction.

These studies do establish a need for caution in taking single-station wind records to determine long-term patterns of probabilities of hit and dosages.

10. LONG DISTANCE TRANSPORT AND DIFFUSION TO 100 KM

A need exists to understand transport, diffusion, and plume depletion effects upon airborne material carried out to about 100 km and lasting for many hours. Extensive diffusion measurements have been painstakingly made in the past couple of decades and have been summarized and reported by many authors (e.g., Heffter, 1965; Slade, 1968). In general, these measurements have described diffusion at the shorter distances or have dealt with large instantaneous sources at long distances, high altitudes, or both. The intent of our study was to improve understanding of the transport and diffusion of quasi-continuous effluent releases dispersed within the planetary boundary layer.

At the initial stages of such a measurement program, the most reliable course of action seemed to be one that would include several simultaneous types of measurements (a) to determine the consistency of the different measurement techniques, (b) to combine the complementary data types to gain a more complete overview of the effluent behavior, and (c) to identify and emphasize data measurements that appeared to be the most vital ones. At the beginning of such a study, it is crucial to directly measure effluent concentration in order to evaluate the effective plume trajectory and dilution. The key information available from this testing was the measurement of tracer ground-level concentrations of successive distances downwind. Based on these measurements, the downwind change of relative axial concentration and lateral tracer dispersion could be examined. Along with these direct tracer measurements, this testing included unique, simultaneous measurements of low-level winds from an encompassing network of tower-mounted wind sensors and trajectories from serially released tetroons. The information presented illustrates the successful field implementation of a unique combination of complementary and valuable measurements that

could be a useful technique for achieving a better understanding of regional dispersion of airborne material.

Two field tests have been conducted to date. The first test (NOAA Tech. Memo. ERL ARL-32, 1971) was of limited use because of the presence of a wind shear or discontinuity zone across the sampling grid some 40 km downwind. The second test, conducted on August 31, 1971, was highly successful and illustrates comparisons of the various transport and diffusion estimation techniques. A third test was aborted due to the failure to achieve suitable testing conditions.

The measurements described in this study were conducted over the Upper Snake River Plain in southeastern Idaho at the NRTS and adjacent areas. The Upper Snake River Plain is approximately 1500 m above sea level and is enclosed by mountains that rise 1200 to 1800 m above the valley floor along all but the southwestern edge of the rectangular study area. The irregular boundary in figure 43 outlines the NRTS.

The tracer used in this investigation was methyl iodide gas labeled with the radioisotope iodine-131. This technique was developed and used during a limited number of diffusion comparisons with uranine dye and molecular iodine gas for downwind travel distances less than 3.2 km (Start, 1970). This gas is chemically inert, for practical purposes, and allows a control of plume depletion due to dry deposition. Sampling checks have not revealed a tendency for ultraviolet decomposition of the methyl iodide into reactive (depositing) iodine species. Time integrated air

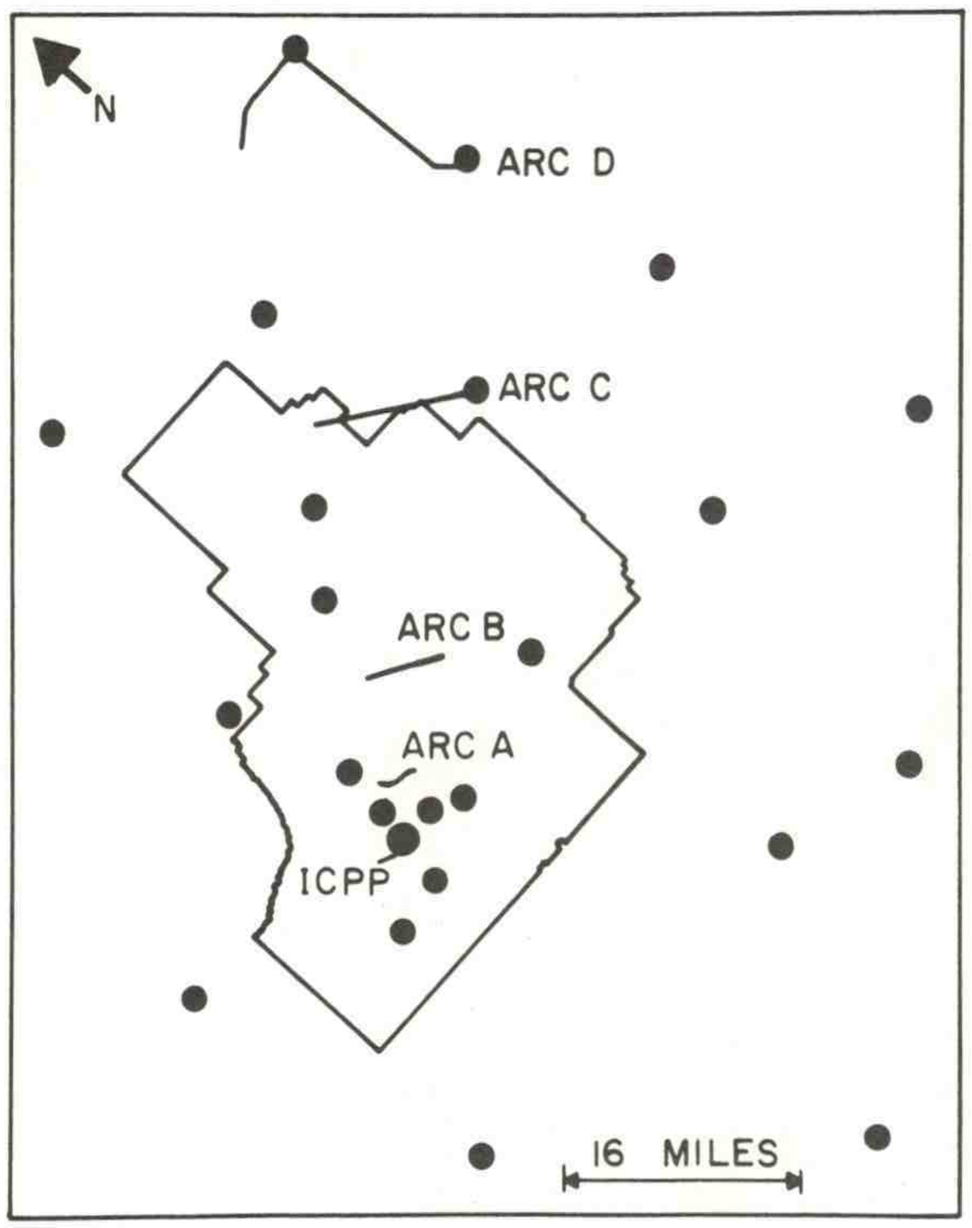

Figure 43. Field measurement area with wind tower locations (dots) and tracer sampling arcs (A, B, C, and D). The tracer release location is designated ICPP.

samples were collected by a network of high volume air samplers, each loaded with an iodine impregnated charcoal cartridge and a glass fiber type prefilter. The sampler collection efficiency for methyl iodide was 0.75. Four sampling arcs, with from five to eight high volume air samplers per arc, were located at approximately 6, 19, 48, and 80 km downwind. Iodine-131 in the samples was qualitatively and quantitatively identified using gamma spectroscopy and conventional well scintillation counting techniques. Methyl iodide gas was released for 65 min from the 76-m stack at the Idaho Chemical Processing Plant.

Twenty-four tower-mounted wind sensors were operated within the rectangular area of figure 43. Wind directions and speeds measured at somewhat randomly located tower sites within the grid were interpolated to a rectangular mesh of points. Calculated trajectories were derived from these "windfields" for comparison with observed plume centerline positions and tetroon trajectories.

A transponder-equipped tetroon was released about $1\frac{1}{2}$ hr before the methyl iodide release. Other such tetroons were launched at the beginning of the release and at approximately 20-min intervals during the ensuing hour. In all, five tetroons were launched. The tetroon-transponder flights were tracked by a M-33 radar. Since a single radar was following several tetroons at the same time, positioning of individual tetroons was accomplished about once every 5 min. Detailed tracking information was not determined from any one tetroon; rather; the general position of each one was determined so that the lateral and vertical envelopes of their positions for the series of launches could be estimated. The tetroons remained within 600 m of the surface much of the time. All tetroon positions during vertical height oscillations dipped to within 1600 m of ground level. The Boise radiosonde data and the 700 and 500 mb analyses for 1200 GMT on August 31 and 0000 GMT on September 1, 1971, were examined. From this information and the surface temperatures in the test area, a maximum adiabatic mixing depth of 1400 m was estimated. This value was similar to the 1600-m depth that contained the tetroon oscillations.

Normalized axial concentrations versus downwind distance were plotted in figure 44. NRTS curves for stability classes B and C are plotted for reference. The methyl iodide decrease of slope with distance — a decrease that was not explained simply by sampling inaccuracies or the occurrence of the peak concentrations at positions between samplers — should be noted. Two additional curves, those labeled C_{LID} and B_{LID}, are shown to illustrate the effect upon the climatological curves if vertical tracer dispersion were confined within a layer 1400 m above ground level. These two additional curves are discussed later.

Lateral standard deviations measured for methyl iodide were plotted versus downwind distance in figure 45. The NRTS curves for uranine dye (Yanskey et al., 1966), labeled for stability classes B, C, and D, are included for reference. Statistically, the methyl iodide slope was the same as the NRTS slopes of 0.85.

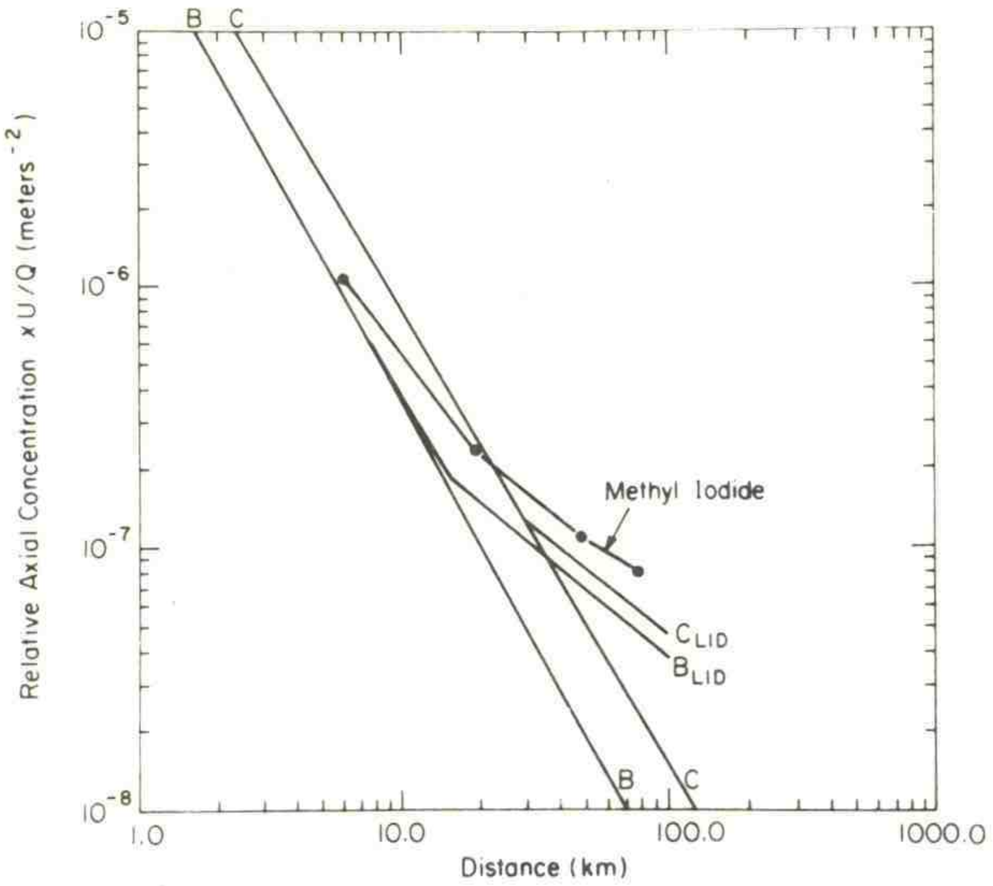

Figure 44. Methyl iodide measurements and NRTS climatological curves of relative axial concentrations versus downwind distances.

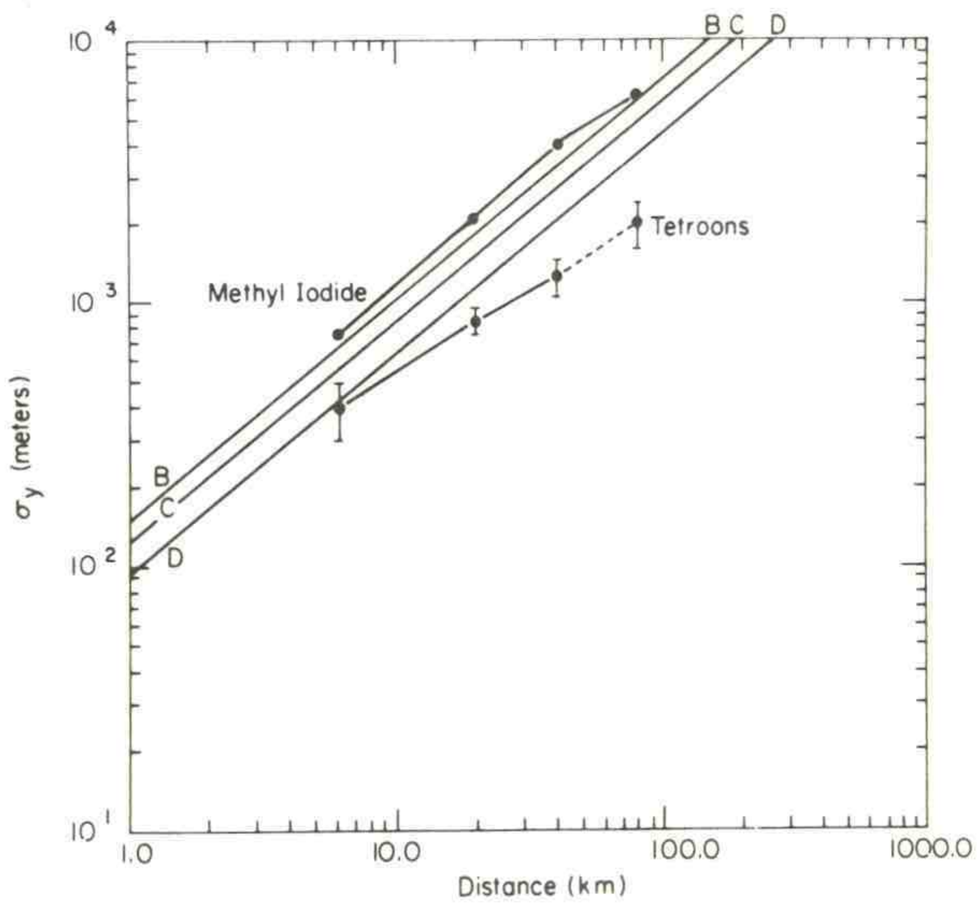

Figure 45. Lateral dispersion values from NRTS climatology, methyl iodide measurements, and approximations from envelopes of tetroon trajectories.

The horizontal trajectories derived from the tower wind measurements are compared with the tetroon flights (fig. 46). A tetroon trajectory is not plotted for a release time of 1430 MST (the beginning of the methyl iodide release). This flight ended about 60 sec after launch. Letter symbols are located along the plotted trajectories at successive 15-min intervals, with times for windfield derived trajectories denoted by upper case letters and tetroon times denoted by lower case letters. The tetroon positions generally led the corresponding calculated trajectory positions by a few kilometers (in agreement with pibal observed wind speeds

(A) 1303 08/31/71

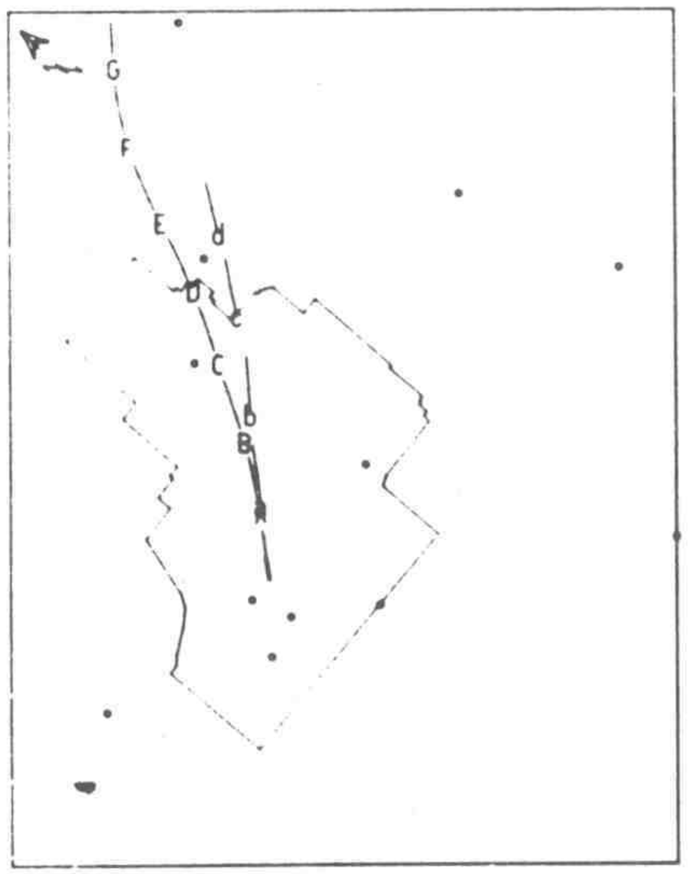

(B) 1430 08/31/71

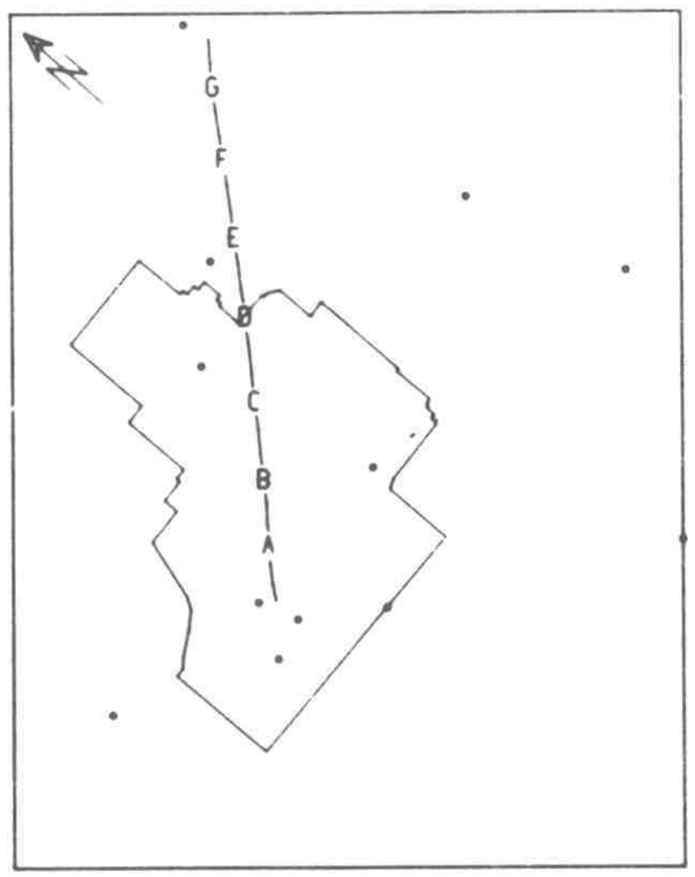

(C) 1444 08/31/71

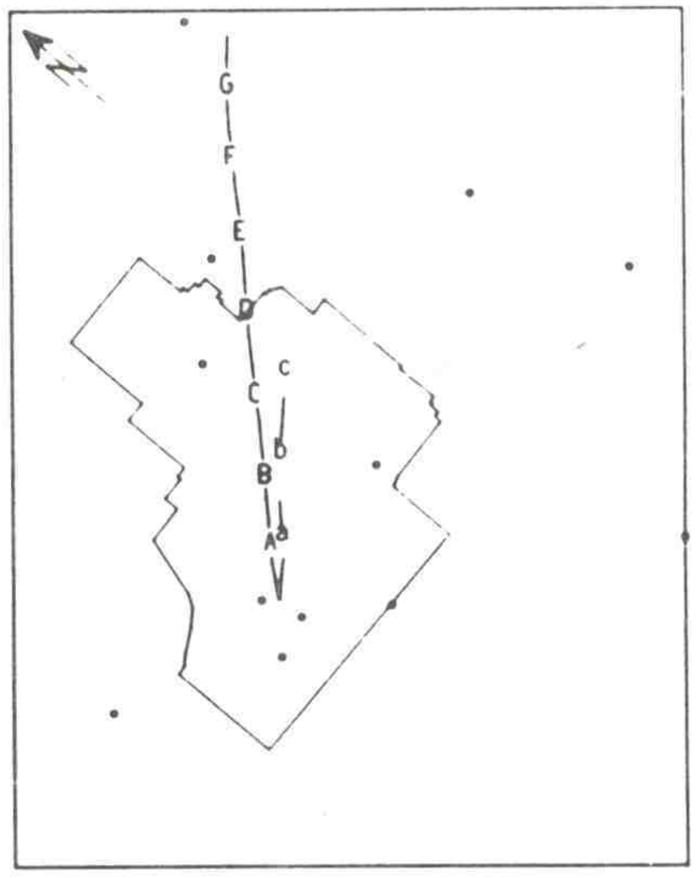

(D) 1507 08/31/71

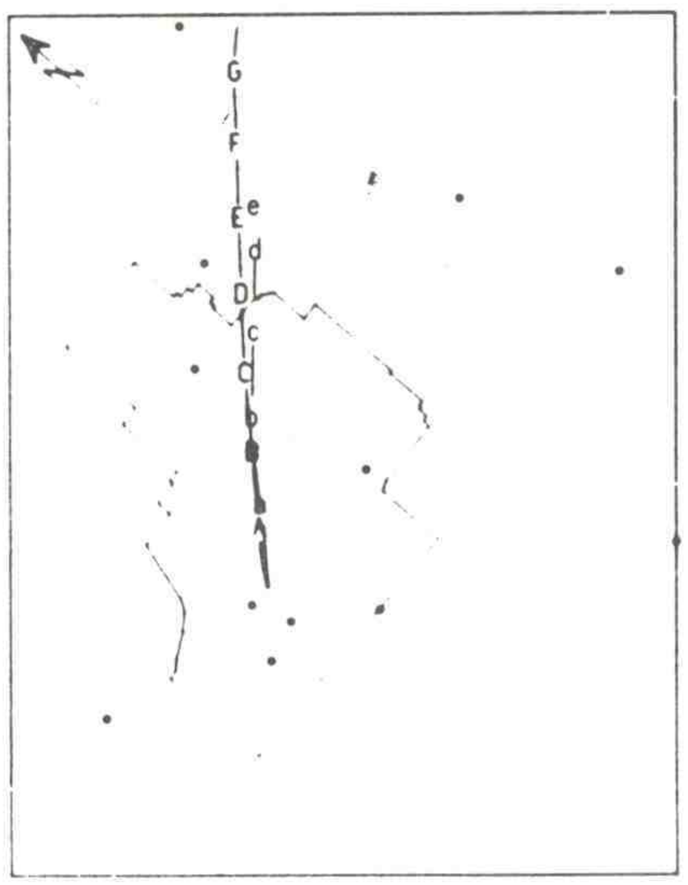

(E) 1539 08/31/71

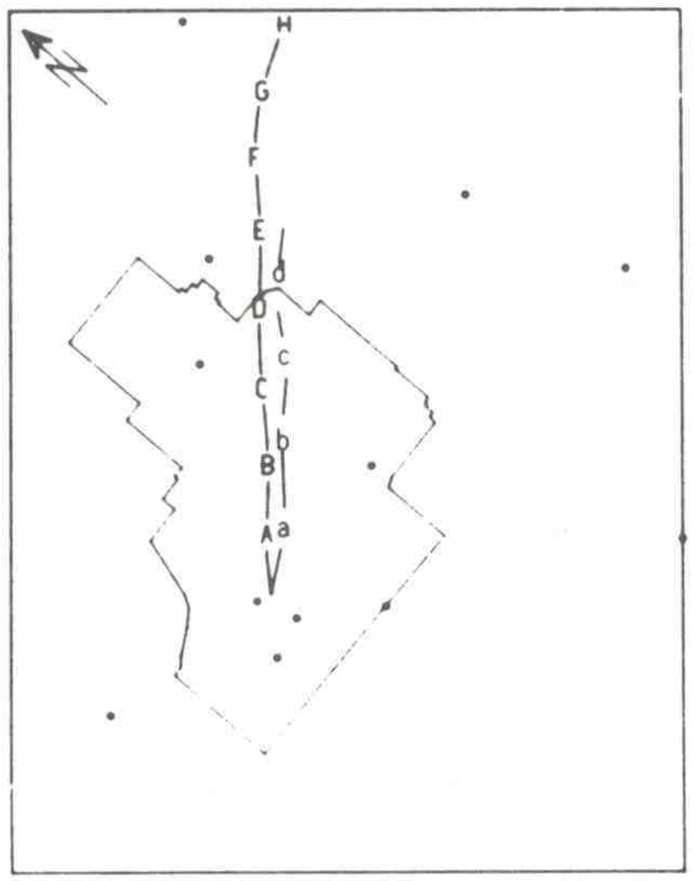

Figure 46. Paired horizontal trajectories at 15-min intervals for tetroons (lower case letters) and windfield advected (upper case letters) hypothetical particles. Trajectory beginning times are listed above each plot.

2 to 3 m sec^{-1} greater at tetroon flight altitudes). In every case, the tetroon trajectories deviated to the east of the windfield-determined trajectories. The smallest lateral separation between a windfield-derived trajectory and a tetroon trajectory occurred for the flight begun at 1507 MST. This tetroon consistently flew at lower altitudes for more time than any other tetroon in this series.

The angular displacements between windfield and tetroon trajectories were on the order of 5°. Pibal winds within the first 800 m above the surface supported a wind direction turning consistent with this separation. These same trajectories are shown in figures 47 and 48. In figure 47, all tetroon trajectories are plotted together. The dashed line is the windfield determined trajectory computed at the same time as tetroon release No. 2. This dashed line seems to be a reasonable estimate of the extreme northwestward position of the tetroons. Open circles were plotted to note the points of peak sampled methyl iodide on each arc. At 6 km, the windfield derived trajectories (fig. 47) may be the best locaters of the peak concentration; at greater distances the tetroons were best (fig. 48).

To convert the trajectory data into a form similar to methyl iodide lateral dispersion, we arbitrarily assumed that the lateral width of the envelope of the trajectories contained 95 percent of all the possible trajectories that might have occurred in this period, or in other words, that they represented $\pm 2\sigma$ about the (undefined) mean. There is no justification for this assumption, although intuitively it seemed reasonable. Although it rendered the absolute values of the plume spread suspect, the

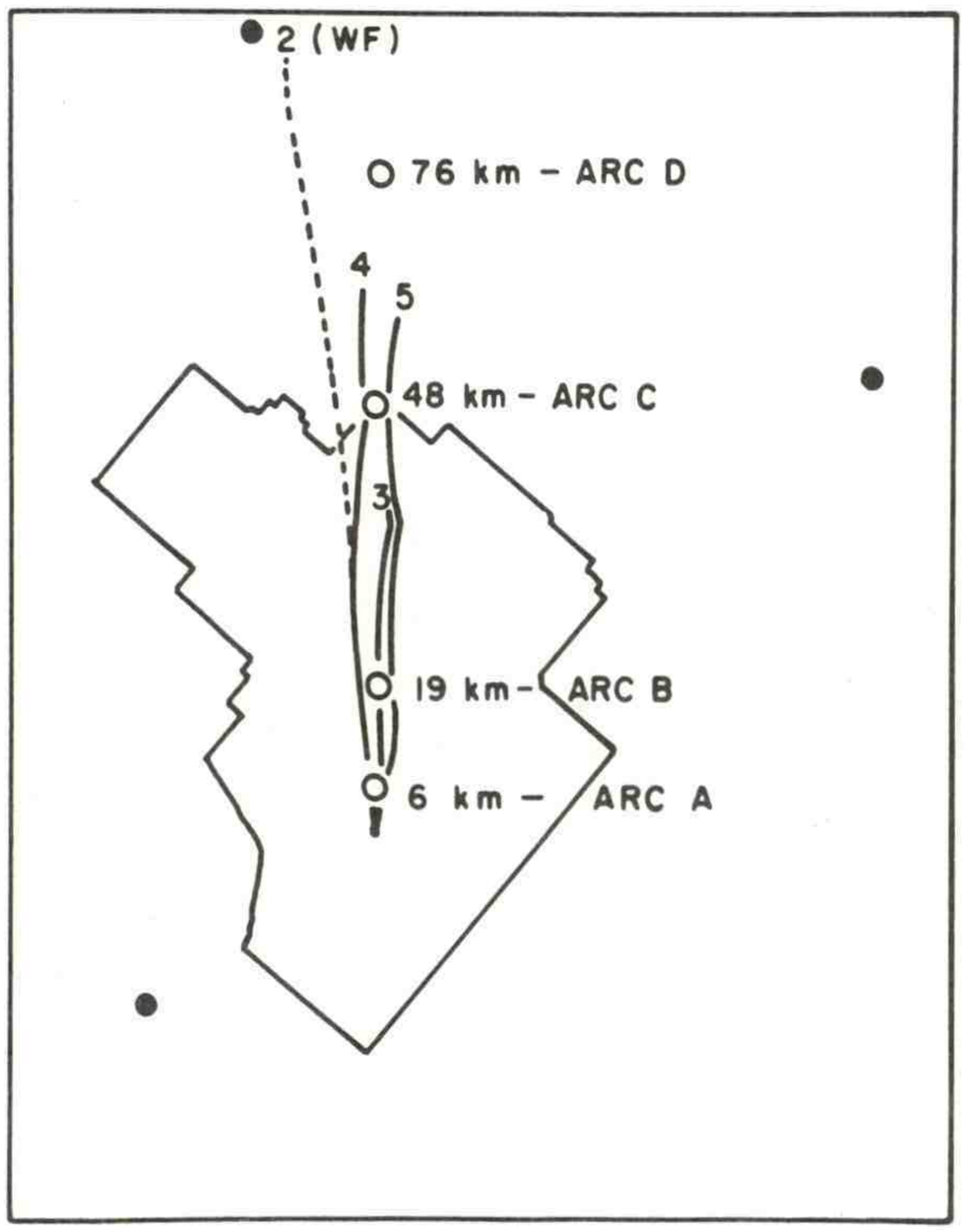

Figure 47. Composite plot of tetroon trajectories No. 3, 4, and 5. Dashed line locates windfield derived trajectory beginning at 1430 MST. Locations of peak-measured methyl iodide concentrations are denoted by open circles.

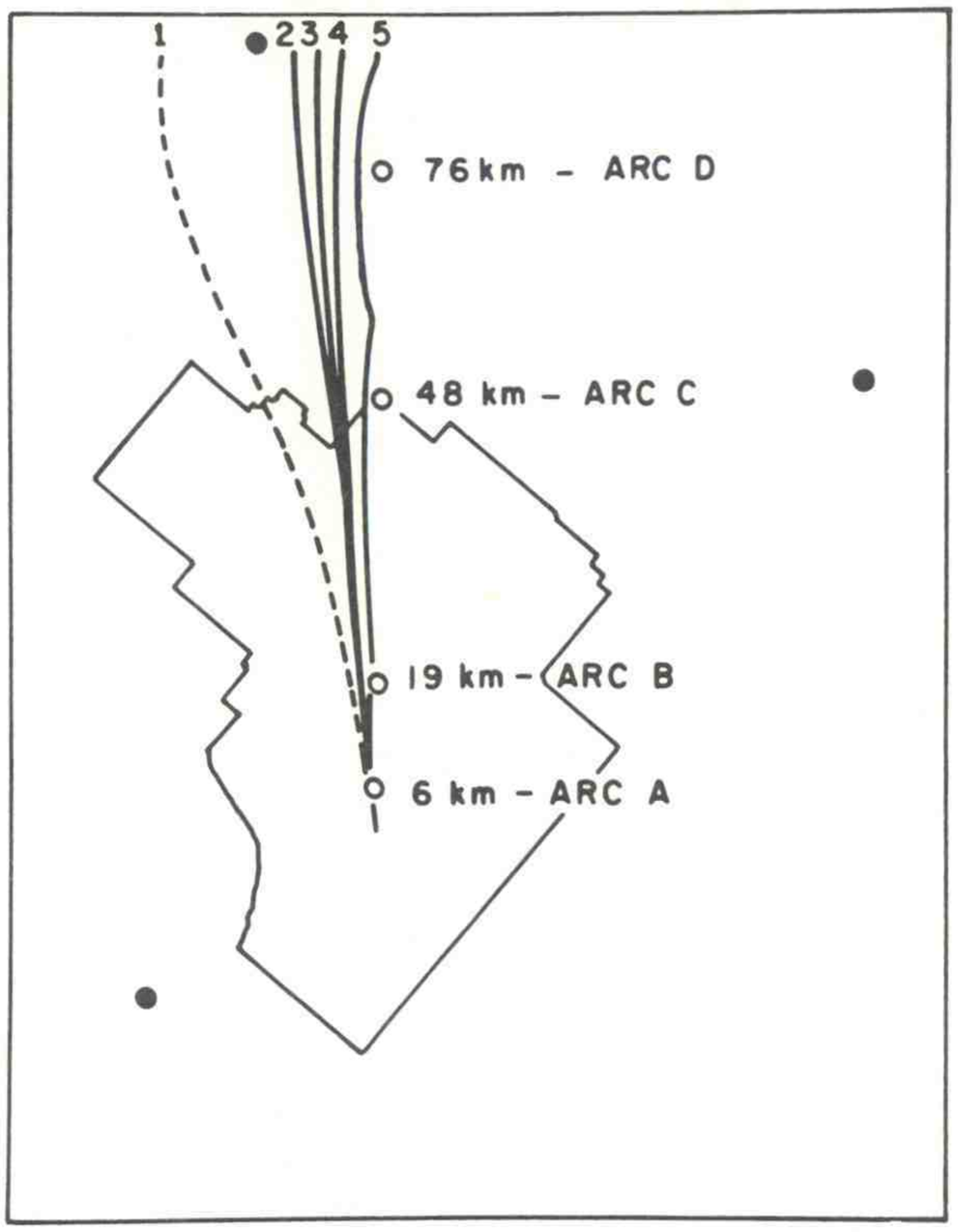

Figure 48. Composite plot of windfield derived trajectories. Dashed line locates trajectory for 1 hr before the methyl iodide release. Locations of peak measured methyl iodide concentrations are the open circles.

rate of spreading was unaffected by the particular choice of numerical σ value. The line in figure 45 labeled tetroons is a plot of these envelope widths after division by four. Since all of the tetroons were tracked short of arc D at 76 km, the data point at 76 km was estimated from extrapolations from the last trajectory end points. The vertical lines through these points illustrate the maximum variability likely from uncertainties in defining the edges of the envelope of tetroon trajectories. When the variability at each point was considered, the slope of these tetroon-derived σ_y values did not significantly differ from either the NRTS curves or the methyl iodide measurements. The envelope-derived values are a factor of 2 to 3 less than the methyl iodide measured lateral dispersion. In the study of tetroon trajectories in the Los Angeles Basin, the trajectory envelope width divided by 4 estimated the lateral dispersion determined by the running mean variance statistic (Pack and Angell, 1963). This systematic difference, always found to be less than a factor of 2, may explain some of the differences in σ_y values. When figures 47 and 48 were reexamined, an interesting σ_y feature was noted. When the envelopes of windfield and tetroon trajectories were superimposed, the width of the combined envelopes was $1\frac{1}{2}$ to 2 times wider than the individual envelopes at the longer distances. The average difference in angular bearing of the trajectories (and their envelope means) was close to 5°. If lateral dispersion was reestimated from the pooled envelopes of trajectories, values of σ_y approaching the methyl iodide measurements resulted. These systematic differences in the near surface windfield trajectories and the corresponding tetroon trajectories suggested the effect of vertical wind direction shear. Five sequential pibal observations, made at the release

point and moving with the plume, substantiated a wind direction change of this magnitude with height.

Limiting σ_z (the standard deviation of the vertical effluent concentration) to 80 percent of the depth of the mixing layer (Pasquill, 1962), a maximum σ_z of 1120 m resulted. When the effects of the vertical lid were incorporated to modify the rate change of normalized axial concentrations with distance (Smith and Singer, 1966), a slower rate of dilution resulted. When the value of 1400 m for the lid was used to modify the curves in figure 44 for NRTS stability classes B and C, the value of σ_z became a maximum at 15 and 29 km, respectively. The effect of a lid appeared to reasonably account for the observed slower rate of dilution.

Assuming a ground source (h = 0) and solving (6) for σ_z,

$$\sigma_z \text{ (effective)} = \frac{Q}{\pi U \sigma_y} \frac{1}{\chi_p} , \qquad (12)$$

where Q is rate of tracer release, U is the effective wind speed, χ_p is the measured (methyl iodide) peak axial concentration, and σ_y is the standard deviation of methyl iodide in the lateral direction. Figure 49 shows the calculated effectuve σ_z values for methyl iodide. The line labeled tetroons represents the values of σ_z estimated from the envelope of lateral spreading of tetroons. Since the tetroon envelope derived values of σ_y had been shown to systematically underestimate lateral spreading, the calculated effective σ_z would obviously be an overestimate. This deviation from tracer-derived estimates should not be viewed as a failing of the tetroons; instead, it illustrates the crude (consistent) estimate possible by using only horizontal, unadjusted information. NRTS curves of σ_z for stability classes B and C are plotted for comparison.

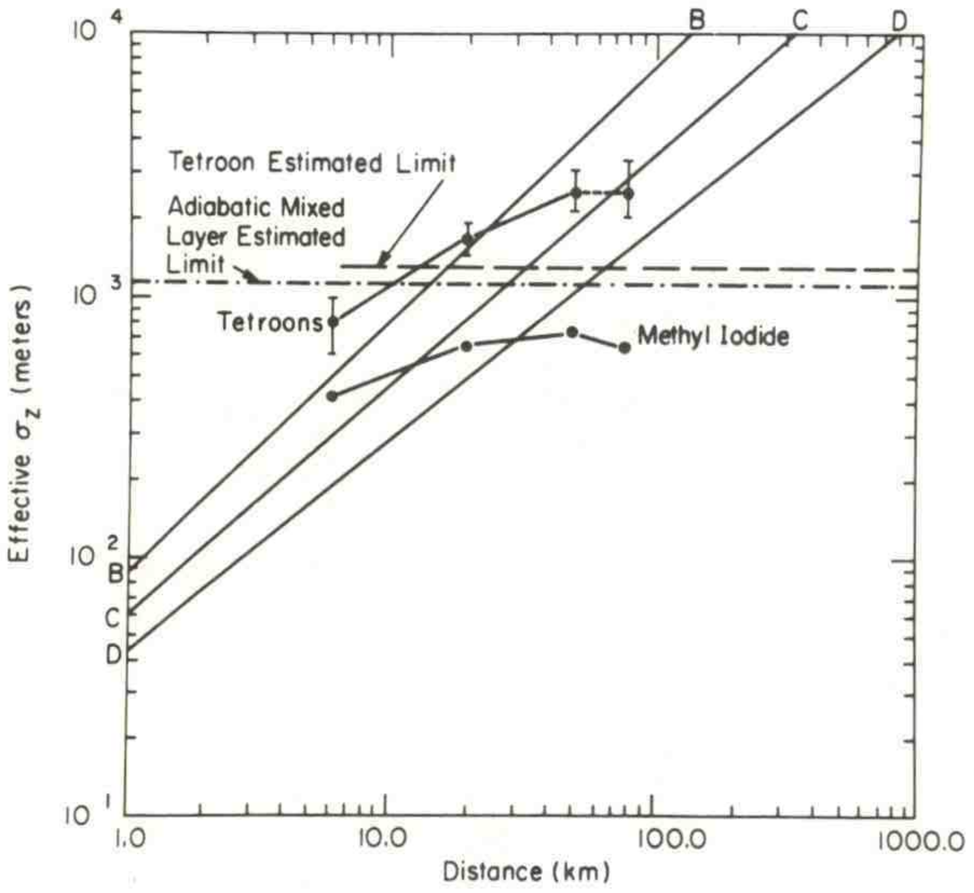

Figure 49. Vertical dispersion values from the NRTS climatology, and the effective values determined from methyl iodide measurements. Estimates based on horizontal tetroon trajectory envelopes used to define lateral dispersion are labeled tetroons.

The dot-dashed line in figure 49 shows the maximum σ_z value estimated from the depth of the adiabatically mixed layer. The dashed line labeled tetroon estimated limit represents a maximum σ_z equal to 80 percent of the height of the extreme tetroon vertical oscillation. This treatment was somewhat analogous to the arbitrary treatment of the lateral width of the horizontal trajectory envelopes. Since the tetroon envelope width divided by 4 underestimated the lateral dispersion, the "tetroon envelope" effective σ_z derived from (12) must have been overestimated by a factor of 2 to 3. Likewise, use of 80 percent of the maximum attained tetroon height probably overestimated the effective height of limited vertical dispersion. The σ_z determined from tetroon height oscillations was 516 m. The mean effective σ_z for methyl iodide tracer was near 650 m. Since the tetroon data are known to slightly underestimate vertical dispersion, the tetroon σ_z value was reasonable and as expected.

The various measurements from this test have shown that lateral tracer spreading behaved as expected. The relative axial concentration decreased more slowly with distance than would be expected from an extrapolation of measurements at short distances. The effect of a lid, which inhibited vertical dispersion, seemed to explain this slowed rate of dilution. The tracer centerline trajectory was well described by both the windfield derived trajectories and the tetroon trajectories. At the longer distances and in the presence of vertical shear, the tetroon trajectories were the best indication of transport. The lateral tracer dispersion can probably be well approximated by the running mean variance statistic; less detailed information such as the trajectory envelope width should be used only with considerable caution. The standard deviation of tetroon height oscillations provided a reasonable estimate of the mean effective σ_z for the methyl iodide tracer.

11. DIAGNOSTIC APPLICATIONS OF WIND SPEED AND COMPONENT SPECTRA

The comparison of the energy spectra of horizontal wind speed with the summed spectra of the horizontal wind components has been shown to provide some interesting insight into the fluctuating nature of the wind at a single location (NOAA Tech. Memo. ERL ARL-32, 1971). It was demonstrated, with a model wind composed of a simple harmonic, that the energy distributions for speed and component velocity can be drastically different. The energy distribution for the velocity had all the energy appearting at the frequency of the oscillation in the velocity. The energy distribution for the speed had less than 20 percent of the energy appearing at twice the frequency and the rest appearing as the energy of the mean flow (zero frequency). The reason for the difference was that the speed in the model could not reflect the sign change in the velocity due to direction reversal. Applying this information to the energy spectra of real data, one would surmise that, if the speed energy in a given frequency band is much less than the combined component energy, the wind fluctuations in that frequency band would be caused by direction reversals. If there is not much difference in the speed energy and combined component energy in a

given frequency band, then the wind fluctuations would be primarily due to fluctuations in the speed alone.

The single harmonic approximation to the wind is an extremely simplified version of what occurs in reality, as may be observed from the spectral distributions of atmospheric kinetic energy. The variations in the motion of the air flowing past a point in the free atmosphere are influenced by phenomena of several scales. For transport considerations, the primary influences seem to be the synoptic scale weather patterns, and local scale topographic influences (including land-water proximity). The combination of these influences can cause a time series of wind data from a given location to be quite complex. In figures 50 through 53, time series of wind components and speed are plotted for July and February 1969, for two levels on the CFA tower at the NRTS. For comparison, the data shown are from the data set used to obtain the energy spectra for 1969 (NOAA Tech. Memo. ERL ARL-32, 1971). The coordinate axes have been rotated 49° clockwise to provide a clear look at the variation along the principal axis of oscillation (V component). Figure 50 shows that at 76 m during February, the velocity variation involves a large number of NE-SW direction reversals with periods around 2 to 4 days. During July, figure 52 shows the prominent velocity variation is a diurnal reversal of the wind. These significant wind reversals cause the speed traces in both of these cases to appear quite different from the velocity traces. The direction

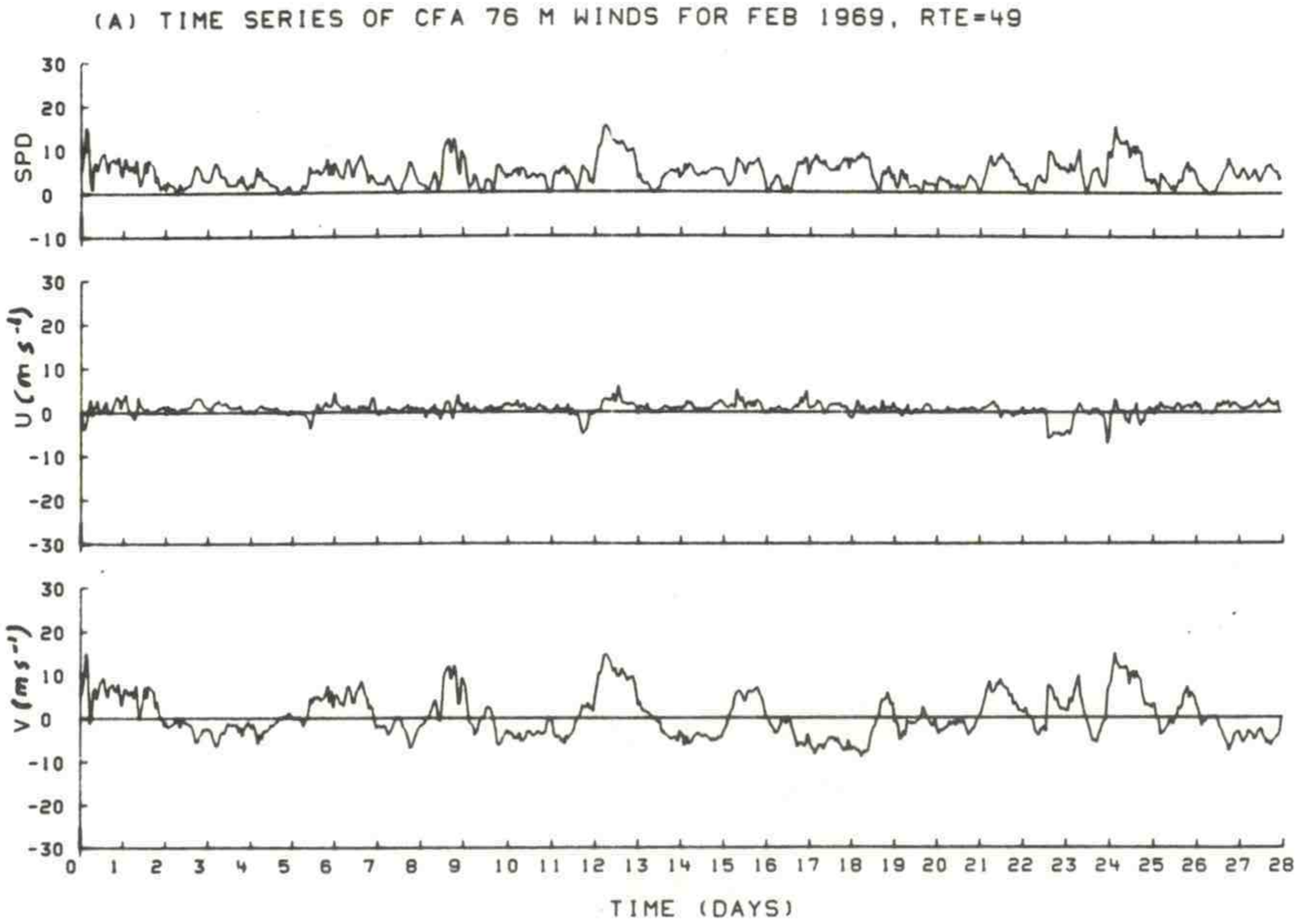

Figure 50. Plots of time variation during February 1969, of wind components and wind speed for the 76 m level of the tower at the Central Facilities Area (CFA) of the NRTS. The 49° clockwise rotation of the coordinate areas causes the V component to represent a NE or SW wind.

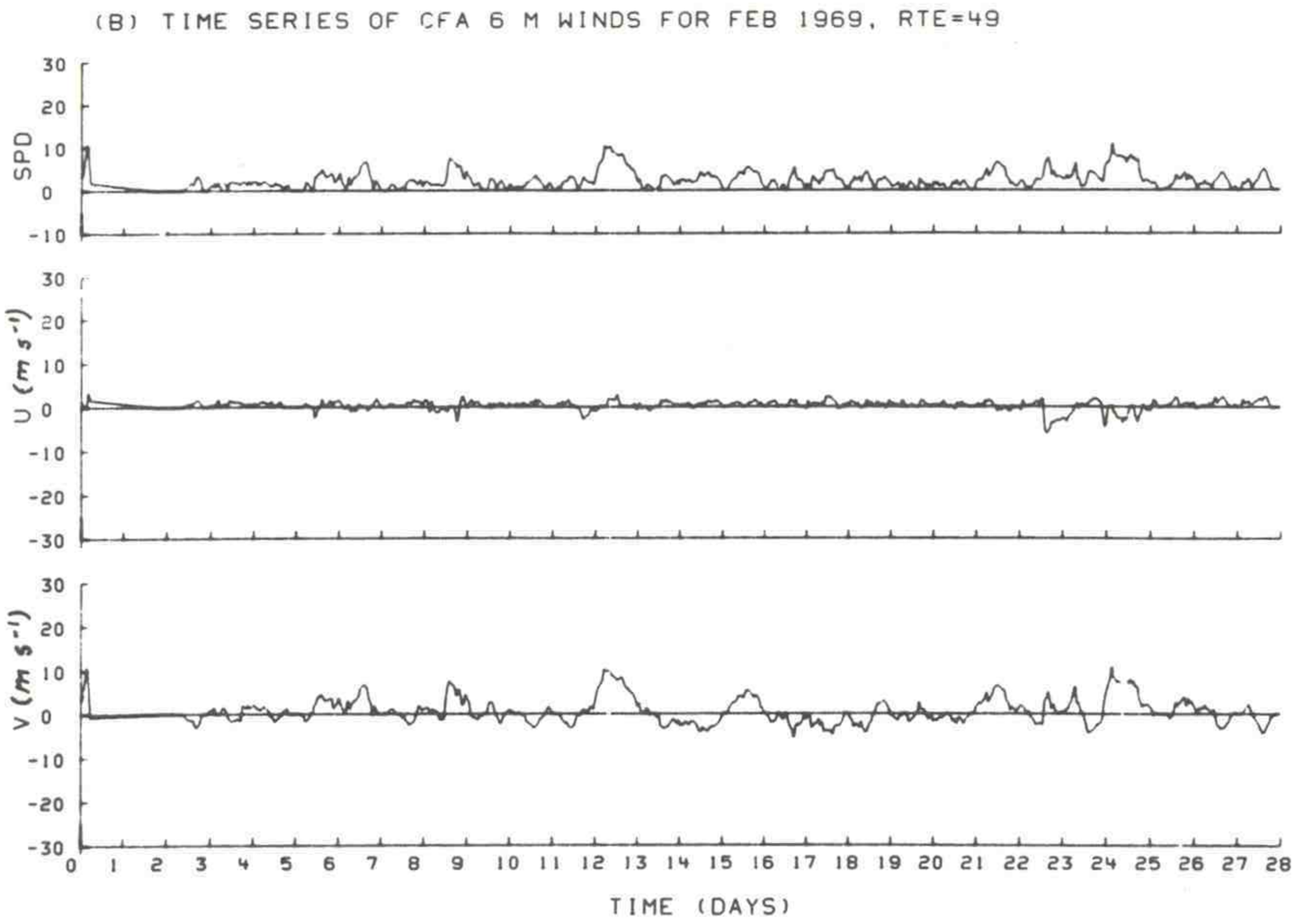

Figure 51. Same as fig. 50 except for 6-m level.

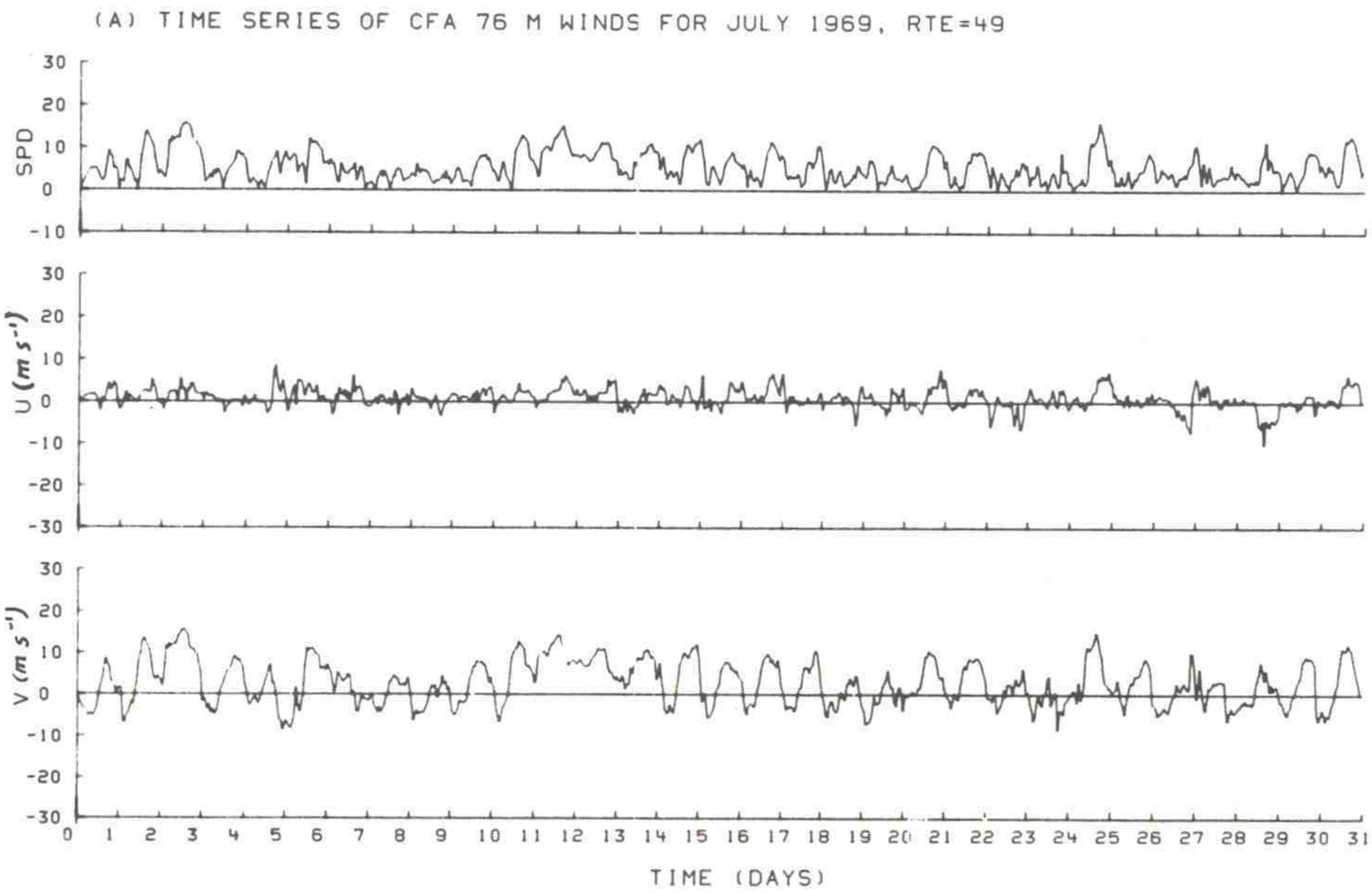

Figure 52. Same as fig. 50 for July 1969.

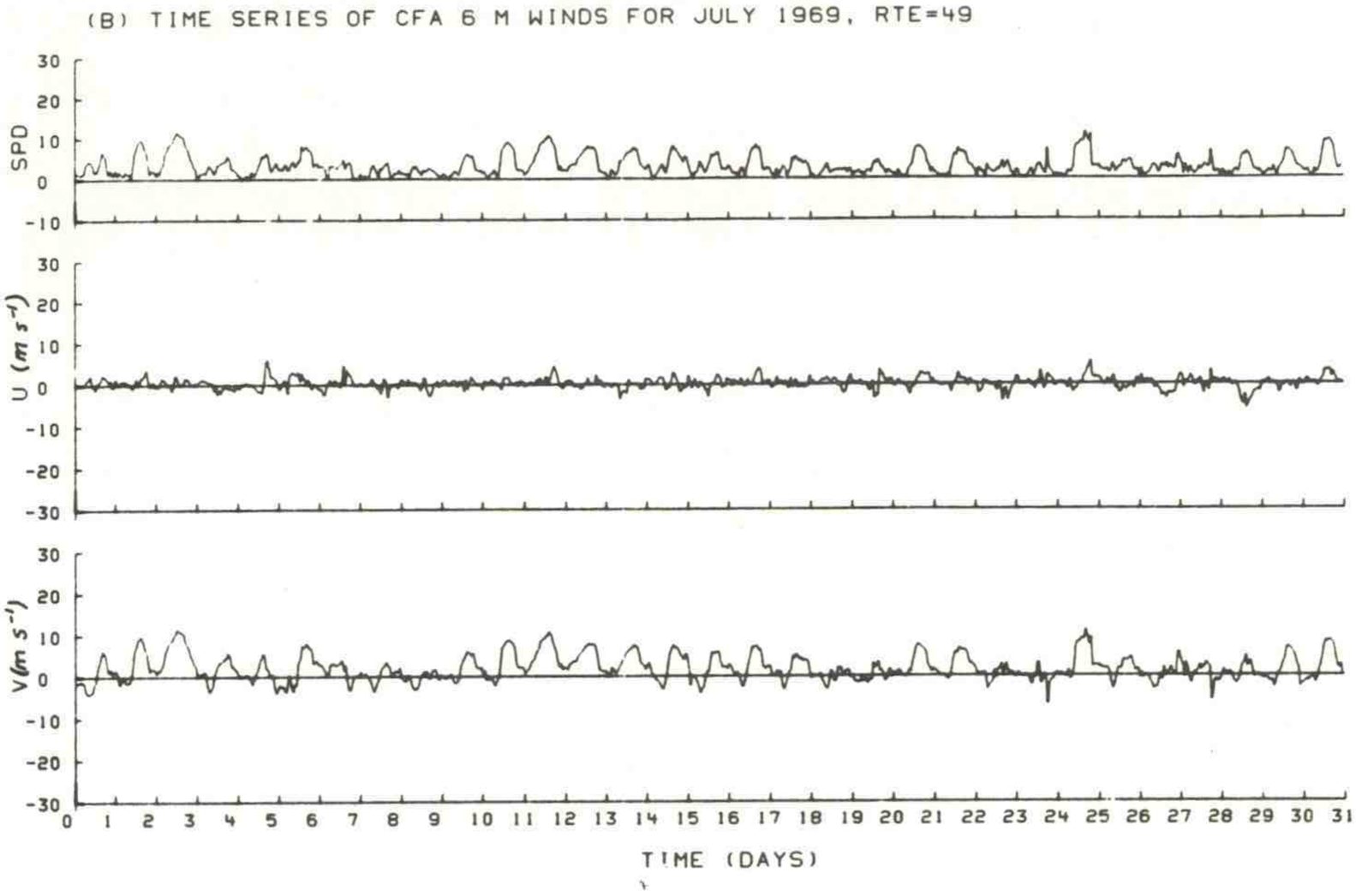

Figure 53. Same as fig. 51 for July 1969.

reversals of many frequencies compared with many other smaller amplitude oscillations cause the redistribution of energy in the speed spectra to be more subtle and complex than for the modeled wind containing a reversal at a single harmonic. However, the predominant effect for those frequencies involving direction reversals is a significant reduction of energy in the speed spectrum at those frequencies. Apparently, for a given frequency band, one can safely attribute the loss of energy in the speed spectra to direction reversals in the wind.

Comparing the spectra at 6 m showed that the speed energy was about the same as the component energy for the frequency band containing the diurnal cycle. The reason for this may be seen by comparing the plots in figures 52 and 53. The velocity fluctuations at 6 m involve a much less significant amount of direction reversal than observed at 76 m. This causes the 6 m speed and component trace to resemble the diurnal variations closer. Examining these time series plots was to substantiate the findings previously deduced from the spectral comparisons. Even though the spectral comparisons yield only qualitative information, they provide a quick and inexpensive method to investigate the importance of local terrain features on boundary layer flow.

For the data on the CFA tower, the spectral comparisons indicated a strong possibility for an unusual amount of low-level shear. When the local terrain around the tower is considered, the cause of the phenomenon begins to emerge. A relief map of the upper Snake River Plain containing the location of the CFA tower is shown in figure 54. Note that the general

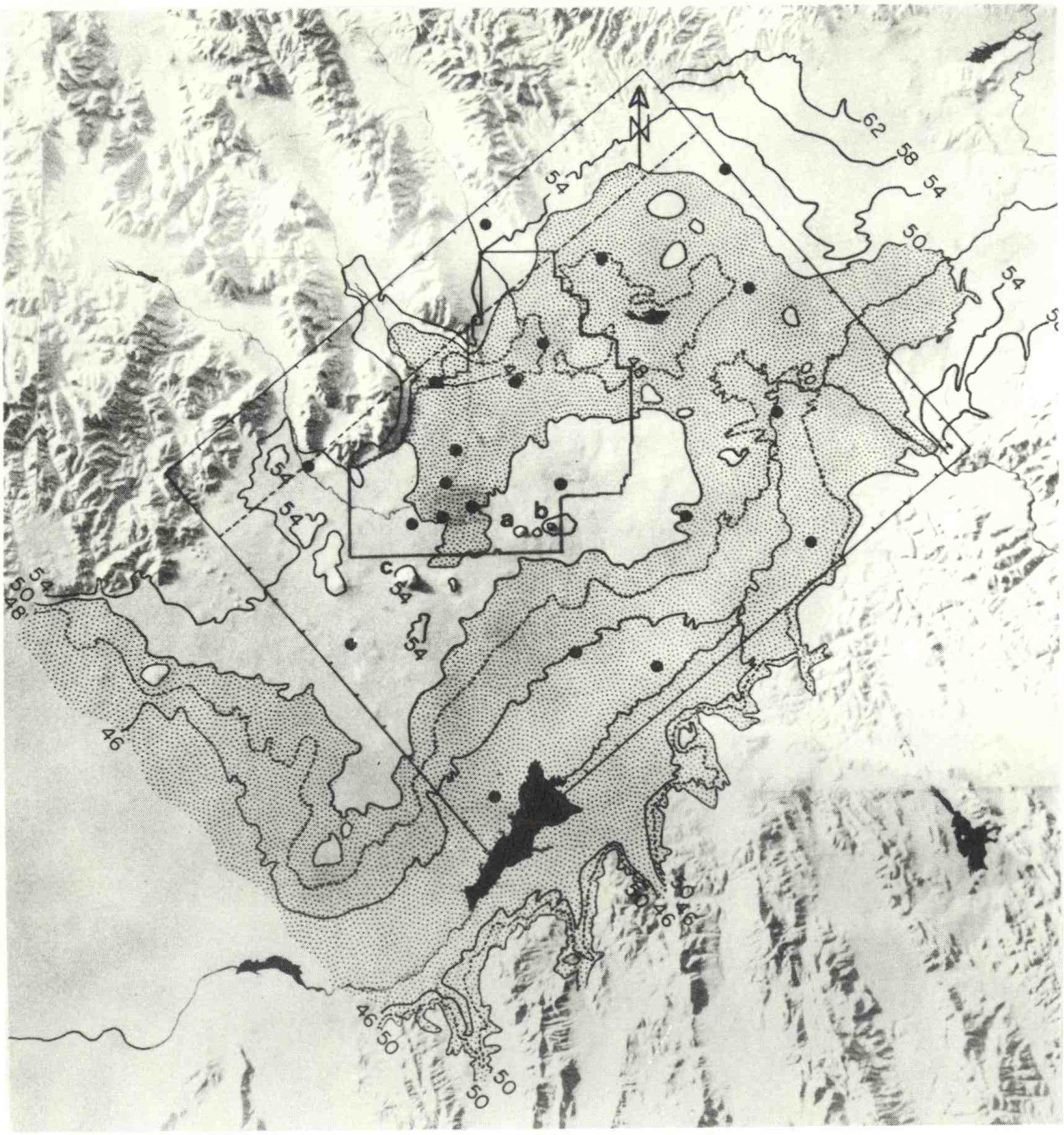

Figure 54. Relief map of the upper Snake River Plain in SE Idaho. The values shown on the few contour lines over the plain are in hundreds of feet. The stippled area within and adjacent to the grid indicates the area below 5000 ft MSL. The tics along the border of the grid indicate the grid point separation, 5.33 mi. (a) CFA 76-m tower location, (b) Grid III 61-m tower location.

slope near the tower is from SW to NE. The magnitude of this local slope is apparently great enough to significantly oppose the general drainage flow from the NE. A dramatic example of this is shown in figure 29 in which an early morning smoke release from different levels on a tower about 6 km north of the CFA tower was photographed. The smoke from the top level (61 m) is traveling SW at about 8 m sec^{-1}, while the smoke from the bottom is traveling ENE at about 2 m sec^{-1}. The results of the spectral comparison indicate that this is not a rare phenomenon.

An opportunity arose to apply the diagnostic spectral techniques to some data from a 61-m tower on the Arnold Engineering Development Reservation in south central Tennessee. The terrain variation near the tower is similar to that in central Oklahoma with streambed erosion causing a moderate amount of small-scale roughness. On a scale of tens of kilometers, the terrain is quite flat except for an abrupt height change at the beginning of the mountain range about 16 km to the east. To illustrate the proximity of the tower to the mountain range, the 1100 ft (330 m) and 1900 ft (570 m) contours are shown in figure 55. In many areas, this 800-ft (240 m) change in elevation occurs in less than 2 km, but then the high ground abruptly levels off to the east. Few heights are above 2,000 ft (600 m).

If we were trying to determine what type of flow might be induced by the terrain under conditions of weak synoptic pressure gardient, the question of whether drainage flow from the mountains would reach the tower location would be difficult to answer. The abruptness and brevity of the slope and its separation from the tower by several miles of relatively flat ground would raise doubt that the wind measured at the tower would reflect a diurnal effect caused by the mountains to the east.

The wind data from the 61- and 10-m levels taken during 1964 were used in a spectral comparison test and are shown in figures 56 and 57,

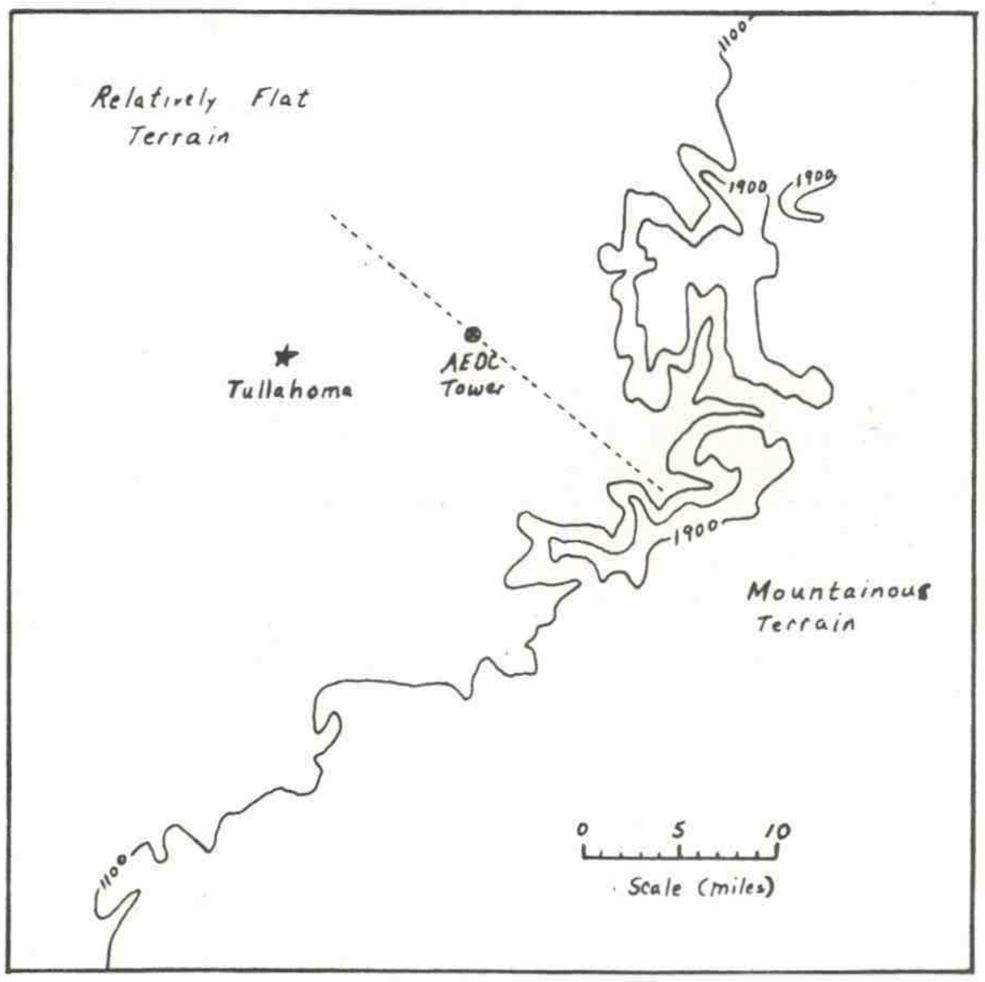

Figure 55. Relative locations of the Arnold Engineering Development Center (AEDC) tower with respect to relatively flat ground and mountainous terrain. The dashed line shows the orientation of the principal axis of oscillation of diurnal cycle in the wind at 61 m.

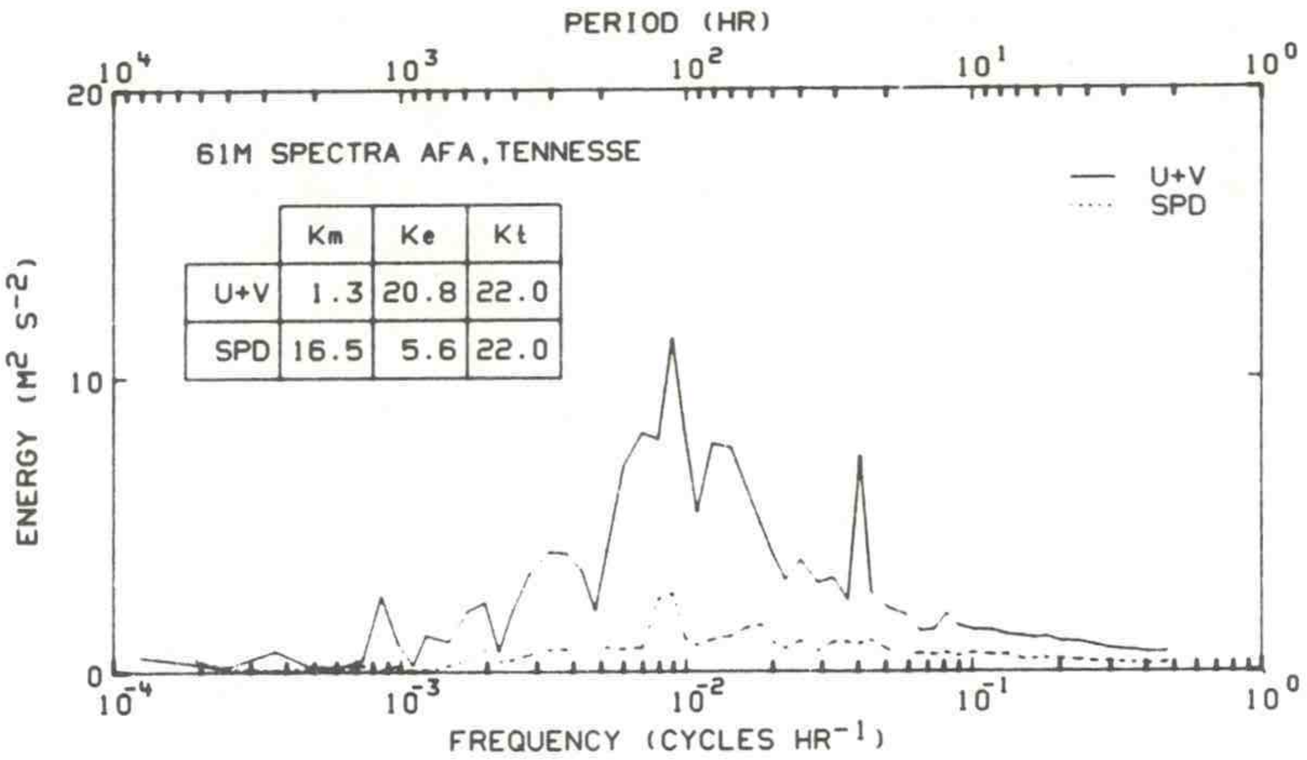

Figure 56. Energy spectra for wind speed and combined spectra of the u and v components of the wind at 61 m on the AEDC tower for 8192 hours beginning December 1, 1964.

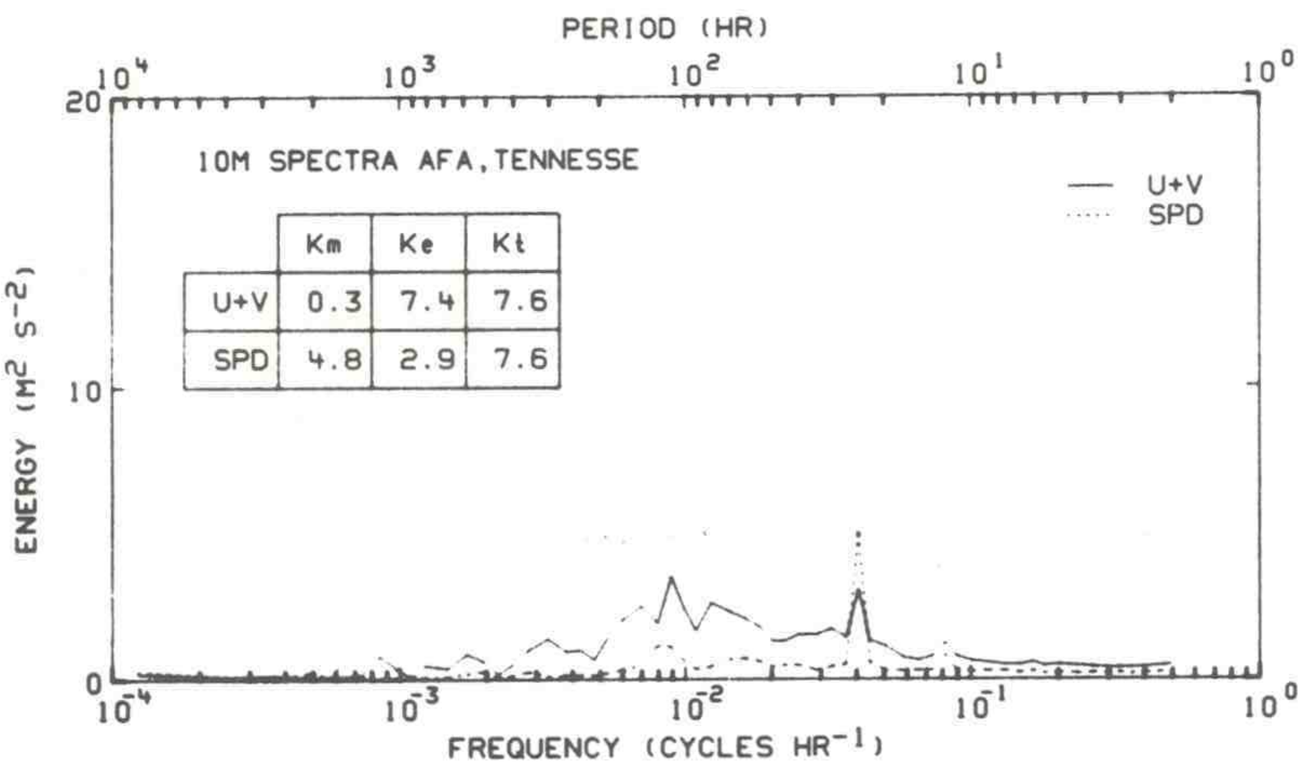

Figure 57. Same as fig. 56 except at 10 m.

respectively. In comparing these results with those for the NRTS, we find the total energy at the Tennessee tower to be little more than half that at the NRTS. According to a logarithmic extrapolation, the 15-m height discrepancy accounts for only a small fraction of the difference. The mean wind speed for the Tennessee data was 4.1 m sec^{-1}, and for the Idaho data, it was 5.0 m sec^{-1}. The spectral distribution of component energy for the 61-m level in the Tennessee tower shows the contribution to the eddy energy from synoptic disturbances coming from a narrower band of frequencies (periods from 2 to 3 days) than at the NRTS (1.5 to 14 days). This difference could reflect the effect of the mountains as cyclonic storms pass through the Northwest.

The most striking difference in the Idaho and Tennessee data at the 76- and 61-m levels is the relative size of the energy contribution from the diurnal cycle. The diurnal cycle in the wind variation measured at the tower in Tennessee is significant but much less so than at the Idaho tower. Since no indication of a peak at the diurnal frequency appears in the speed spectra, the diurnal variation in the speed can be attributed to a wind reversal, as was the case for the NRTS data. The spectral comparison for 10-m level of the Tennessee data indicates that the diurnal variation is due primarily to a speed fluctuation rather than a direction reversal.

In contrast to the 6-m Idaho data, the energy contribution of the speed spectrum at the 10-m level in the Tennessee data is significantly greater than the energy contribution of the combined component spectra. This result is similar to one obtained for Caribou, Maine (Oort and Taylor, 1969). One difference is that, in a line-by-line investigation of the spectra, they found the diurnal spike in the speed spectra to be two orders of magnitude greater than in the component spectra. A comparison of this type for the Tennessee data shows the spike in the speed spectra to be only a factor of 3 greater than in the component spectra. As a test of the significance of the spikes in the component spectra, we recomputed them using the same time-varying direction but a constant value in place of the time-varying speed. The result showed no significant decrease in the relative magnitude of the spike in the component spectra. This would indicate that, at least in this case, the extra energy in the speed spectra at the diurnal cycle is a reflection "beating" by direction reversals at other frequencies.

The directional nature of the wind variation was examined by recalculating and plotting the component spectra at 61 m while rotating in 10° increments the coordinate axes clockwise through 80°. The spectra for the N-S orientation and the 40° rotation are shown in figures 58 and 59. For the N-S orientation, the total energy for the v component (along the ordinate) is over twice that for the u component (along the abscissa). The plot clearly shows that the variation in the N-S component of the wind is the major contributor to the eddy energy over the range of the synoptic scale disturbances, but not at the diurnal cycle. As the axes were rotated clockwise, the difference in contribution at the diurnal cycle was a maximum at 40°, with the u component being significantly larger. This would indicate a diurnal oscillation in a SE-NW direction. It is interesting to note the relative balance between the energy contributions of the components through the range of frequencies for the synoptic disturbances. This contrasts with the situation for the Idaho data, in which the principal axis of oscillation was the same for both the synoptic disturbances and diurnal oscillations because of the strong channeling effect of the mountains on either side of the Upper Snake River Basin.

In relating the spectral results for the Tennessee data to the topography, we find that N-S orientation of the principal axis of oscillation for the synoptic range of frequencies is probably caused by some deflection

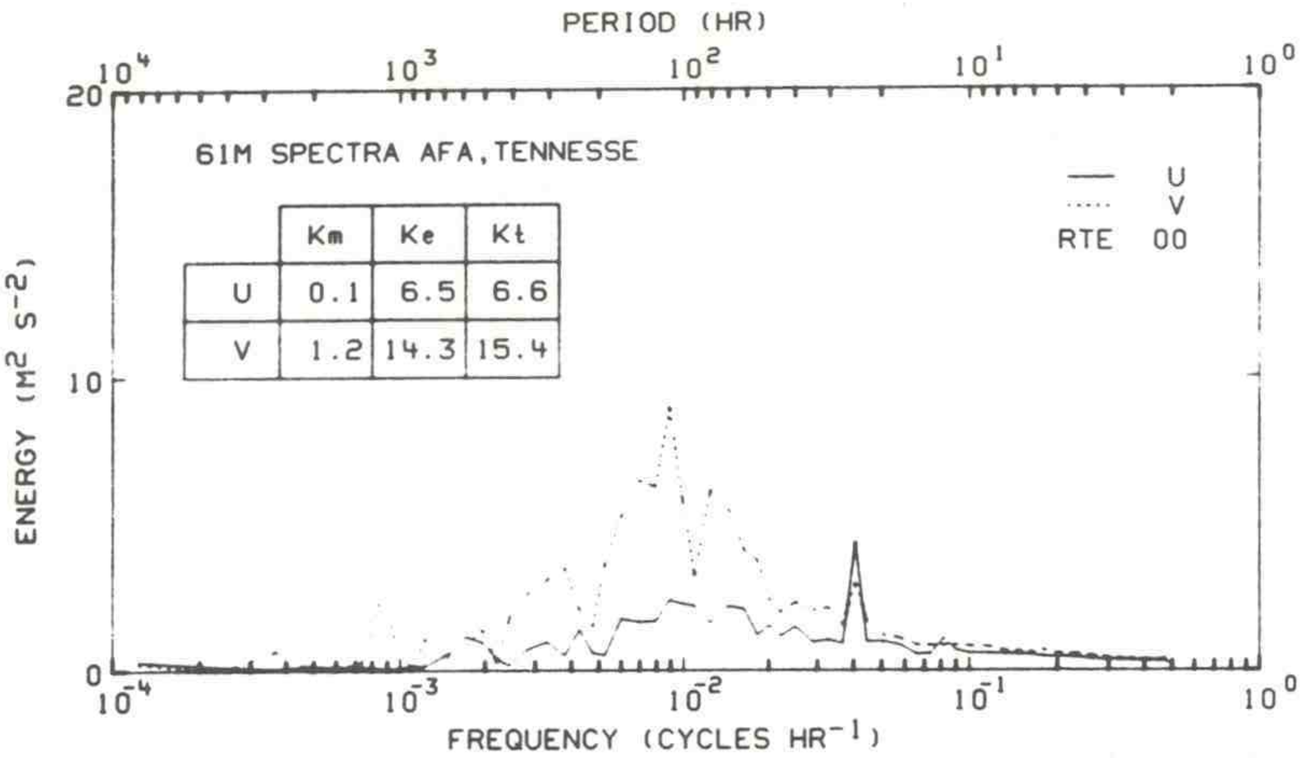

Figure 58. Energy spectra for the u and v components with v being the N-S component.

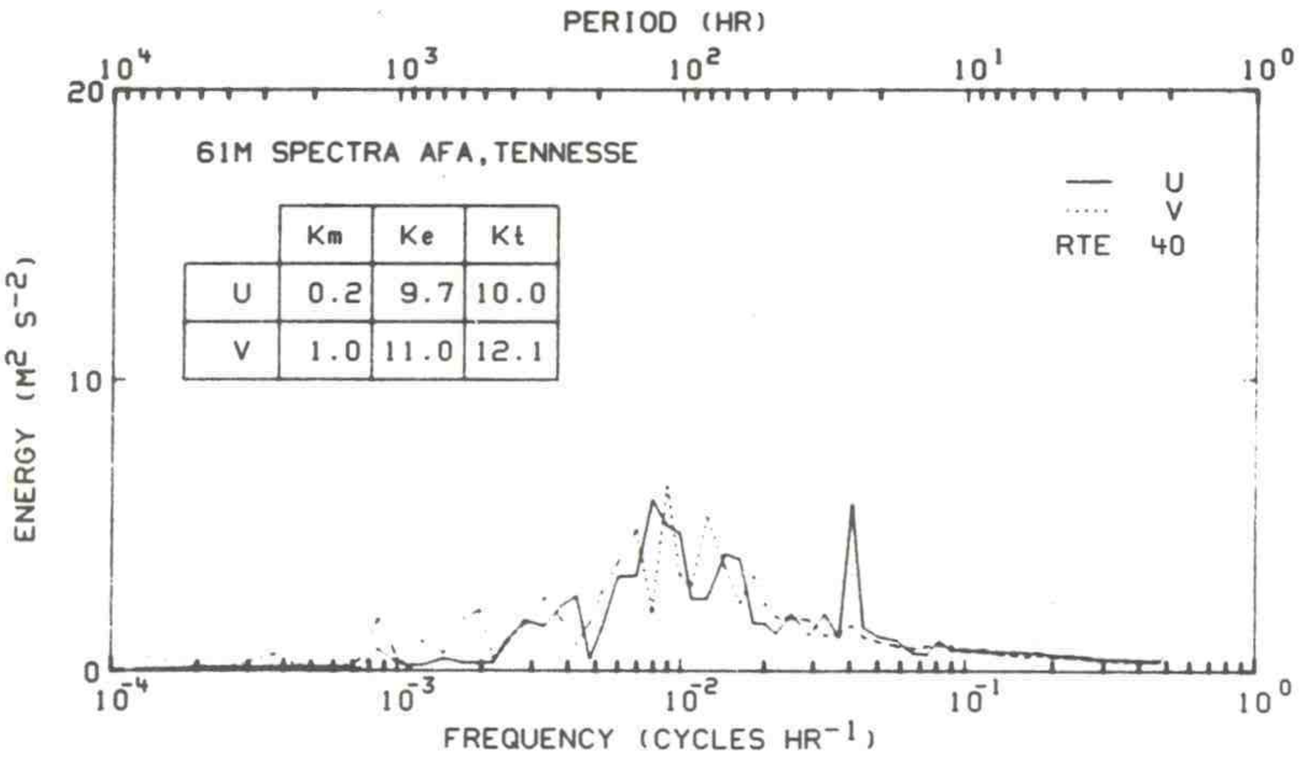

Figure 59. Energy spectra for the u and v components with v being the NE-SW component.

of the flow by the mountain range to the east. The NW-SE orientation of the diurnal oscillation indicates a mountain-valley effect, at least at the 61-m level, due to the valley SW of the tower. The effect seems to be nullified at 10 m, since only a speed fluctuation occurs at this level. This is probably due to the relatively flat terrain between the tower and valley as well as a large reservoir about 5 km south of the tower.

Seasonal spectral comparisons for 1964 show about what to expect. The diurnal oscillation varies from undiscernable in the winter to the major contribution from a single frequency band in the summer. The total variance is a minimum in summer (10.6 m^2sec^{-2}) and a maximum in winter (31.3 m^2sec^{-2}). This difference can be attributed to the large variation in the contributions from the synoptic scale frequencies.

To summarize these results in terms of transport, we could say that a moderate preference for transport to the north or south exists during the fall, winter, and spring with the predominant periods for wind reversals being 4 to 8 days during the spring and fall, but 2 to 4 days during the winter. During the warm months, transport for a stack release would be strongly affected by the diurnal circulation from the valley to the SE. This demonstrates again that, for the meteorological aspects of reactor safety analyses, diagnostic spectral techniques provide valuable insight concerning the influence that local topographic features have on the wind at a given location. Such information pertaining to the oscillatory nature of the wind would be impossible to obtain with a standard wind rose analysis.

12. FORECASTING AND WEATHER WARNING SERVICE

The number of specific NRTS subcontractor and contractor requests can be estimated as follows. About six subcontractors ran projects in which daily or twice-daily requests for weather information were made for periods of 2 to 10 weeks. This represents about 200 to 250 forecast requests. There were 13 weather warnings (excepting December and January) given to AEC Warnings and Communications for general broadcast at the NRTS. December 1971 and January 1972 were the stormiest of record, and 29 individual weather warnings were issued in the 2 months. A description of the unusual wind storm of January 11 and 12 , in which the NRTS transportation buses were stranded at the NRTS overnight, follows. Requests for weather advisories and forecasts occurred between two and three times daily as a minimum, and upwards of 30 requests daily during the unusual weather. Admittedly, a number of these requests were from individuals satisfying their own curiosity; however, a large percentage were from administrators of NRTS functions such as plant operations, transportation, repair services, etc.

Certain teletype and facsimile data — normally received to provide the weather warning and advisory services — are also filed for possible future reference in research on transport.

The storm of January 11 and 12, 1972, involved about 36 man-hours of closely watching the available data, issuing warnings, personally consulting with management, and cooperating with Warnings and Communications. From late morning of Tuesday, January 11, to the predawn hours of Wednesday, January 12, we recorded the strongest winds over snow-covered ground ever observed at the NRTS. These record-breaking winds were due to a possibly record-breaking surface pressure gradient between the high pressure in the intermountain region and the low perssure on the east side of the Rocky Mountains. At 1700 MST of January 11, the low was in central Montana with a central pressure of only 976 mb, while Pocatello, Idaho, was still at 1006 mb — a 30 mb difference. Most of the difference was concentrated within about 500 km. Table 7 shows the average hourly

Table 7. Hourly Average Winds and Peak Gusts Recorded During the Hour ending at the Time Indicated (direction-speed-peak gust).

Time (MST)	CFA 20' Level	Grid III 200' Level	TREAT 50' Level
	January 11		
0100	236-21-30*	235-32-40	225-18-31
0200	252-14-23	240-32-40	225-20-30
0300	252-19-38	250-22-33	225-25-38
0400	234-30-41	260-18-34	225-28-42
0500	230-31-43	235-35-45	228-31-42
0600	231-27-40	235-44-53	235-38-52
0700	238-31-46	237-49-59	235-38-52
0800	236-33-47	245-53-67	235-38-52
0900	237-36-53	245-59-68	238-40-54
1000	238-38-55	240-59-70	237-44-56
1100	237-37-51	240-52-68	237-42-56
1200	234-34-49	235-49-60	240-43-64
1300	234-36-60	232-48-60	235-51-67
1400	234-40-61	238-52-66	235-53-68
1500	237-44-61	240-61-72	235-46-61
1600	237-44-63	240-64-79	240-47-63
1700	240-43-61	242-64-77	240-49-68
1800	240-44-61	243-65-76	241-47-65
1900	244-44-60	245-63-75	245-50-69
2000	245-46-70	245-65-79	245-51-71
2100	244-43-70	245-62-76	245-48-66
2200	243-44-65	245-64-77	245-47-63
2300	243-48-64	245-63-79	245-46-61
2400	243-42-63	245-56-67	245-45-61
	January 12		
0100	241-38-57	245-54-65	245-44-58
0200	240-36-54	243-50-67	245-42-56
0300	244-37-53	245-52-62	245-40-55
0400	246-35-51	248-41-57	252-37-49
0500	261-27-43	265-30-47	255-30-43
0600	270-18-30	300-13-30	320-10-30
0700	351-10-21	335-16-34	350-5-10

* Direction in degrees, speed in knots.

winds and peak gusts for a 30-hr period at three locations starting the morning of January 11 and ending the morning of the 12th. Table 8 shows the altimeter setting differences at selected hours. A difference of 0.10 inches of Hg between Pocatello and Idaho Falls is unusual, and usually produces average wind speeds of 30 to 35 mph.

Table 8. Altimeter Setting Differences in Inches of Mercury

Date	Hour	PIH-IDA	IDA-DLN
Jan	MST		
10	2300	0.03	0.16
11	0500	0.09	0.25
11	0800	0.11	0.30
11	1100	0.11	0.35
11	1400	0.11	0.32
11	1700	0.20	0.25
11	2000	0.18	0.19
11	2300	0.16	0.08
12	0200	0.09	0.01
12	0500	0.10	-0.06
12	0800	-0.02	-0.02

PIH - Pocatello, Idaho
IDA - Idaho Falls, Idaho
DLN - Dillon, Montana

13. ACKNOWLEDGMENTS

Sections 1 and 2 were joint research efforts of several Air Resources Laboratories with the sponsorship of both NOAA and the AEC Division of Reactor Development and Technology. Section 5 is work sponsored by the AEC Directorate of Licensing.

The Oklahoma field program was carried out by ARL personnel from Silver Spring, Maryland, and the National Reactor Testing Station (NRTS), Idaho Falls, Idaho. Support was provided by the National Severe Storms Laboratory (NSSL), Norman, Oklahoma, which operated the slow-response tower sensor system and provided assistance in numerous other ways, and by the 6th Weather Squadron (Mobile), Air Weather Service, U.S. Air Force, which operated the pibal-radiosonde network.

14. REFERENCES

Angell, J. K., D. H. Pack, C. R. Dickson, and W. H. Hoecker (1971), Urban influence on nighttime air flow estimated from tetroon flights, *J. Appl. Meteorol.* **10**:194-204.

Bellamy, John C. (1945), The use of pressure altitude and altimeter corrections in meteorology, *J. Meteorol.* **2**(1):1-79.

Bonner, W. D., and J. Paegle (1970), Diurnal variations in the boundary layer winds over the south central United States in summer, *Monthly Weather Rev.* **98**(10):735-744.

Briggs, G. A. (1969), Plume rise, U.S. Atomic Energy Commission, Division of Technical Information, TID-25075.

Camp, D. W., R. E. Turner, and L. P. Gilchrist (1970), Response tests of cup, vane, and propeller wind sensors, *J. Geophys. Res.* **75**:5265-5270.

Dingle, A. Nelson, and Charles Young (1965), Computer applications in the atmospheric sciences, Univ. of Michigan, Ann Arbor, Mich., 214-221.

Drinkrow, R. (1972), A solution to the paired Gill-anemometer response function, *J. Appl. Meteorol.* **II**:76-80.

Gill, G. C., L. E. Olsson, J. Sela, and M. Suda (1967), Accuracy of wind measurements on towers or stacks, *Bull. Am. Meteorol. Soc.* **48**:665-674.

Heffter, J. L. (1965), The variation of horizontal diffusion parameters with time for travel periods of one hour or longer, *J. Appl. Meteorol.* **4**(1):153-156.

Holmes, R. M., G. C. Gill, and H. W. Carson (1964), A propeller-type vertical anemometer, *J. Appl. Meteorol.* **3**:802-804.

Kaimal, J. C., and D. A. Haugen (1969), Some errors in the measurement of Reynolds stress, *J. Appl. Meteorol.* **8**:460-462.

NOAA Tech. Memo (1970), Atmospheric transport and diffusion in the planetary boundary layer, Air Resources Laboratories Semi-Annual Research Program Review, Jan-July 1970, ERL-ARL-28, 47 pp.

NOAA Tech. Memo (1971), Atmospheric transport and diffusion in the planetary boundary layer, Air Resources Laboratories Annual Research Program Review, July 1970-June 1971, ERLTM-ARL-32, 71 pp.

Oort, A. H., and A. Taylor (1969), On the kenetic energy spectrum near the ground, *Monthly Weather Rev.*, **97**:632-636.

Pack, D. H., and J. K. Angell (1963), A preliminary study of air trajectories in the Los Angeles Basin as derived from tetroon flights, *Monthly Weather Rev.* **91**(10-11):583-604.

Pasquill, F. (1962), *Atmospheric Diffusion* (D. Van Nostrand Co., Ltd., London).

Slade, D. H., ed. (1968), Meteorology and atomic energy 1968, TID-24190, Clearinghouse for Federal Scientific and Technical Information, Natl. Bureau of Stands., U.S. Dept. of Commerce, Springfield, Va.

Smith, M. E., and I. A. Singer (1966), An improved method of estimating concentrations and related phenomena from a point source emission, *J. Appl. Meteorol.* **5**(5):631-639.

Start, G. E. (1970), Comparative diffusion and deposition of uranine dye, molecular iodine gas, and methyl iodide gas, Proc. 5th Annual Mid-year Topical Symp. on Health Physics of Nuclear Facility Siting, Health Physics Soc. Nov.

Teweles, S., and H. Wobus (1954), Verification of prognostic charts, *Bull. Am. Meteorol. Soc.* **35**:455-463.

Wendell, L. L. (1970), A preliminary examination of mesoscale wind fields and transport determined from a network of towers, NOAA Tech. Memo. ERLTM-ARL 25, Air Resources Laboratories, Silver Spring, Md.

Wendell, L. L. (1972), Mesoscale windfields and transport estimated determined from a network of wind towers, *Monthly Weather Rev.* **100**(7):565-578.

Yanskey, George R., Earl H. Markee, Jr., and Alden P. Richter (1966), Climatography of the national reactor testing station, IDO-12048, AEC Opeartions Office, Idaho Falls, Idaho.